Utrecht University

A global remote-sensing assessment of the mobility of coastal dunes

Petya Georgieva Petrova (7861451)

Master thesis for the partial fulfilment of the Master of Earth Sciences at Utrecht University

Utrecht University supervisors:

Prof. Dr. Gerben Ruessink, Department of Physical Geography

Prof. Dr. Steven de Jong, Department of Physical Geography

2022

Abstract

Over the last decades, many coastal dunes have lost their natural geomorphologically dynamic character due to spatial expansion of vegetation. This "greening" may not only adversely affect the resilience of dune systems to climate change, but already puts at risk their ecological diversity. While climate has been considered the dominant factor for greening in areas where human activities are limited or rare, on a regional scale over the last century, the role of human interventions has been significant. Whether dune greening is limited to the effects of global warming or is site-specific is largely unknown. Therefore, the aim of this work is to detect and assess the change in vegetation cover over time, at a large number of dunefields worldwide, by using Landsat satellite imagery, and to correlate the identified trends with the trends in the main climatic variables, such as temperature, precipitation and wind speed, in order to decide on the drivers of the change.

The Climate Engine App (http://climateengine.org/) has been used to retrieve the multitemporal series of the Normalized Difference Vegetation Index (*NDVI*; Landsat 4, 5, 7 and 8) and those of the climatic variables for the period 1984 – 2021. This has been done for 186 individual coastal dune sites from different continents: Europe (69); South America (33); North America (31); Africa (20); Oceania (29); and Asia (4). The dune systems are evolving locally under different climatic and environmental conditions, and are subjected to different levels of human pressure.

The main results confirm that greening trends are indeed dominant on a global scale (87.1%), as compared to a few dune sites with sand mobilising trends (9.1%), where the aeolian process dominates the stabilisation, and sites with no change (3.8%). Steeper trends are mostly associated with denser average vegetation cover (greener sites) which is typical for the temperate climates. Those sites also exhibit pronounced *NDVI* seasonality. About 63% of all significant changes show acceleration over the second half of the study period. The other important result is that the vegetation trends show no statistical relationship with the trends of the climatic variables which has been additionally corroborated by a multiple regression analysis. On one hand, possible explanation may be that the current climate has already reached the threshold of being sufficiently warm and wet, so that the dunes are greening anyway. Therefore, further changes in the climatic variables may become irrelevant to the greening. On the other hand, other regional factors (atmospheric pollution, decline in rabbit population) may play a role. Also, management interventions can explain some of the accelerated greening trends, as well as cases of reduced *NDVI* at other dune sites, despite local climate favouring greening.

Keywords: *Coastal dunes; Dune dynamics; NDVI time series; Dominant fluctuations; Human interventions; Coastal management*

Acknowledgements

Firstly, I wish to thank my academic supervisor Professor Gerben Ruessink, for his guidance and continuous enthusiasm during this project in spite of the lockdown. Due to his support, the initial confusion was substantially reduced and there was time to learn and enjoy the virtual trip across amazing dunescapes. I should also thank him for the indirect motivation to choose the topic of coastal dunes, as well as for the opportunity to participate at the NCK Days 2022 and get back the feeling of being a researcher and of socialising with people.

Secondly, I want to thank Professor Steven de Jong for accepting to be my second supervisor. I am sure that under different circumstances I would have asked him a lot of questions.

Dordrecht, the Netherlands

May, 2022 *Petya Petrova*

Contents

List of figures

List of tables

1. Introduction

1.1. Coastal Dunes

Dunes are globally present aeolian features associated with sandy, wave-dominated coastal landscapes with sufficient sediment supply (Martínez and Psuty, 2008; Davidson-Arnott and Law, 1996). They arise from the interaction between wind, sand and vegetation cover and have an important role in the sediment budget of the beach-dune system (Arens and Wiersma, 1994; Hesp, 2002). The undisturbed exchange of sediments is responsible for the dynamic equilibrium of the system and shoreline stability (Davidson-Arnott et al., 2018; da Silva and Hesp, 2010). Providing coastal stability and protection of the hinterlands against marine flooding is commonly viewed as the main role of the dunes for humankind. This role is particularly important nowadays, in view of the changing climate, associated rise of the mean sea level and increasing threat by more frequent and destructive storms and coastal floodings (Claudino-Sales et al., 2008; Nicholls and de La Vega-Leinert, 2008).

The functions of dunes, however, include also natural values. From an ecological perspective, they are rich in habitats for rare plants and animal species, therefore holding high biodiversity value (Everard et al., 2010; Martinez et al., 2004). Dunes also contain natural resources, like sand and drinking water (Arens and Geelen, 2006; Barbier et al., 2011; van der Meulen et al., 2004). And, very importantly, the beach-dune landscapes have invaluable recreational potential (Jackson and Nordstrom, 2011).

In this context, the changing perception that dunes need to be controlled and the growing concern that stabilised dunes have deteriorated functionality in all of the above aspects imply that dunes need measures for their conservation and protection (Van der Biest et al., 2017; Everard et al., 2010; Ruessink et al., 2018).

1.2. Factors controlling the dune dynamics

Coastal dunes have been going through a period of stabilisation over the last decades due to spatial expansion of vegetation, with a tendency for dominance of late successional stages, such as scrub and woodland species. Some examples of increasingly vegetated dune surfaces at different geographical locations, including Brazil, Mexico and southern Australia, are given in Figure 1.1.

The above tendency has been recently discussed by Jackson et al. (2019) and Gao et al. (2020), among others, with respect to the major driving forces behind the stabilisation process. According to

the first group of authors, greening and the resulting dune fixation are due to changes in the main climatic variables on a global scale (i.e., increasing temperature and precipitation, combined with decreasing windiness), as well as due to atmospheric deposition of various pollutants and nutrients (NO_2, CO_2, N, P, etc.). Such hypothesis excludes the human factor or reduces its effect to minimum.

Gao et al. (2020) on the other hand conducted a more extensive research based on a literature review, for a significantly larger number of dune sites worldwide. They concluded that although climate could have dominated the dune evolution in areas where human activities are limited or rare, on a regional scale the human interventions have played a significant role over the last century which led primarily to dune stabilisation. It is, however, still unclear how important are the natural versus anthropogenic drivers of greening and whether greening is a global trend resulting from global warming, or the changes in the dune dynamics are site-specific responses to regional and local environmental and climatic conditions (Lancaster and Helm, 2000; Delgado-Fernandez et al., 2019; Miot da Silva et al., 2013; Jackson and Nordstrom, 2011).

It is considered that natural dune mobility is driven primarily by three groups of factors: (1) climate (wind regime, precipitation, temperature); (2) sediment supply and availability, and (3) extent of vegetation cover (Arens et al., 2013; Provoost et al., 2011; Tsoar, 2005). Furthermore, the drivers promoting vegetation growth can be generally described as (Provoost et al., 2011; Jackson et al., 2019, Gao et al., 2021): anthropogenic (e.g., stabilisation activities, introduction of exotic species to promote dune formation or landscape fixation), and climate-driven (e.g., increased temperature, reduced wind speeds). Figure 1.2 (modified from Jackson et al., 2019) is a conceptual illustration of the potential drivers of greening and their long-term global trends. It shows that the combination of warmer, wetter and less windy climatic conditions favours vegetation growh and thus dune stabilisation with time, especially for cool temperate environments.

The relationship between climate and dune dynamics can be better understood looking at the history of dune formation. Provoost et al. (2011) compared chronologies of dune formation and development at several dune sites across northwest Europe and pointed to clear links with periods of substantial aeolian activity. Such periods exhibit worsened climatic conditions (low temperature and strong winds) as compared to the climate today (warmer, wetter, calmer). The Little Ice Age (1300 to 1850 AD) has been associated with the formation of several dune systems in NW Europe, e.g., in Denmark (Clemmensen and Murray, 2006; Clemmensen et al., 2014) and United Kingdom (Wilson et al., 2001). Significant aeolian activity has been also reported for the SW coast of France (the Aquitaine coast; Clarke et al., 2002), the Portuguese coast (Costa de Caparica; Costas et al., 2016) and the SW Spanish coast (Zazo et al., 2005) where some of the largest and active dunes nowadays exist. Moreover, according to Dillenburg et al. (2018), aeolian deposits on the coast of southern Brazil can be also correlated with the same historical periods of cold climate and increased storminess.

On the other hand, the improved climatic conditions that followed those periods coincide with dune stability. For example, Clemmensen et al. (2014) reported strong correlation between the stabilised

dunes on the Skagen Odde spit in Denmark and the declining storminess in NW Europe over the last century, although the stabilisation can be partially attributed to dune management.

Therefore, it is clear that the long-term dune activity is cyclic. The dune systems go from highly active states (strong aeolian activity on bare sand) to stabilised dunes (fully fixed by vegetation) in response to large-scale climatic fluctuations (Hugenholtz and Wolfe, 2005). Furthemore, it can be considered that the global increase of dune vegetation at present, although largely influenced by stabilisation practices, appears to be a natural response to the improved climatic conditions following the Little Ice Age.

Figure 1.1. Dune greening. *Source*: Prof. Patric Hesp (Coastal Dynamics 2021, Dune Dynamics short course, June 28th; https://www.coastaldynamics2021.nl/).

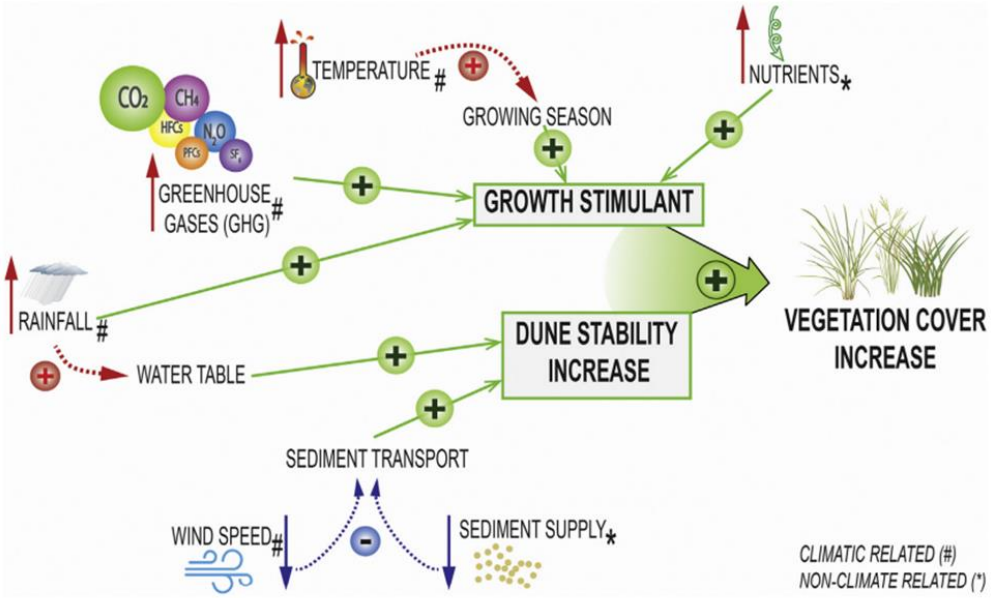

Figure 1.2. Likely relationships between potential drivers and dune vegetation expansion. *Source*: Jackson et al. (2019).

The importance of the regional and local climatic conditions has been broadly discussed in the literature (Miot da Silva et al., 2013; Delgado-Fernandez et al., 2019; Hesp et al. 2021; Moulton et al., 2019; Psuty and Silveira, 2010; Jackson et al., 2019; among others). The climatic variables are acting together on a global scale, but their relative role is to a great extent site-specific. A small temperature increase in the temperate zones leads to vegetation growth and dune fixation. However, dunes in arid climates are naturally more mobile since the scarse rainfalls do not allow significant vegetation growth (Hesp, 2013). Low precipitation, warm temperatures and high wind energy determine the generally higher dune activity in dune systems from arid and semi-arid settings, such as the Maspalomas dunefield on Gran Canaria, Canary Islands (Hernández-Cordero et al., 2018; García-Romero et al., 2019).

Active dunes therefore exist at locations where the sand transport is facilitated by favourable atmospheric conditions. This makes the wind power the most important physical factor for dune mobility. It is commonly represented as a sand drift potential, i.e., the wind strength that keeps the sand in saltation mode. High drift potential (high sediment transport) limits the growth of vegetation by sand burial and/or wind erosion; low drift potential (low sediment transport) leads to vegetation expansion, therefore to dune greening (Tsoar, 2005). The actual sand drift further depends on the grain size, surface roughness and vegetation cover, as well as on the sand moisture and wind directionality (Yizhaq et al., 2009). Wind direction can influence the dunefield width, since offshore and alongshore winds do not contribute to sand migration landward, thus restricting the dunefield growth (Martinho et al., 2010).

Precipitation and potential evapotranspiration, on the other hand, control the sand transport through the moisture content, since greater moisture delays the sediment availability and requires higher wind

speeds for aeolian transport (Anthonsen et al., 1996; Tsoar, 2005). The rainfall amounts and their annual distribution determine the vegetation growth, which controls the dune mobility and size (Pye et al., 2014; Delgado-Fernandez et al., 2019; Martinho et al., 2010). Sparse vegetation in arid and semi-arid climates, as in the Mediterranean region, is sensitive to precipitation, therefore the dunes are expected to respond directly to it, with fast greening (Martinez and Gilabert, 2009). In more humid coastal areas, precipitation can significantly increase the local water table, thus changing the sand availability, the vegetation cover and dune mobility (Miot da Silva and Hesp, 2013).

Although precipitation works as a limiting factor for dune development and mobility (Pye et al., 1982), extensive dunefields can be found along the tropical coast of Brazil. Furthermore, some of the largest and most active dunes are located within 2 – 3º from the Equator in the NE Brazil, where the regional climate is controlled by a long dry period with very strong onshore winds (Hesp, 2008; Buynevich et al., 2010; Jimenez et al., 1999; Maia et al., 2005). Extensive dunefields, with coexisting vegetated and active dune forms, can be also found in the humid tropics of the Mexican Gulf coast (19–21°N).

Dune sites with increased precipitation and decreased windiness show higher rates of vegetation growth, e.g., those from the cool temperate regions of Europe and North America. On the other hand, Huang et al. (2018) found local temperature rise to be the reason for shrub encroachment on Hog Island, a barrier island on the east coast of US. The greening of the Irish dunes is yet another example of local climate change favouring greening: increasing temperatures (especially in winter, leading to a longer growing season), slightly increased trend for rainfall and reduced windiness (Jackson and Cooper, 2011; Provoost et al., 2011). Furthermore, most of the remote Irish dunes are expected to be close to their natural state, similarly to the Hog Island dunes. The recent years have also seen stabilising trends in some of the tallest dunes in the central region of the Gulf of Mexico which is partially attributed to natural greening promoted by the warm and wet climate.

Similar combinations of climatic conditions, as those above, can explain why over the last century the dunes in southern Brazil are greening faster than those in NE Brazil (Martinho et al., 2010; Miot da Silva et al., 2013; Miot da Silva and Hesp, 2013; Mendes and Giannini, 2015). In particular, Martinho et al. (2010) described the temporal changes in dune systems on the norhern and midlittoral Rio Grande do Sul coast of sourthern Brazil. They explained the observed significant morphological differences with characteristics of the local climate, sand supply and coastal orientation. In the north, the dunefields are narrower (~1 km) due to higher precipitation caused by local orography, lower sand drift potential and sand supply. Additonally, locally warmer conditions make the dunes there more vegetated. Southwards, the dunefields are wider (> 6 km), since the precipitation decreases while the wind energy and sand supplies increase. Moreover, as the northern dunefields are smaller and have less sand, they stabilise faster, in contrast to the southern dunefields where larger amount of sand and ongoing coastal erosion delay the stabilisation process.

The extensive research on dune activity has led to the development of indices (usually based on wind power, precipitation rate and potential evapotranspiration) to quantify the mobility and predict shifts between active and stable phases of the sand dunes (Lancaster, 1988; Tsoar, 2005). These indices, along with developed numerical models predict the hysteretic behaviour of the dune system, and the lag necessary for the dunes to respond and recover from disturbances in the vegetation cover (Hugenholtz and Wolfe, 2005; Yizhaq et al., 2007; Yizhaq et al., 2009). The model of Yizhaq et al. (2009) further predicts possible coexistence of active and fixed sand dunes in the dune systems (bistability). Bistability occurs under the same climatic conditions of a particular geographical area, provided that the local wind regime and precipitation rates support vegetation (Barbosa and Dominguez, 2004; Martinho et al., 2010).

Bistability is explained by the existing hysteresis between vegetation cover and wind power. It contradicts the predictions of the mobility indices since the latter are based on the local climate which implies that for particular climatic conditions the dune forms should be the same: fixed, active, or semi-fixed. Bistable mode is illustrated for the dunes from the Lençóis Maranhenses dunefield in NE Brazil (Figure 1.3a) where the mean annual precipitation reaches 2.4 m (Yizhaq et al., 2009). Irrespective of the extremely high rainfall rates, many of the dunes are active due to strong winds during the dry period. It should be noted here that bistability is characteristic for the Brazilian coast, Figure 1.3(a, b) (Tsoar et al., 2009), but can also be found for dunefields elsewhere (among them, Ampalaza chevrons, Madagascar, Figure 1.3c; Alexandria, South Africa, Figure 1.3d). In the extreme cases of very low/high wind speeds, the dunefields will display a single mode – fixed or mobile, respectively.

Furthermore, above a certain threshold of annual precipitation required for vegetation growth (50 mm/year; Tsoar, 2005), the amount of rainfall stops restricting the dune mobility, and the wind factor becomes dominant for the dune evolution (Yizhaq et al., 2009). Below that threshold, however, and if ignoring the wind effects, the amount of rain is important for the vegetation dynamics, since in that case, dry conditions are necessary to maintain the dunes active (Hugenholtz and Wolfe, 2005). This is in agreement with the results of Anthonsen et al. (1996) on the dynamics of Råbjerg Mile dune in Denmark. They showed that, considering the high energy winds at the site, reduction of sand transport due to local rainfall would be expected only if the wind speed drops below 13 m/s.

Other climatic factors affecting the dune dynamics and morphology are energetic storm events and relative sea level rise, as they may trigger substantial coastal erosion and sediment transport (Hinkel et al., 2013). Therefore, the importance of episodes of increased storminess in the past for formation of dune complexes, and the importance of periods of stillness for their stabilisation, are frequently discussed (Provoost et al., 2011; Costas et al., 2012; Dillenburg et al., 2018). Recently, Levin (2011) explained the decreased dune mobility on Fraser Island, Australia, with reduced frequency and intensity of the tropical cyclones.

Figure 1.3. Coexisting mobile and fixed dunes (bistability): (a) Lençois Maranhenses, NE Brazil; (b) Joaquina dunefield, S Brazil; (c) Ampalaza chevrons, Madagascar; (d) Alexandria dunefield, South Africa.. *Source*: Climate Engine 2022, http://climateengine.org/.

Tropical cyclones shape the coastal environments in subtropical and tropical settings (Claudino-Sales et al., 2008; Houser et al., 2015; Houser et al., 2008). While the beach and dunes during such extreme events may be eroded within hours, the recovery of the dune system may take years to decades, depending on the duration and intensity of the storm (Houser et al., 2015). In this sense, the rate of post-storm recovery reflects the resilience of the coastal system. For example, dunes in northern France impacted by severe storms were shown to recover over approximately 5 years (Héquette et al., 2019). On the other hand, it took about 10 years for the recovery of the Santa Rosa barrier island in NW Florida, US, after the passage of the hurricane Ivan in 2004 (Houser et al., 2015).

In the future, as the sea level continues to rise due to climate change, the storm surge levels are expected to be higher and extreme water levels causing dune erosion – to occur more frequently (e.g., the water level during the storm Xaver on the French coast in 2013 reportedly exceeded the 100-year

prediction and caused severe dune erosion; Hequette et al., 2019). This, along with the projected reduced time for dune recovery between the storms, will result in excessive erosion in the beach-dune system, especially where the sediment supply is low. However, at locations with high sediment supply, dunes may continue to develop and prograde seaward even under rising sea level (Hequette et al., 2019).

Together with the regional climate, sufficient sand supply is the other environmental factor supporting natural dune mobility (Aagaard et al., 2007; Psuty and Silveira, 2010; Delgado-Fernandez and Davidson-Arnott, 2011; Hesp, 2013). An example of highly active dune today due to abundant sand supply from the beach is Dune du Pilat in France (Tastet and Pontee, 1998). Although the sediments feeding the dunes most often originate from the beach, they can also have fluvial origin. Examples are the dunes at the mouth of Sigatoka River in Fiji (Kirkpatrick and Hassall, 1981), the Oregon dunes in US (Gao et al., 2021), the São Francisco River dunes (updrift and downdrift) and dunes on the northeast coast of Brazil (Barbosa and Dominguez, 2004). However, reduction of sediments from the rivers to the oceans due to entrapment in reservoirs upstream has been globally observed (Syvitski et al., 2005). On the other hand, river channelisation can explain the lack of sediments delivered by the Segura river (Spain) which leads to beach erosion (Pagán et al., 2017). Decline of sediments in the littoral zone due to coastal structures for shoreline protection, which modify the longshore transport and cause beach erosion downdrift, was also reported (e.g., at Playa Chachalacas, Mexico; Martínez et al., 2019), among others.

Human interventions over the last century may further explain significant deviations from the expected natural dynamics and functioning of the dunes globally (García-Romero et al., 2019). In particular, coastal dune ecosystems have suffered continuous transformations due to urban expansions, land reclamations for agriculture, stabilisation and destabilisation programmes, which has led to the destruction of many dune habitats worldwide and loss of plant communities (Schlacher et al., 2007). In Belgium, 50% of the coastal dunes degraded due to urbanisation and coastal squeeze (Van der Biest et al., 2017; Martínez et al., 2014). In addition, the beaches and dunes have become preferred place for recreation which has led to an increase of tourism infrastructure (e.g., the Sefton coast, UK, Delgado-Fernandez et al., 2019; Gran Canaria, Spain, Hernández-Calvento et al., 2014; García-Romero et al., 2019; Playa Chachalacas, Mexico; Martínez et al., 2019). Similar examples of dunes suffering from human pressure can be also given for the Mediterranean coast (Miccadei et al., 2011) and the Adriatic coast (Malavasi et al., 2013; Sytnik and Stecchi, 2015). The most significant modifications of the coast, however, can be probably found in Asia, in response to the need of accommodating the growing human population there (Nehren et al., 2016).

To stop the mobile dune sand from invading urban zones, as well as other infrastructures and natural features along the coastline (e.g., wetlands, forests), dune stabilisation projects by planting, afforestation and fencing have been implemented over the last centuries worldwide, e.g., in Europe (Arens et al., 2007), South Africa (Avis, 1989); US (Reckendorf et al., 2019); New Zealand (Hilton and Konlechner, 2010; Konlechner et al., 2015). Examples for dune stabilisation attempts are the two

active dunefields on the SW Atlantic coast of Cadiz, Spain: Valdevaqueros and Bolonia (Navarro-Pons et al., 2016). Despite numerous stabilisation measures since 1930s, these dunes, particularly Valdevaqueros, continue to pose a risk with their landward migration and growth due to unlimited sediment supply combined with favourable strong winds.

A worrying consequence from the dune stabilisation is the loss of biodiversity. Namely, pioneering plants involved in the dune formation and growth become rare, species and habitats in many stabilised dunes decline and eventually disappear (Arens et al. 2013; Pye et al., 2014). Furthermore, the fixed dunes lack the flexibility of an unconstrained beach-dune system, which can adjust shape and extent in response to the climate change and sea level rise (Schlacher et al., 2007). However, with respect to the projected impact by energetic storms, Jackson et al. (2019) argued that the vegetation cover may actually increase the dune potential to withstand marine erosion and may further support the recovery process. In particular, the resilience to wave-induced erosion is found to increase by 30% for largely vegetated dunes which is explained by the fact that sand may accumulate shoreward of the dunes and may be used to make the dunes higher and wider. This provides margins both against flooding and scarping (Ajedegba et al., 2019; Feagin et al., 2015). Moreover, the plant roots bind the sediments, thus increasing the dune resistance against wave action (Feagin et al., 2015).

The review on the factors causing dune greening shows that the dune dynamics should be viewed as an integrated response to all local environmental boundary conditions for the dune system, enhanced by climate variability and human-related disturbances (Nordstrom et al., 2000; Delgado-Fernandez et al., 2019). Therefore, it is necessary not only to understand the connections between the geomorphic, ecological and human processes in the coastal zone, but also to assess the relative contributions of these factors to the long-term dune dynamics which would allow to make decisions on the management measures for more resilient coasts.

Furthermore, when attempting to answer which factors contribute to the dune vegetation at a particular location, it should be taken into account that the natural, climatic and anthropogenic changes in the dune fields span a variety of spatial and temporal scales (Martínez and Gilabert, 2009). At a very fine temporal resolution, the changes result from the vegetation phenology (intra-annual or seasonal changes). At a low temporal resolution they are land-cover related, thus reflecting the climate variability (interannual changes or the trend). The characterisation of these two types of change is necessary for better understanding of the vegetation dynamics. The question is then whether dune greening is only the long-term trend in the vegetation signal, or other signal components at shorter temporal scales, such as the seasonal fluctuations or short-term changes caused by storm events, are also involved.

The present study offers a fully global remote-sensing assessment of the long-term dune dynamics based on multitemporal *NDVI* time series. The selected dune systems represent different regional climates and environmental conditions. An advantage of the study is the larger number of sampled dunefields, as compared to those studied by Gao et al. (2020), and particularly by Jackson et al. (2019).

This allows for a more comprehensive approach to investigate the potential contribution of natural local factors to the dune mobility. Another advantage is the procedure used to decompose the original *NDVI* signals to their temporal constituents which is applicable to non-uniformly sampled time series, as well as series with missing data without necessity of pre-processing to fill in the data gaps.

The assessment focuses on: (1) quantifying the changes in the vegetation cover in terms of key metrics derived from the *NDVI* constituents (seasonal fluctuations, trends and trend jumps), and (2) coupling of the *NDVI* time series with ERA5 reanalysis time series of the main climatic variables relevant to the process of dune fixation. Such approach is expected to allow to identify the drivers of the vegetation dynamics.

1.3.Aim and outline of the research

The purpose of the study is to: (1) identify whether coastal dunes are indeed greening on a global scale, or there are distinct local features involved, and (2) identify and characterise the major climatic drivers of the observed dune greening or mobilisation. For the purpose, the following research questions need to be answered:

RQ1. Which are the dominant fluctuations in the NDVI records on a global scale?

- Is the *NDVI* signal dominated by interannual changes, seasonal variations or sudden individual/multiple jumps in the identified trend?
- How is the greening trend in the time-series expressed: as a linear or nonlinear response?

RQ2. What factors have caused the dune greening?

- How do dunes respond to climatic variables forcing?
- What is the relative importance of other drivers of coastal dune dynamics, e.g., sediment supply and human interventions?

The remainder of this thesis is organised in four chapters. Chapter 2 describes the data source and the criteria for selection of dune sites. It also introduces the methodology for data analysis in order to answer the research questions. The obtained results are presented in Chapter 3 and are followed by a discussion in Chapter 4. The global dune mobility trends and the importance of potential contributing factors are summarised in Chapter 5. Appendices A to C provide additional information on dune sites and relevant results supporting the analysis in the main body of the thesis.

2. Materials and methods

2.1. *Selected coastal dune sites*

The choice of coastal dune sites is determined to a great extent by the recent reviews and discussions on the topic of dune mobility by Jackson et al. (2019) and Gao et al. (2020). It is complemented here by few more sites, following visual inspection of different coastal dune systems worldwide in the Google Earth Pro engine (https://www.google.com/earth/about/versions/).

As a result, a total of 186 individual dune sites have been selected for the present study (Figure 2.3). They are geographically distributed as follows: 69 in Europe (e.g., Clemmensen et al., 2014; Clarke et al., 2002; Delgado-Fernandez et al., 2019; García-Romero et al., 2019; Ruessink et al., 2018; Tastet and Pontee, 1998; Pye et al., 2014; Jackson and Cooper, 2011; Arens et al., 2013; Costas et al., 2016; Provoost et al., 2011; Navaro-Pons et al., 2016; Pagan et al., 2019; Sytnik and Stecchi, 2015; Łabuz et al., 2018); 33 in South America (e.g., Miot da Silva et al., 2013; del Valle et al., 2008; Jimenez et al., 1999; Martinho et al., 2010; Nehren et al., 2016; Hilbert et al., 2016); 31 in North America (e.g., Reckendorf et al., 1985; Hesp et al., 2010; Girardi and Davis, 2010; Mathew et al., 2010; Pickart and Hesp, 2019; Ajedegba et al., 2019; Gaspar de Freitas, 2021; Huang et al., 2018; Jewell et al., 2014); 20 in Africa (Harris et al., 2011; Miguel and Castro, 2018; Abbott et al., 2016); 29 in Oceania (Hilton and Konlechner, 2010; Konlechner et al., 2015; Levin, 2011; Levin et al., 2017; Moulton et al., 2019; Tribe and Kennedy, 2010); and 4 in Asia (Mujabar and Chandrasekar, 2012; Nehren et al., 2016).

The first criterion for dune selection, as suggested by Jackson et al. (2019), is the size of the dunefield. They chose areas exceeding 5 km^2 to assure, on one hand, better coverage of large transgressive dune systems like those along the tropical coast of Brazil (Hilbert et al., 2016; Jimenez et al., 1999) or on Frazer Island, Australia (Levin, 2011), and, on the other hand, to remove the limitations of the relatively low resolution of Landsat images (30 x 30 m). This approach has been also adopted for the present study where possible (geographical locations and areas of the sampled dunefields can be found in the provided supplementary material). The smallest dune area considered here has only 0.03 km^2 since it represents a section of a largely fragmented foredune due to tourism infrastructure (Marina di Ravena, Italy; Sytnik and Stecchi, 2015). The largest area, on the other hand, comprises 273.95 km^2 from the extensive transgressive dunefield Lençóis Maranhenses in NE Brazil, with a total area of 1052 km^2 (Hilbert et al., 2016). Both fields are illustrated in Figure 2.1.

a) **b)**

Figure 2.1. Examples of selected coastal dunefields (a) with the smallest area (0.03 km^2) on Marina di Ravena beach, Italy; and (b) with the largest area of 273.95 km^2 from the transgressive Lençóis Maranhenses dunefield in NE Brazil**.** *Source*: Google Earth Pro 7.3.4.8248.

Following Jackson et al. (2019), the other criterion for dune choice is the natural aspect of the dune sites. In this respect, the focus of the present study is on relatively natural dune landscapes with varying degrees of human impact to allow comparison between sites with reduced and no artificial disturbances. However, it is difficult to exclude the artefacts of human presence at the coastal zone, since many dune systems are located in the vicinity of human structures or near urbanised areas. For example, a number of selected dunes from the United Kingdom have been subjected to modifications in time, e.g., the dunes on the Sefton coast, England (Delgado-Fernandez et al., 2019; Esteves et al., 2012), see Figure 2.2(a). The Irish dunes, on the other hand, are relatively pristine due to their isolated character, according to Jackson and Cooper (2011), e.g., the Inch dunes in Figure 2.2(b).

The dune selection is relatively broad in terms of geographical locations and climatic regions to compare and study, as it is expected that local and regional climatic factors are controlling the dune mobility over time. Dunes from arid to semi-arid areas have been also selected here for analysis, as opposed to Jackson et al. (2019). Nevertheless, Jackson et al. (2019) still considered Los Médanos de Coro dune site in Venezuela, which belongs to a tropical dry climate and to one of the semi-arid zones of the world. In addition, apart from the sites from dry tropical settings, already reviewed by Gao et al. (2021), other dune cases have been also investigated, such as the chevrons on the Island of Madagascar (Abbott et al., 2016; Vimpere et al., 2019), as well as the nebkhas of the Guerrero Negro back-barrier dunefield in Baja California, Mexico (Hesp, 2008; Fryberger et al., 1990).

a) **b)**

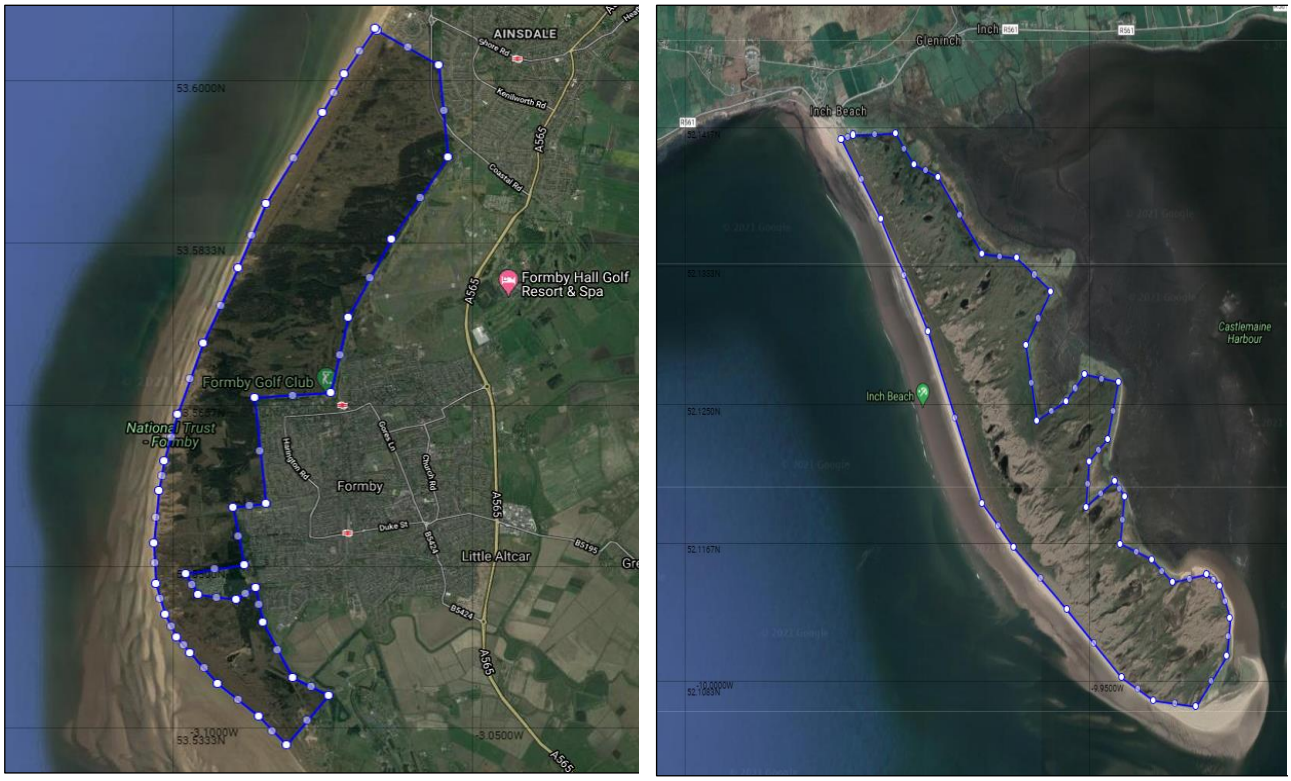

Figure 2.2. Examples of selected coastal dune fields (a) with significant direct anthropogenic influence (the Sefton coast, England); and (b) with negligible human impact (Inch dunes, Ireland)**.** *Source*: Google Earth Pro 7.3.4.8248.

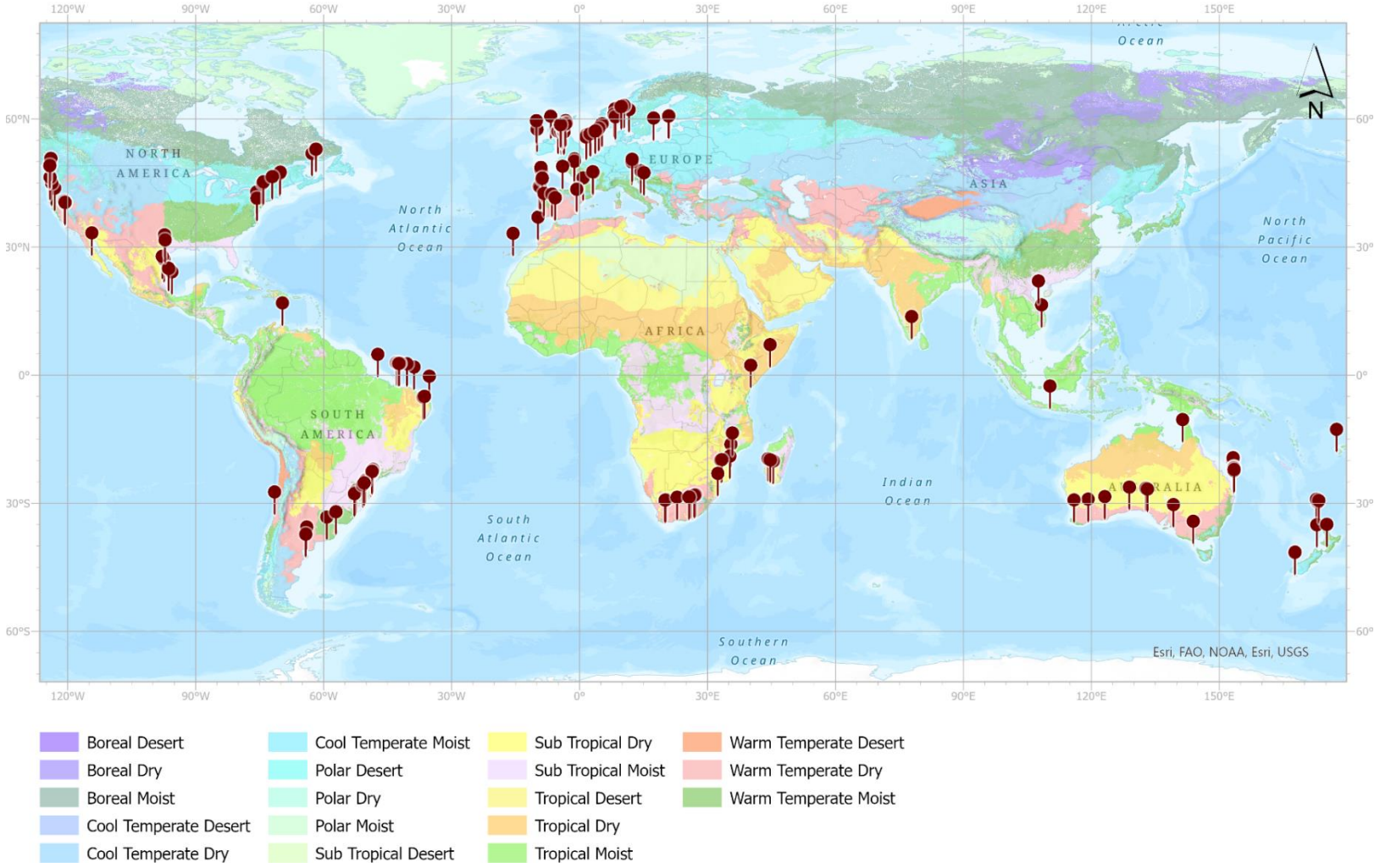

Figure 2.3. Map of the selected dune sites superimposed on a map of the world climate regions (18 classes; acc. to Sayre et al., 2020). The climate regions are produced as a geospatial integration of the world temperature and moisture domains. *Source*: Esri, USGS, TNC (World Terrestrial Ecosystems Pro Package - Overview (arcgis.com)). The software used to prepare the map is ArcGIS Pro 2.6.0.

2.2. Research Question 1: Coastal dune mobility trends

2.2.1. Remote sensing *NDVI* datasets

A series of multitemporal remotely-sensed Normalized Difference Vegetation Index (*NDVI*) records have been used to study the dune dynamics in terms of vegetation cover, for the period between 1984 and 2021. The *NDVI* data were requested from the Climate Engine App of the Google's geospatial tool Google Earth Engine (http://climateengine.org/; Huntington et al., 2017). They represent spatial averages over the areas of the selected dunefields (Figure 2.1 – Figure 2.3). The *NDVI* time series originate from the compilation of Landsat 4/ 5/ 7 and 8 satellite imagery covering coastal dune sites across all continents, with a wide range of climate types and environmental conditions. The duration of the time series is from 1984 to 2021.

The *NDVI* is calculated from the spectral reflectance measurements in the visible red part of the electromagnetic spectrum (*RED*; 0.6 – 0.7 μm) and in the near-infrared part (*NIR*; 0.7 – 1.1 μm) as (Tucker, 1979)

$$NDVI = (NIR - RED)/(NIR + RED) \quad (1)$$

where the spectral reflectance is defined as the ratio between reflected and incoming radiation in each spectral band. It may take values between 0 and 1.

The *NDVI* and the associated trends are commonly used in the evaluation of landscape vegetation greenness (Myneni et al., 1995), as well as for quantification of the response of vegetation to changes in the local hydro-climatic conditions. *NDVI* ranges between −1 and 1, where increasing values describe healthy vegetation, which is characterised by low reflectance in the visible range of the spectrum and high reflectance in the *NIR* range. For example, a dense green vegetation shows high *NDVI* values (0.6 – 0.9); shrubs and grassland have low positive values (0.2 – 0.5); bare soil, active dune sand or snow have values close to 0, e.g. -0.1 – 0.1. Water bodies and clouds result in low, positive or slightly negative *NDVI* values.

The remotely-sensed images used here to calculate the *NDVI* have a relatively low spatial resolution (30 x 30 m) and a temporal resolution of 16 days. Therefore, as discussed by de Jong et al. (2011), a trade-off between temporal and spatial coverage exists regarding the *NDVI* sampling. This means that while the multitemporal series allow for more climatic cycles and significant changes in land use over time to be included, any non-accounted single pixel due to low spatial resolution may contain several land use types or ecosystems. In the present case, however, the interest is in having longer time series, as they are suitable for detecting and quantifying the temporal dynamics of the dune systems. This dynamics is caused by variable climatic conditions which are discernible on a decadal scale. It should be kept in mind though that factors other than climatic forcing may potentially be the reason for long-

term gradual changes (trends) and abrupt changes in the trend (disturbances). Among those factors, for example, is the cumulative effect of direct and indirect changes due to coastal management with the purpose of making the coast more resilient to flooding (Delgado-Fernandez et al., 2019; Evans and Geerken, 2004).

The workflow to answer the first research question is illustrated in Figure 2.4. Prior to performing any statistical trend analysis (the second column of the flow chart), the *NDVI* signals need to be visually inspected and initial years with scarce data – removed. The signals are also corrected for outliers, the presence of which could affect the trend estimates by showing less significant or no trend when there is a real change present. This applies particularly to the performance of the linear regression analysis. Local outliers are identified with a moving window procedure from the Matlab® built-in functions library (‘*isoutlier’*), using a window length of 5 elements (the default option). The procedure returns an outlier when the value exceeds the median *NDVI* by more than three scaled median absolute deviations. The scaled deviation is formulated as: $A\,median\left(abs\left(y - median(y)\right)\right)$, where $A = -1/\sqrt{2}\,erfcinv(3/2)$, with $ercinv(\cdot)$ – the inverse complementary error function and y – the investigated time series.

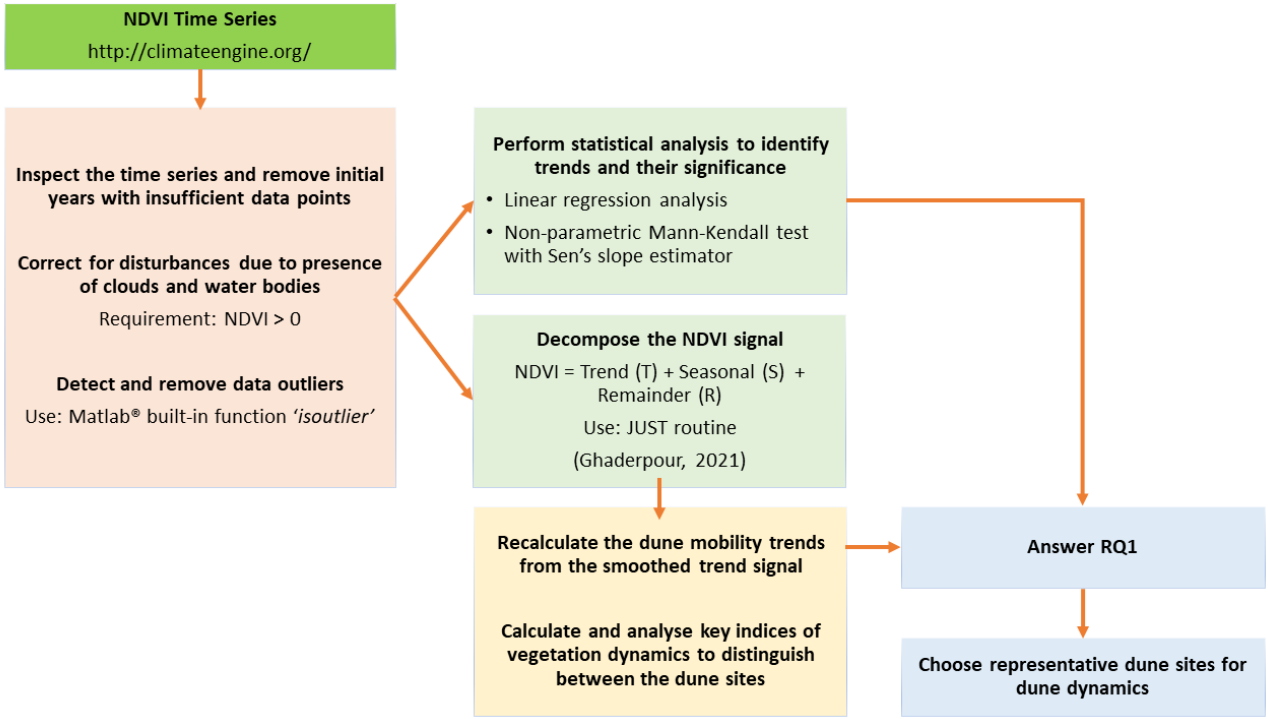

Figure 2.4. Workflow diagram for RQ1: Identification and quantification of the dune mobility on a global scale.

In the following, the statistical steps in the middle column of the workflow diagram will be described.

2.2.2. Trend analysis methods

Statistical parametric test (linear regression) and non-parametric Mann-Kendall test with Sen's slope estimator have both been applied to identify significant long-term changes in the *NDVI* and climatological multitemporal time series. While the parametric trend tests have the disadvantage of requiring independent and normally distributed data, the non-parametric tests only require that data are independent.

Among the group of non-parametric tests, the rank-based Mann-Kendall (MK) test (Mann, 1945; Kendall, 1975) is the most frequently used for trend detection in hydro-meteorological data (see Gocic and Trajkovic, 2013; Delgado-Fernandez et al., 2019; Helsel et al., 2020). Positive test statistic indicates an increasing *NDVI* trend (greening, in the context of the coastal dunes) and negative test statistic defines a decreasing trend (increase of open dune spaces with mobile sand). The test procedure is described next, following Gocic and Trajkovic (2013).

2.2.2.1. Mann-Kendall trend test

The assumption of the Mann-Kendall test is that the data originate from independent realisations. This constitutes the null hypothesis of the test, H_0 (i.e., the data show no trend). The alternative hypothesis, H_A, is that the data follow the detected monotonic trend at a chosen level of significance. The MK analysis is robust even when data in the time series are missing (Helsel et al., 2020).

The test statistic, *T*, is defined as

$$T = \sum_{i=1}^{n-1} \sum_{j=i+1}^{n} sgn(x_j - x_i) \tag{2}$$

where *n* is the length of the time series; x_i and x_j are sampled data with $j > i$. The *sgn* function has the form

$$sgn(x_j - x_i) = \begin{cases} +1 \;\; if\ (x_j - x_i) > 0 \\ 0\ if\ (x_j - x_i) = 0\ (tied\ data) \\ -1\ if\ (x_j - x_i) < 0 \end{cases} \tag{3}$$

If no tied data are present and the sampled data are ordered randomly, the *T* statistic (Eq. 2) has zero mean, $E[T] = 0$, and variance $var(T) = \sigma_T^2 = n(n-1)(2n+5)/18$. In the general case, however, the variance needs to be corrected for ties so that (Gocic and Trajkovic, 2013)

$$\sigma_T^2 = \left\{ n(n-1)(2n+5) - \sum_{i=1}^{p} t_j(t_i - 1)(2t_i + 5) \right\} / 18 \tag{4}$$

where *p* is the number of tied groups in the data set and t_i is the number of data points in the *i*th group. A tied group is a set of data with the same value.

T would be approximately normally distributed if the sample of independent variables is large enough (Kendall, 1975). For $n \geq 10$, the standardized normal test statistic Z_T can be written as (Gocic and Trajkovic, 2013)

$$Z_T = \begin{cases} (T-1)/\sqrt{var(T)}, & for\ T > 0 \\ 0, & for\ T = 0 \\ (T+1)/\sqrt{var(T)}, & for\ T < 0 \end{cases} \quad (5)$$

The significance of the identified trends depends on the following conditions (for a two-sided test): for $|Z_T| > Z_{1-\alpha/2}$, the null hypothesis is rejected and a significant trend in the time series is returned for level of significance α. The critical value $Z_{1-\alpha/2}$ is obtained from the standard normal distribution table, where $Z_{1-\alpha/2} = 1.96$ for α = 0.05 (5%), and $Z_{1-\alpha/2} = 2.576$ for α = 0.01 (1%).

The T-statistic is related to the Kendall's correlation coefficient, τ, through the relationship

$$\tau = T/D \quad (6)$$

where

$$D = \left[\frac{1}{2}n(n-1) - \frac{1}{2}\sum_{i=1}^{p} t_j(t_j-1)\right]^{1/2} \left[\frac{1}{2}n(n-1)\right]^{1/2} \quad (7)$$

Examples of the application of the MK test to hydro-meteorological data can be found in Gocic and Trajkovic (2013), Delgado-Fernandez et al.(2019), among others.

2.2.2.2. Sen's slope estimator

The defined trend slope is an approximation of the change over time. Having detected a statistically significant change with the MK test, the next step is to apply the Sen's slope estimator (Sen, 1968) to quantify the magnitude of the change, as the MK test only assesses its significance. The slope for a sample of N pairs of data is written as (Gocic and Trajkovic, 2013)

$$Q_i = (x_j - x_k)/(j-k), for\ i = 1, \dots, N; 1 \leq k < j \leq n \quad (8)$$

with x_j and x_k – the data at times j and k ($j > k$) and n – the sample size.

If there is only one measurement in each time interval, then $N = n(n-1)/2$, where n equals the number of time periods. If there are multiple observations in one or more time periods, then $N < n(n-1)/2$, where n equals the total number of observations. Then, the N values of the slope Q_i are ranked from the smallest to the largest and the Sen's slope is estimated as the median of all estimates as

$$Q_{med} = \begin{cases} Q_{\left[\frac{N+1}{2}\right]}, if,\ N\ is\ odd \\ \left(Q_{\left[\frac{N}{2}\right]} + Q_{\left[\frac{N+2}{2}\right]}\right)/2\,, if\ N\ is\ even \end{cases} \quad (9)$$

where the sign of Q_{med} determines the direction of the trend, and the magnitude of Q_{med} – its steepness.

Hereafter, $Q_{med} = Q_{NDVI,}$ for the Sen's slope of the *NDVI* time series, and $Q_{med} = Q_T$, Q_P or Q_W, for the slopes of the daily averaged meteorological variables (temperature, precipitation and wind speed, respectively).

The above formulations for the Mann-Kendall test and the Sen's slope are implemented in the Matlab® routine by Burkey (2006, 2012) which has been adopted for the analysis here.

2.2.2.3. Statistical significance of the trend slopes

The statistical significance of a trend slope can be assessed by Analysis of Variance test (ANOVA), for the linear regression, and a *Z*-test (Eq. 5), for the Mann-Kendall's trend (de Jong et al., 2012). A slope is also statistically significant if the two-sided probability of the trend (*p*-value) does not exceed the chosen level of significance, beyond which an observed change can be considered a random occurrence. In the present case, the trend is evaluated against level of significance $\alpha = 0.01$ (1%). In addition to the level of significance of 1%, an upper limit of 10% is used to distinguish moderately significant changes. The significance of the long-term trend also follows from the coefficient for the null hypothesis (h), where $h = 0$ indicates a non-significant slope (therefore, no trend), and $h = 1$ refers to a non-zero slope which can be either positive (in the case of greening dunes) or negative (in the case of dunes with increasing sand drift).

Depending on the sign of the associated Sen's slope, Q_{NDVI}, and the *p*-value, Forkel et al. (2013) divide the temporal trends in 6 categories. They are shown in Table 2.1 along with description of the vegetation change they represent. A "no change" result implies either that the test probability value is larger than the applied upper threshold of α, i.e. $p > 0.1$, or that the magnitude of the detected change is less than 1%.

Table 2.1. Criteria for assessment of the trend slope and its significance (cf. Forkel et al., 2013). In addition, it has been imposed that the magnitude of the *NDVI* change over the study period should exceed 1%.

Class	***Change***	Q_{NDVI}	***p***
Significant positive trend	Greening	> 0	≤ 0.01
Moderate positive trend	Greening	> 0	0.01 < *p* ≤ 0.1
No trend with positive tendency	Stable	> 0	> 0.1
Significant negative trend	Mobilisation	< 0	≤ 0.01
Moderate negative trend	Mobilisation	< 0	0.01 < *p* ≤ 0.1
No trend with negative tendency	Stable	< 0	> 0.1

In addition to fulfilling the conditions in Table 2.1 (Forkel et al., 2013), the magnitude of a change for a considered period of time is expected to exceed a certain threshold. In the present case, this threshold is set at 1%, for the period of study between 1984 and 2021.

2.2.3. Change detection and time series decomposition

The trends of vegetation greenness identified in remotely-sensed *NDVI* time series are not always monotonic (increasing/decreasing) but may vary in time in terms of direction and magnitude (Forkel et al., 2013; de Jong et al., 2013). The change itself can be either a gradual change over multiple decades (interannual fluctuations) or a sudden jump (breakpoint) as a result of short-term changes in the dune vegetation cover. The latter can be a result of, e.g., energetic storms leading to dune scarping or destruction (Claudino-Sales et al., 2008), or dune rejuvenation projects (Ruessink et al., 2018). Such events are identified by abrupt reduction of the *NDVI* values, followed by a gradual recovery of the dune system. The latter may take decades (Houser et al., 2015).

Therefore, change detection methods should be able to detect sudden jumps and also distinguish between variations at different temporal scales, i.e. they need to identify interannual changes (trends) in the presence of intra-annual (seasonal) fluctuations. The reason is that while interannual changes in the vegetation signal are largely explained by climatic variability, which is the major controlling factor for the natural dune dynamics (Forkel et al., 2013), the climatic variability also affects the seasonal patterns. And, seasonality may introduce correlation in the *NDVI* signal which may mask the trend.

Statistical season-trend models have been proposed to detect and quantify changes in the vegetation signals and decompose them into trend, seasonal and remainder components. The algorithms manage to detect changes while accounting for the effect of seasonality. For example, the Breaks For Additive Seasonal and Trend statistical model (BFAST; Verbesselt et al., 2010a; Verbesselt et al., 2010b) combines iterative decomposition of the *NDVI* signal with methods for breakpoint detection. However, it performs poorly for non-uniformly sampled time series with missing data (Awty-Carroll et al., 2019), which is the case with the studied *NDVI* series here. The performance of other change detection methods have been discussed and compared with BFAST by Awty-Carroll et al. (2019), but similarly to BFAST they are not able of dealing with missing data in the signals. Furthermore, none of them takes into account observational uncertainties.

For the purposes of the present study, the Jumps Upon Spectrum and Trend method (JUST) for change detection and time series analysis has been adopted (Ghaderpour and Vujadinovic, 2020). Moreover, an open-source software package implementing the method has been recently developed for Matlab® (Ghaderpour, 2021). JUST is recommended as a robust approach for the detection of jumps in the trend component of both equally and unequally sampled non-stationary time series, which is the case of the collected *NDVI* records.

The method may take into account also observational uncertainties (e.g., presence of clouds), to improve the estimation of the location of potential jumps, the trend and the seasonal component. It does not require pre-processing of the data in terms of interpolation to fill in gaps of missing data due to non-availability of the satellite imagery. The method is based on spectral analysis where statistically significant spectral components are detected within consecutive moving windows from the *NDVI* signal (Ghaderpour and Vujadinovic, 2020).

The algorithm for the seasonal-trend model which returns the locations of potential jumps and the optimal set of sinusoids and trendlines that best approximate the vegetation time series is the Anti-Leakage Least-Squares Spectral Analysis (ALLSSA). ALLSSA operates on a moving window base of fixed size (number of observations) which is particularly useful when data are missing. A linear function of two pieces is fitted to the temporarily chosen segment of the data series along with the fitted harmonic components based on least-squares analysis. The jump direction and magnitude are used to characterise the gradual and/or sudden changes in the time series.

Once the trend and the seasonal components are found, Least Squares Wavelet Analysis (LSWA; Ghaderpour and Pagiatakis, 2017; Ghaderpour, 2021) can be further applied to decompose the vegetation signal in the time-frequency domain to study the contribution of different frequency constituents to the intra-annual signal. LSWA is an alternative of the Fourier transform, as it decomposes unequally spaced, non-stationary time series in the time-frequency domain. It also returns the spectrogram of the time series which is based on the least-squares fit of sinusoids with different cyclic frequencies to the time series segments.

The choice of input values for the JUST software and LSWA has been influenced by the results for the dune site illustrated in Figure 2.5. The area is a fragment of the South Kennemerland dunefield (the Netherlands) analysed here. It reveals blowouts and foredune notches excavated in the period between the beginning of 2012 and 2013, with the aim to restore the mobility of the inland dunes by reconnecting them with the beach, as well as to increase the biodiversity in the dune ecosystem (Ruessink et al., 2018). As a result, 75% of the sand previously deposited on the seaward side of the foredune was found landward of it by 2016 which corroborates the effectiveness of the applied dynamic approach for dune rejuvenation. This effect can be traced in the *NDVI* time series in Figure 2.6. The plot reveals a clearly non-monotonic trend between 1984 and 2021, showing first an increase in the *NDVI* over the first decade, followed by a relatively stable period of approximately 10 years, and a decrease over the remaining decade. The reduction in the *NDVI* over the tail years, corresponding to an increase of bare sand in the area, may be regarded as a lagged response to the rejuvenation measures in the dune area.

The South Kennemerland site was therefore chosen to test the ability of the JUST software (*JUSTjumps* routine) to detect sudden changes in the trend, because the known change from the beginning of 2012 was expected to be detected. The encountered jumps are then used to split the vegetation signal to its temporal components (trend, seasonal and remainder) using *JUSTdecompose*

or, alternatively, using the LSWA routine to decompose the signal in the time-frequency domain to obtain the spectrogram.

Figure 2.5. Area with excavated notches and blowouts at South Kennemerland, the Netherlands. *Source*: Google Earth Pro 7.3.4.8248.

The JUST software was run for different combinations of window size, translation step and thresholds for the magnitudes of the potential jumps and the number of years between two consecutive breakpoints (Ghaderpour, 2021). Table 2.2 shows three sets of tested values which led to the results in in Figure 2.6. As expected, small translation step and very low thresholds for the jump magnitude and direction (Figure 2.6a) return a number of jumps. However, the expected jump location is not clearly defined, which could be also partially attributed to missing values in the *NDVI* record. By increasing the values of the input parameters, the trendline becomes smoother but JUST still does not return the expected jump location (Figure 2.6b).

To avoid uncertainties while detecting the real jumps and to automate the process, given the number of sites to be analysed, it has been chosen to run *JUSTjumps* and *JUSTdecompose* using more conservative initial values for the JUST parameters (Table 2.2; Figure 2.6c). This approach has been recommended by Ghaderpour (2021) when discussing the automation possibility. The chosen higher thresholds reduce the chance for detecting a breakpoint but still permit to detect changes in the trend direction over the period of interest (1984 – 2021). For the moving window, a size of three tail years was chosen as an input, with translation step equal to the size of the longest tail year. The tail years contain the largest number of measurements which allows to cover at least one full cycle of existing seasonal fluctuations.

Table 2.2. Input parameters of *JUSTjumps* and *JUSTdecompose* acc. to Ghaderpour (2021).

Input	***Default value***	***Tested value***	***Chosen value***	***Description***
t				Time
f				*NDVI* observations
Step	M	34	34 (the longest tail year)	Translation step, δ
Size	3M	90	90 (3 tail years)	Window (segment) size, R
Season	ALLSSA	ALLSSA	ALLSSA	Season-trend model
ω	[0.8:0.2:3.8]	[0.1:0.1:4]	[0.1:0.1:4]	Cyclic frequency for performing ALLSSA
Level	0.01	0.01	0.01	Significance level, α
Mag. th.	0.05	0.1	0.2	Threshold for the absolute value of the jump magnitude
Dir. th.	0.01	0.1	0.2	Threshold for the absolute value of the jump direction
Jump th.	0.75 (9 months)	2	2	Minimum time difference between jumps, in years
Save	0 (False)	1 (Save)	1 (Save)	Save or not the detected jumps and characteristics

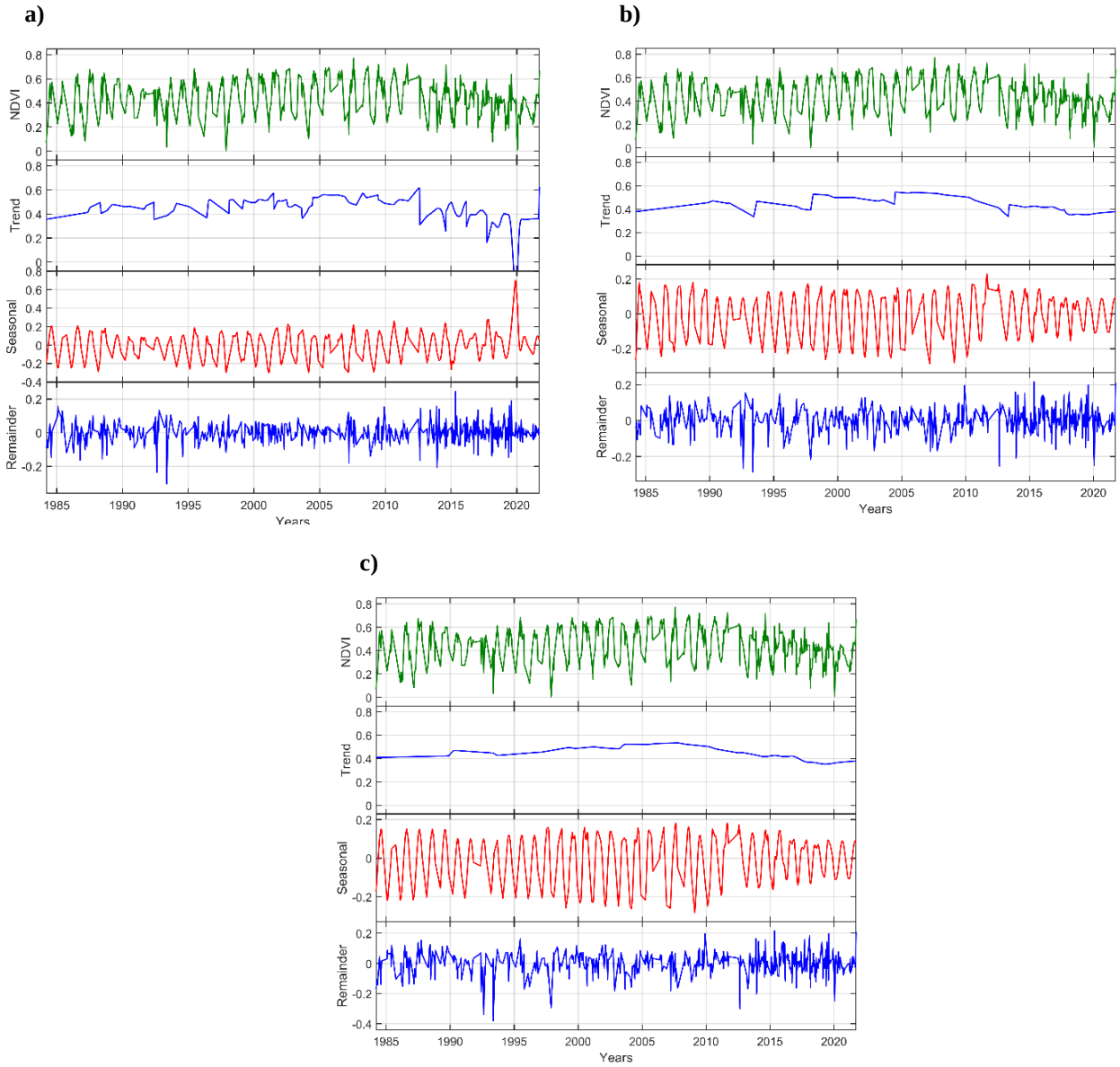

Figure 2.6. South Kennemerland, the Netherlands – area of excavated blowouts and notches. (a) Default values: average sampling rate, M = 16; window size, R = 3M ; sliding window step, δ = M. The threshold for the magnitude of the jump is set at 0.05 and for the direction at 0.1. The minimum time difference between jumps is 9 months; (b) Average sampling rate, M = 16; window size, R = 90 (three tail years); sliding window step, δ = 34 (the longest tail year). The thresholds for the magnitude and direction of the jump are set at 0.1; The minimum time difference between jumps is 2 years; (c) The chosen values for the automated JUST runs: average sampling rate, M = 16; window size, R = 90 (three tail years); sliding window step, δ = 34. The thresholds for the magnitude and direction of the jumps is set at 0.2. The minimum time difference between jumps is 2 years.

2.2.4. Key indices of dune vegetation dynamics

Key indices and ratios quantifying the dune dynamics in terms of vegetation cover can be derived from the trend and seasonal components of the decomposed *NDVI* signals. This approach was proposed by Martínez and Gilabert (2009) when studying the vegetation dynamics of land ecosystems to explain land degradation in Spain. The key features are introduced in Table 2.3 along with two ratios representing the contributions of the interannual and intra-annual temporal components to the total

energy of the signal. The Sen's slope in the table, Q_{NDVI}, is the slope recalculated from the trend component of the *NDVI* signal. The reason behind using the trend signal for statistical testing instead of the *NDVI* time series is that by reducing the dispersion in the data series, the trend estimate could be improved (see Martinez and Gilabert, 2009).

Table 2.3. Key features based on the decomposed *NDVI* signal (extended from Martinez and Gilabert, 2009). Designation for the signal components: Trend (T), Seasonal (S), Remainder (R).

Feature	***Description***	***Meaning***
Q_{NDVI}	Sen's slope of the interannual component (*T*)	Magnitude of the vegetation change
$\overline{NDVI}$	Mean of the interannual component (*T*)	Mean *NDVI* level of vegetation during the period of data
$NDVI_{min}$	10th percentile of the mean interannual and intra-annual variability (*T*+*S*)	Minimum *NDVI* level during the period of data
$\Delta NDVI$	Range of the intra-annual variability (S) as the difference between the 10th and 90th percentile	Amplitude of the annual phenological cycle
var(*T*)/var(*NDVI*)	Ratio of the interannual variability to the variability of the *NDVI* signal	Contribution of the long-term change component to the total energy of the signal
var(*S*)/var(*NDVI*)	Ratio of the intra-annual variability to the variability of the *NDVI* signal	Contribution of the seasonal component to the total energy of the signal

2.3. Research Question 2: Drivers of dune mobility

2.3.1. Climatological dataset (daily averaged wind speed, temperature, precipitation)

The climate data used to examine the association between temporal variations of the vegetated dune status and climate variability were also obtained from the Climate Engine App (http://climateengine.org/; Huntington et al., 2017) for the same dune areas and period (1984 – 2021). They represent ERA5 reanalysis data for the temperature (daily averages at 2 m height; *T* [ºC]), total precipitation (daily sums; *P* [mm/day]) and wind speed (daily averages at 10 m height; *W* [m/s]). The dataset provided by the Climate Engine App is a result of merging the Google Earth Engine dataset (up to 7/9/2020) and data to real-time ingested by the Climate Engine (cf. Copernicus Climate Change Service (C3S), 2017). ERA5 is a 30+ global climate reanalysis data by the European Centre for Medium-Range Weather Forecasts (ECMWF), with spatial resolution of 24 km (0.25º x 0.25º) and time coverage since 1979. However, the time series for the climate variables used here have been retrieved for the same period as the *NDVI* records (1984 – 2021). Furthermore, they are representative averages for the area of each selected dune site.

Figure 2.7 illustrates the workflow for the analysis of the climatic data.

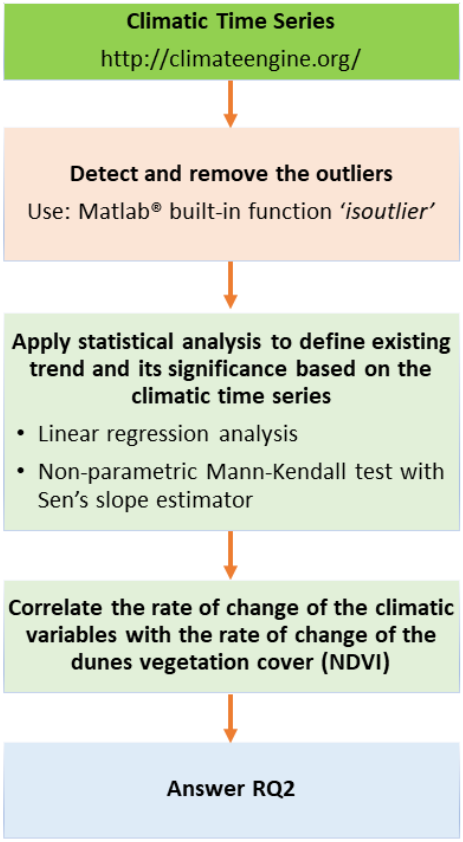

Figure 2.7. Workflow diagram for RQ2. Effect of local climate on the dune dynamics.

It must be noted here that the time series of the daily averaged climatic variables have not been decomposed to their inherent components, as it has been done for the *NDVI* signals, due to significantly time-consuming data processing involved. Instead, the non-parametric Mann-Kendall test has been applied to identify significant trends in the temperature, precipitation and wind speed time series, and then calculate the Sen's slopes (Q_T, Q_P and Q_W).

Next, as the *NDVI* signals are non-uniformly sampled and cannot be directly compared with the climatic signals, it has been decided to base the linear correlation analysis on the estimated rates of change (Q_{NDVI} versus Q_T, Q_P and Q_W) in order to determine dependence between greening and temporal changes in the climate variables. The climatic time series have been also correlated between each other to find statistically significant relationships.

2.3.2. Pearson correlation

The Pearson correlation coefficient, r_{xy}, quantifying the linear association between two variables, x and y, is expressed as

$$r_{xy} = \sum_{i=1}^{n}(x_i - \bar{x})\,(y_i - \bar{y}) / \sqrt{\sum_{i=1}^{n}(x_i - \bar{x})^2 \sum_{i=1}^{n}(y_i - \bar{y})^2} \qquad (10)$$

where n is the sample size; x_i and y_i are the ith observations of x and y; $\bar{x} = \frac{1}{n}\sum_{i=1}^{n} x_i$ is the sample mean of x; $\bar{y} = \frac{1}{n}\sum_{i=1}^{n} y_i$ is the sample mean of y.

Equation (10) can be rewritten as

$$r_{xy} = n\sum x_i y_i - \sum x_i \sum y_i \Big/ \sqrt{n\sum x_i^2 - (\sum x_i)^2}\sqrt{n\sum y_i^2 - (\sum y_i)^2} \quad (11)$$

where $i = 1, \ldots, N; 1 \leq k < j \leq n$

In the context of dune dynamics, r_{xy} serves to evaluate the relative contribution of factors driving the increase or decrease in the vegetation cover (Moulton et al., 2019; Taminskas et al., 2020).

3. Results

3.1. Research Question 1: Coastal dune mobility trends

3.1.1. Linear regression and Mann-Kendall statistical tests for trend analysis

The results from the linear regression and Mann-Kendall trend test with Sen's slope estimator applied on the *NDVI* time series have been found to be quite robust in terms of returning the same trend significance for the majority of the investigated dunefields (181 out of 186 cases). The few exceptions where the tests disagree show wide geographical spread.

Figure 3.1 confirms the consistency of the test results, irrespective of the applied statistical tool, since in both cases the estimated *p*-value is negligibly small, in comparison with the imposed significance level of 1%. Figure 3.1(a) introduces a case of monotonically increasing trend (a greening dune surface) and Figure 3.1(b) – a non-monotonically decreasing trend (increase of bare sand) for a highly active dunefield. The statistical dependencies and the correlation coefficients are also included in the plots for consistency. It can be seen that the dependence based on the non-parametric test is weaker than the one from the linear regression. In general, this holds for the entire sample of dunes. The MK trends and the associated Sen's slopes are further used to study the long-term dune dynamics. This follows the considerations in Section 2.2.2 that the non-parametric MK test performs better for time series with missing data and outliers which is the situation with the analysed *NDVI* records.

The spatial distribution of the trends based on the Mann-Kendall test can be seen mapped in Figure 3.2. The green triangles represent increasing trends, the red triangles – decreasing trends and the empty triangles describe no change, either because the test result is not statistically significant, according to the imposed requirements (Table 2.1; Forkel et al., 2013), or because the change magnitude does not exceed the threshold of 1% for the given period. The remaining trend categories are plotted as light green and light red triangles.

Figure 3.2 reveals a clear dominance of the greening trends globally, as opposed to the few cases of dunes becoming more active with time. These results are clearly consistent with Jackson et al. (2019). In particular, 159 cases (85.5%) show increased stability over the study period; 13 cases (7%) show increased degree of sand mobilisation; 10 cases (5.4%) have experienced insignificant to no change at all, and 3 (1.6%) and 1 (0.5%) cases experienced moderately significant mobilising and greening trends,

respectively. The only dune system with identified moderately significant increase of vegetation is South Kennemerland, the active area of which is illustrated in Figure 2.5.

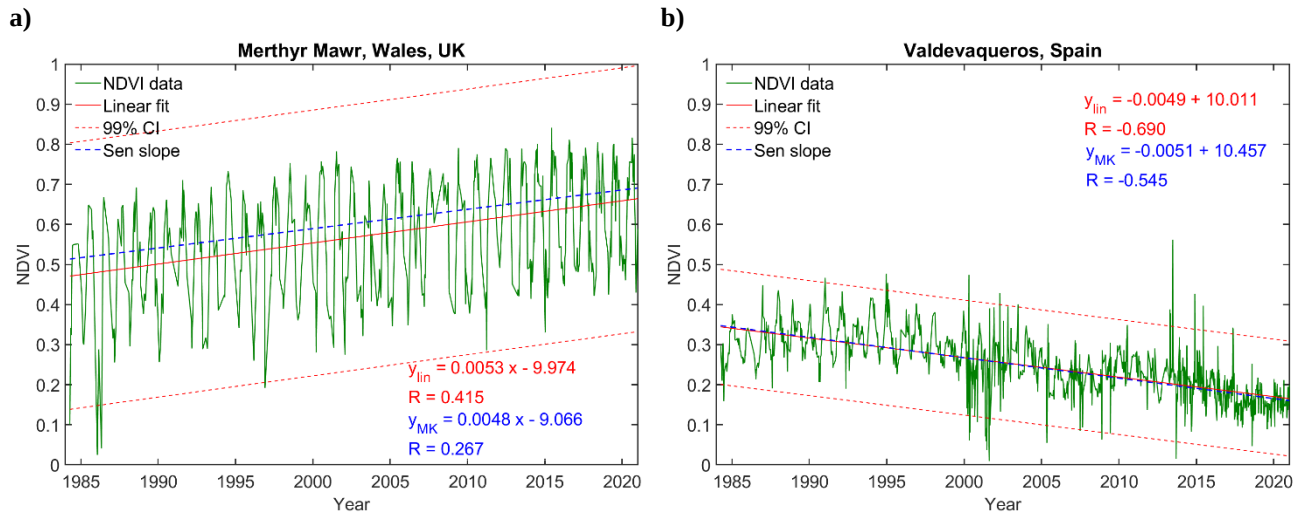

Figure 3.1. Linear regression and Mann-Kendall test results using the *NDVI* signals corrected for cloud disturbances and outliers. (a) Greening dunefield: Merthyr Mawr, Wales, UK; (b) Active dunefield: Valdevaqueros, SW Spain. The 99% confidence intervals are illustrated as red dashed lines in the plots. The linear regression and MK trend equations are also displayed.

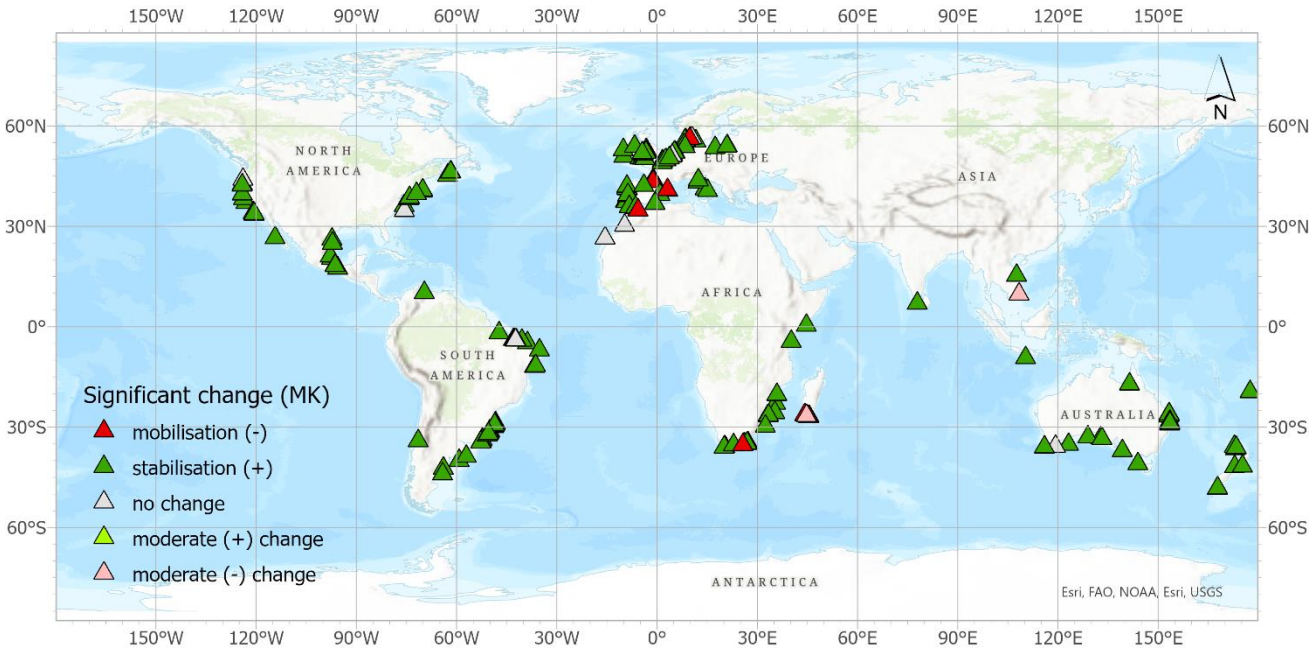

Figure 3.2. Map of the global dune dynamics based on the Mann-Kendall test statistics and the Sen's slopes. The *NDVI* time series are corrected for cloud disturbances and outliers. The decision on existing statistically significant multitemporal *NDVI* change depends on: (1) the magnitude of the change over the research period 1984 – 2021 (minimum of 1%), and (2) the *p*-value in comparison with the imposed levels of significance: α = 0.01 (the threshold for statistically significant greening/mobilisation) and α = 0.1 (the upper threshold for moderate level of significance), acc. to Forkel et al. (2013).

3.1.2. JUST and LSWA decompositions of the *NDVI* signals (Ghaderpour, 2021)

A few examples of decomposition to interannual (trend), intra-annual (seasonal) and short-term (remainder) components, using the JUST routine (Ghaderpour and Vujanovic, 2020; Ghaderpour, 2021), are given in Figure 3.3 for different combinations and dominance of the components of the vegetation signals. Figure 3.3(a) illustrates a case from Mexico (Cabo Rojo dunes) where a nearly monotonously increasing trend dominates the vegetation dynamics while the seasonal component is negligible. Figure 3.3(b), on the other hand, shows a well-defined seasonal pattern with an amplitude of approximately 0.3 *NDVI*. Increased vegetation cover with pronounced seasonality are typical for the most NW European dunes due to favourable climatic conditions combined with well-established management practices for dune stabilisation. A nonlinear gradual change in the *NDVI* can be seen for Ritoque, Chile (Figure 3.3c). Figure 3.3(d) illustrates a jump towards lower *NDVI* after a period of moderate greening. The jump is followed by a period of *NDVI* recovery. In this particular case, the jump reflects the destructive impact of the Hurricane Sandy in October 2012 which caused extensive flooding, and wind and wave damages on parts of the Long Beach Island, US, particularly the areas lacking protective dunes (Irish et al., 2013). Cases of detected trend jumps in the *NDVI* series here are rare, partially because of the imposed relatively high threshold for their detection by the JUST routine. Finally, Figure 3.3(e) and Figure 3.3(f) illustrate active dunes, which dynamic character can be explained by different reasons.

Next, statistically significant results from the Mann-Kendall test performed on the trend components of the *NDVI* series and the recalculated Sen's slopes are presented. Figure 3.4 shows updated map of the spatial distribution of confirmed statistically significant trends. The dunefields have been classified as greening and mobilising in a similar way as before (see Figure 3.2). The new statistics reveal that 162 dune sites (87.1%) became greener over time, as compared to the previously found 159; 17 (9.1%) versus 13 display higher aeolian activity, and 7 (3.8%) versus 10 show "no change" over the study period. Moderate positive and negative changes, as those illustrated in Figure 3.2, were not detected on this occasion.

The 17 cases showing increase of bare sand, i.e. $Q_{NDVI} < 0$, are spread across all continents, except for Australia (Figure 3.4). These cases include some of the few dune systems in Europe that are mobile on a large scale today, e.g., Dune du Pilat in France (the tallest sand dune in Europe) (Tastet and Pontee, 1998; Clarke et al., 2002; Gabarrou et al., 2018), Valdevaqueros and Bolonia dunes in Spain (Gomez-Pina et al., 2002; Navarro-Pons et al., 2016; Rodríguez-Ramírez et al., 2008), and the cliff-top Rubjerg Knude dune in Denmark (Saye et al., 2006).

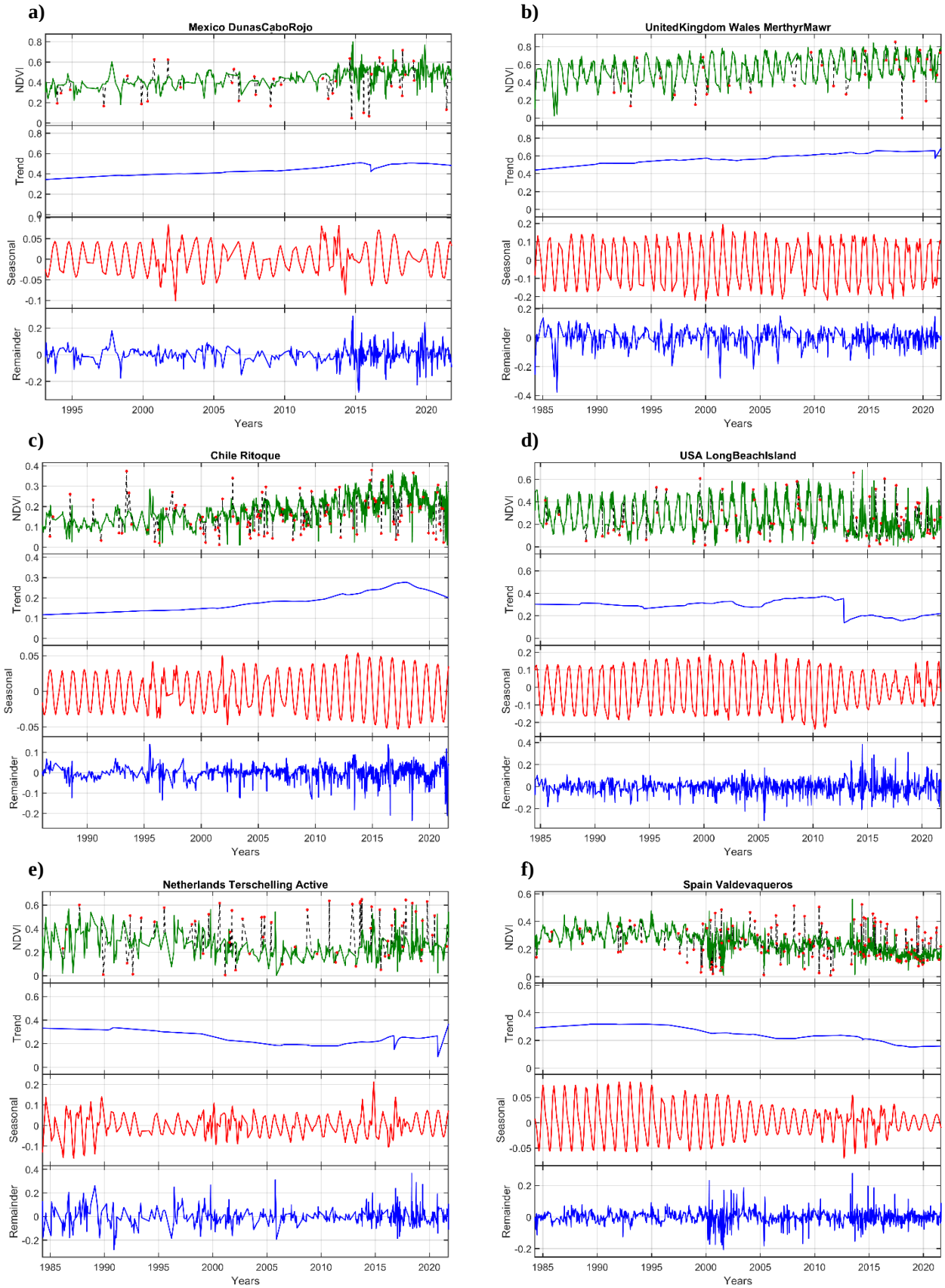

Figure 3.3. JUST decomposition: (a) trend-dominated signal, Dunas Cabo Rojo (Mexico); (b) seasonality dominated signal, De Panne (Belgium); (c) nonlinear gradual change, Ritoque (Chile); (d) trend jump, Long Beach Island (US); (e) remobilisation, Terschelling, the Netherlands; (f) active dunes, Valdevaqueros, Spain. The red dots in the plots of the *NDVI* signal represent outliers.

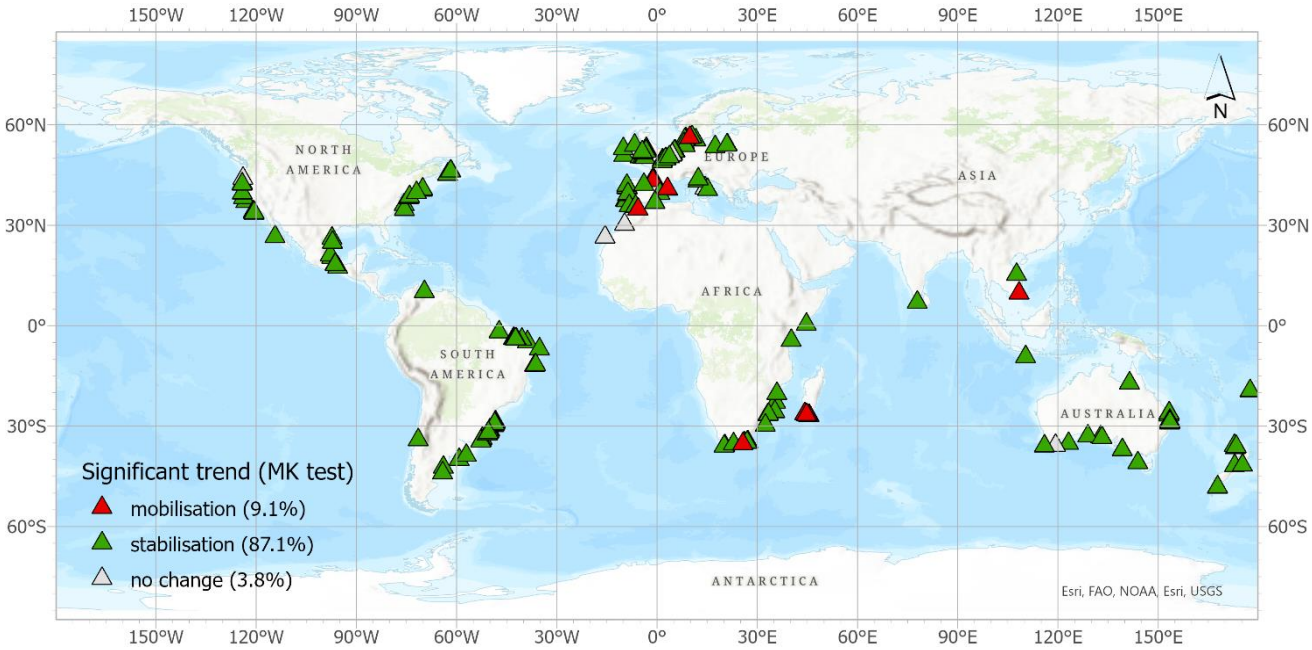

Figure 3.4. Dune dynamics based on Mann-Kendall analysis performed on the trend component of the *NDVI* series. The decision for statistically significant change depends on: (1) the change magnitude (minimum of 1%), and (2) the test *p*-value relative to the imposed levels of significance, $\alpha = 0.01$ (threshold for statistically significant greening and mobilisation) and $\alpha = 0.1$ (threshold for moderate level of significance).

Other dune cases, although characterised at present with high mobility, show signs of greening over the last 70 years. They include Doñana (considered the largest mobile dune system in Spain; Muñoz-Reinoso, 2018); the Listland dunes on the German Wadden island of Sylt (Osswald et al., 2019; Peyrat et al., 2009), and the Łeba Bar in Poland (Peyrat et al., 2009). From the historical perspective of dune formation, all dunes from NW Europe situated on the coasts of the North Sea and Baltic Sea started as highly mobile dune formations which were migrating landward or along islands and spits, and at a later stage became stabilised (Clemmensen et al., 2014).

The strength of the interannual changes is quantified in terms of the Sen's slope magnitude. Figure 3.5 shows a map of the calculated Sen's slopes, where the strongest positive trends depicted in red ($0.009 \leq Q_{NDVI} \leq 0.02$ *NDVI*/year) are identified at several locations: Ovari dune site, southeast India; Thua Thien, Vietnam, and Parangritis, Indonesia, as well as on the eastern Australian coast. Strong greening tendencies are found in NW Europe ($Q_{NDVI} \leq 0.009$ *NDVI*/year).

The advantage of using the trend component of the *NDVI* signal to calculate the Sen's slope is that the calculated slope has less statistical uncertainty than the slope based on the original *NDVI* series, as pointed out by Martínez and Gilabert (2009). The uncertainty decreases due to removal of the noise associated with the seasonal fluctuations in the original signal (de Jong et al., 2011; Hawinkel et al., 2015). The standard error (S_E) of the slope has been used as a measure to quantify and compare the uncertainties. Figure 3.6 provides a box-plot representation to compare the standard error distributions for the two types of statistical analysis: (1) based on the *NDVI* series (left box-plot diagram), and (2) based on the trend component of the decomposed *NDVI* series (right box-plot diagram). Figure 3.6

confirms that the values and the spread of the standard errors for (2) are lower than for (1). Among the descriptive statistics, the sample median can be seen decreasing from 3 x 10^{-4} to 7 x 10^{-5}, i.e., by approximately a factor of 10.

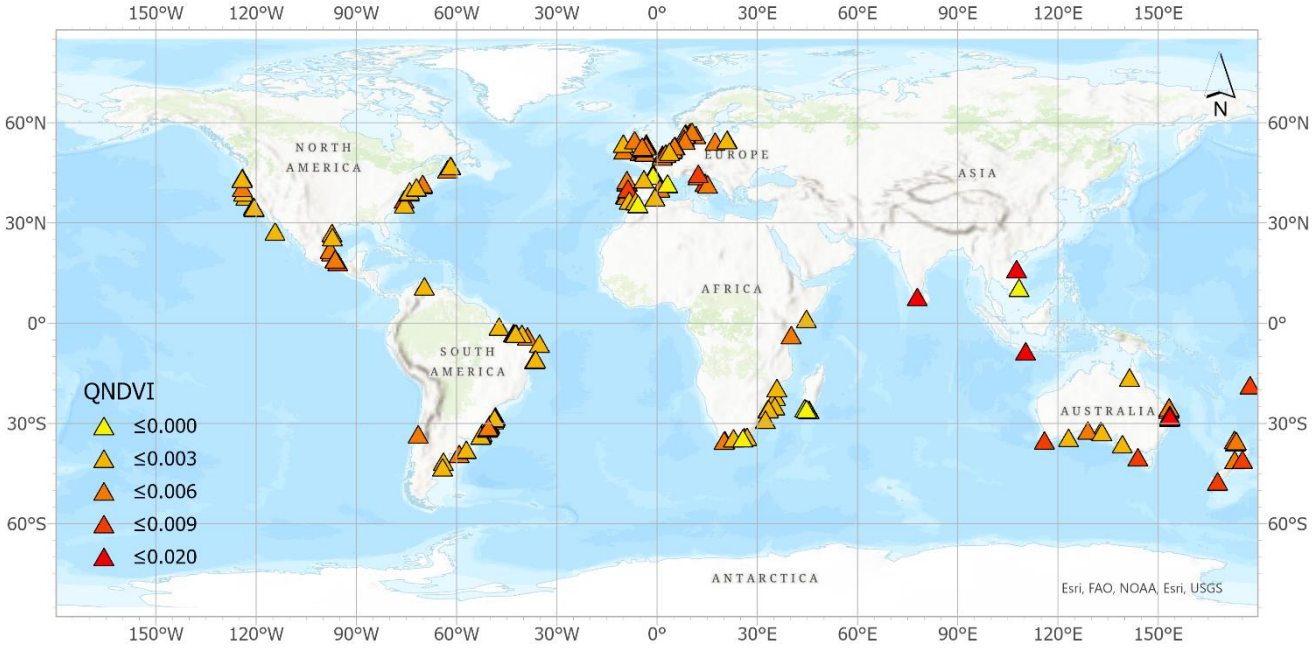

Figure 3.5. Sen's slope based on the trend component of the *NDVI* signal for the period 1984 – 2021.

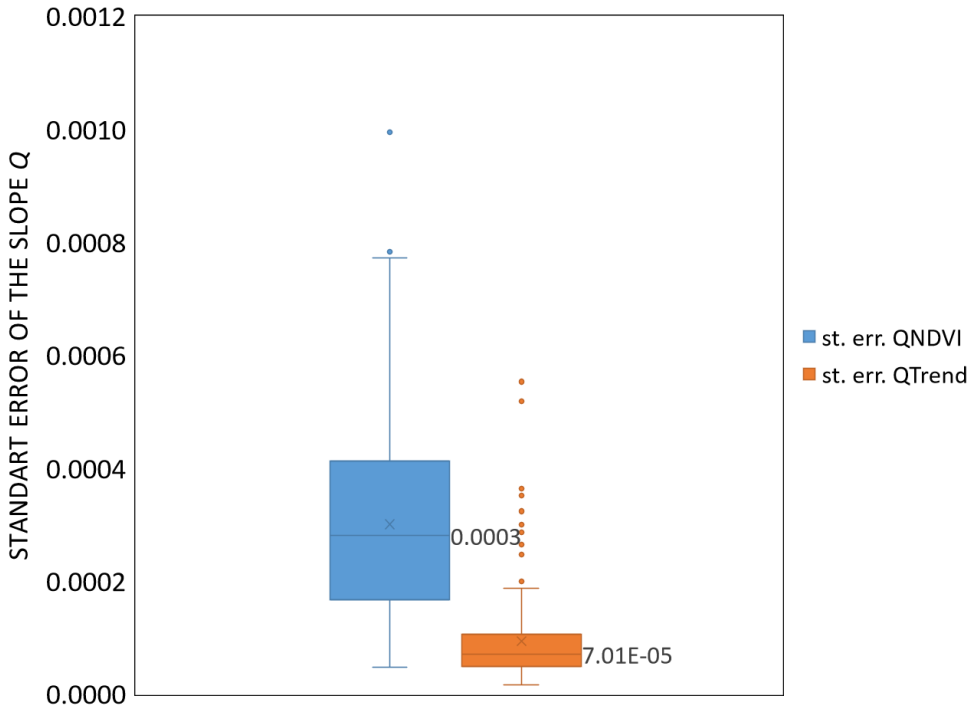

Figure 3.6. Uncertainties of the Sen's slope calculated from the *NDVI* series (the left box-whiskers plot) and from the trend component of the decomposed *NDVI* series (the right box-whiskers plot). The input *NDVI* time series have been corrected for cloud disturbances, outliers and missing data.

The *NDVI* metrics from Table 2.3 are explored further in order to characterise the seasonal and interannual variability. The mean levels of vegetation, $\overline{NDVI}$, are visualised in Figure 3.7. They vary between 0.049 *NDVI*, for the arid conditions of Guerrero Negro barrier islands in Mexico, and 0.605 *NDVI*, for the cool temperate climate of Brownslade Burrows in Wales. The estimated sample mean is 0.290 *NDVI*. From all dune sites with $\overline{NDVI}$ within the largest 25% of the sample, approximately a third (33%) originates from the European coasts.

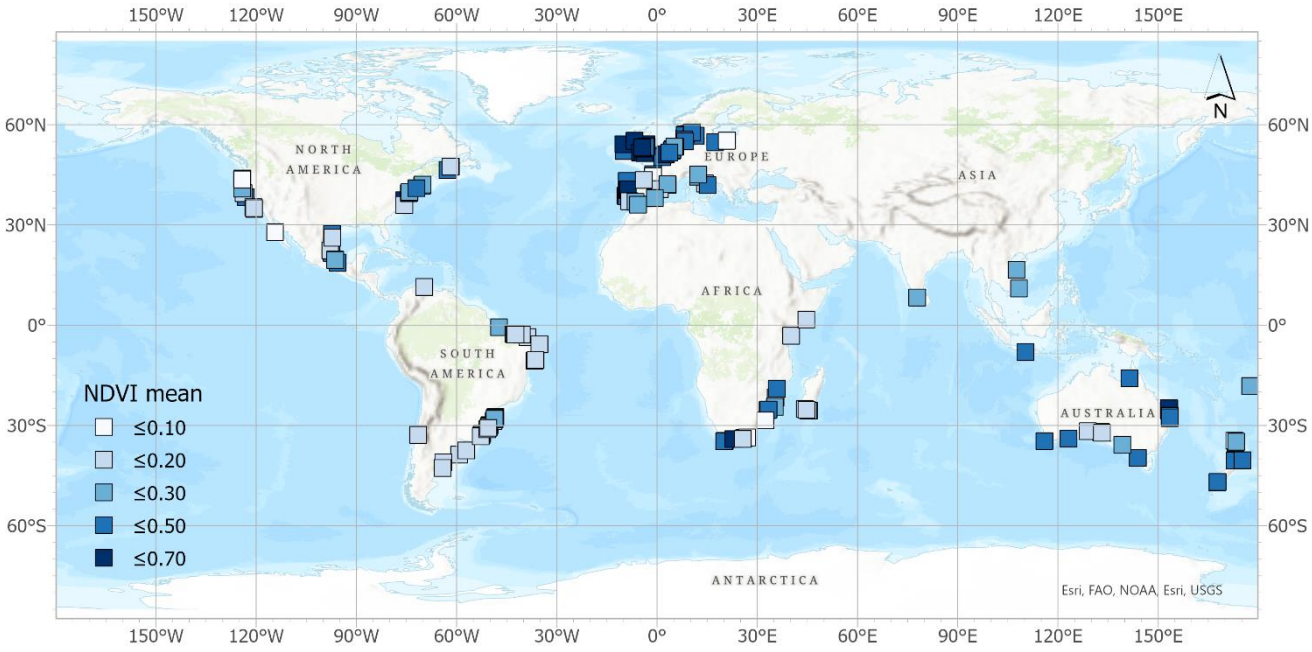

Figure 3.7. Mean levels of vegetation, $\overline{NDVI}$ for the study period 1984 – 2021.

A similar global scale pattern can be also identified for the minimum vegetation cover, $NDVI_{min}$, in Figure 3.8. The lowest value of $NDVI_{min}$ is close to 0 (= 0.044) and belongs to the site with the lowest $\overline{NDVI}$, Guerrero Negro. The largest among the minimum values, on the other hand, reaches 0.522 *NDVI* for the vegetated dunes in the Goukamma Nature Reserve, South Africa, where the dunes are almost fully fixed by vegetation, except for a few blowouts at the backshore.

As expected, in the lowest 25% of the $NDVI_{min}$ sample one can find examples of largely mobile dunes, such as Dune du Pilat in France ($NDVI_{min}$ = 0.081) and the extensive Lençois Maranhenses dunefield in Brazil ($NDVI_{min}$ = 0.058). Very low values of $NDVI_{min}$ also characterise the dunefields of the Ebro delta ($NDVI_{min}$ = 0.125), thus corroborating the observations of Martínez and Gilabert (2009) on the ongoing land cover changes within Spain. They showed that warm temperatures and insufficient rainfall in the semi-arid southeast region of Spain are responsible for ongoing land degradation.

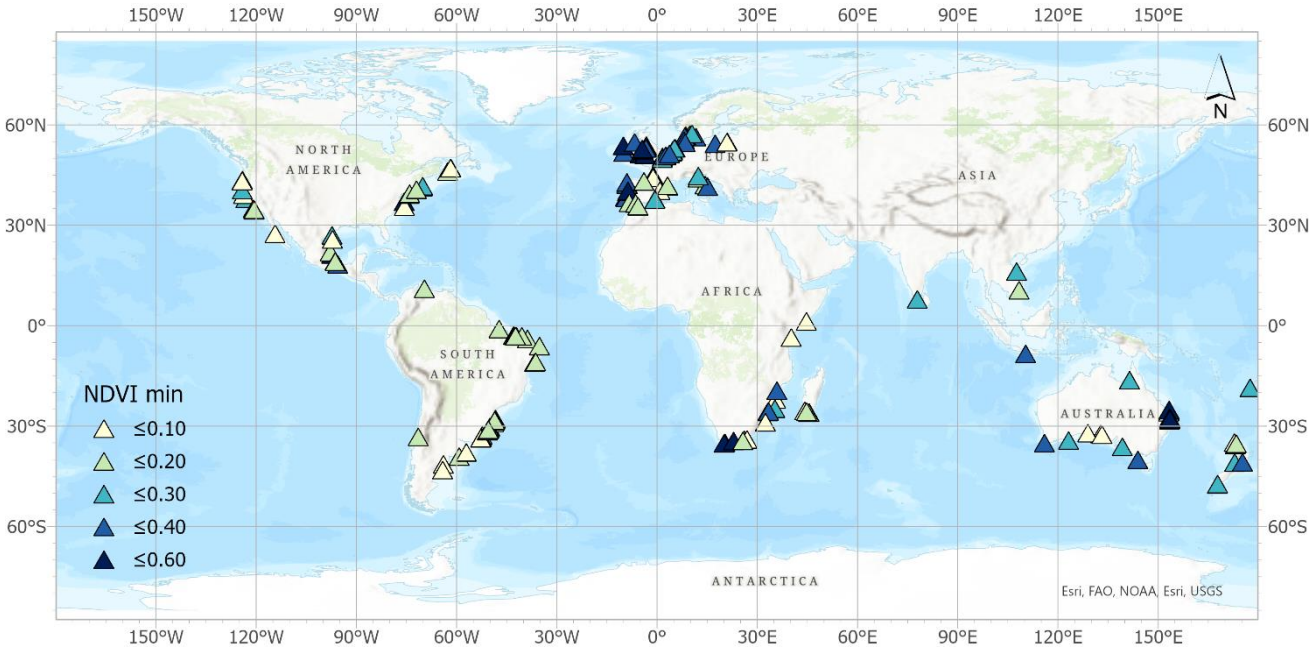

Figure 3.8. Minimum *NDVI* levels reached during the study period 1984 – 2021.

The amplitude of the annual phenological cycle, Δ*NDVI*, has been calculated as the range between the 10th and 90th percentiles of the zero-mean seasonal signal (Table 2.3). The range of seasonal variations is an important feature to judge the status of the dune vegetation. Large Δ*NDVI* can be expected for dune fields developing in humid to wet conditions, while permanently low vegetation in dry conditions shows very low Δ*NDVI*. These seasonality patterns are clearly observed in Figure 3.9, where the largest amplitude of fluctuations is in the northern hemisphere, particularly in NW Europe and at the east coast of US. In N and NW Europe, Δ*NDVI* varies from 0.103, for the Anholt Island (Denmark), to 0.298, for Brownslade Burrows (Wales). The lowest Δ*NDVI* value is reached for the hyperarid conditions of Guerrero Negro, Mexico (= 0.009), and the maximum of 0.345 – for the Greenwich dunes in Canada, within cool temperate, humid conditions. At this point, given the values of $\overline{NDVI}$ and Δ*NDVI* at Guerrero Negro dune site, it can be concluded that the conditions there resemble bare sand dominance.

So far, it has been demonstrated how greening in terms of $\overline{NDVI}$ is distributed globally. It has been concluded that the most significant positive changes occur in NW Europe, on the east coast of US, in the humid subtropics of the SE African coast, in eastern Australia (Queensland) and the west coast of New Zealand.

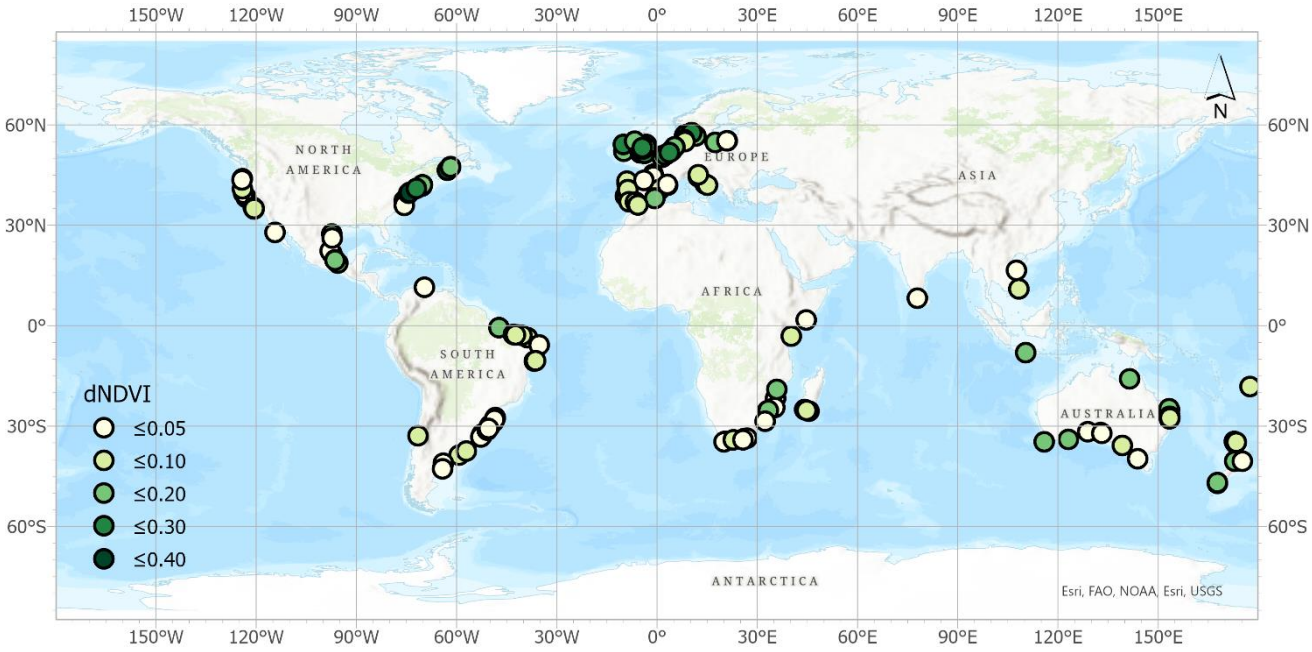

Figure 3.9. Amplitude of the annual phenological cycle, Δ*NDVI*, for the study period 1984 – 2021.

The relative contributions of the seasonal and trend components to the total variance of the *NDVI* signals are visualised in Figure 3.10 and Figure 3.11. The plots corroborate that vegetated dune sites with clear seasonal patterns are typical for the mid- to high latitudes covering NW Europe and the east coast of US. This is also the pattern revealed by the greening dune ridges at the Nassau river mouth in Queensland, NE Australia. On the other hand, for sites with sparse vegetation canopies (e.g., in arid and semi-arid tropical and subtropical climates), it is expected that vegetation responds directly to rainfall, the seasonal fluctuations are low, therefore the trend could become the dominant component in the vegetation signal.

A site suitable for comparison between the relative contributions of the trend and seasonal components is Mangueira Lagoon in the southernmost part of Brazil (Figure 3.12a), where the northern and the southern part of the dunefield exhibit very different vegetation states. At present, the northern polygon is highly afforested, while the southern is mostly free of vegetation. This is reflected in the values of the $\overline{NDVI}$. The fixed polygon appears to be dominated by the trend component, showing a quasi-monotonic increase from approximately 0.1 *NDVI* to 0.6 *NDVI*, and negligible seasonal fluctuations with magnitude of ~0.07 *NDVI* (Figure 3.12, upper right panel). The quasi-bare polygon to the south, on the other hand, is characterised by a relatively constant low trend at around 0.13 *NDVI*; the seasonal variations are negligibly small and are not illustrated in the plot (Figure 3.12, lower right panel). Accordingly, the calculated contribution of the trend to the energy spectrum of the vegetation cover is relatively low for the active dunes (~0.15) and quite high for the stabilised dunes (~0.76).

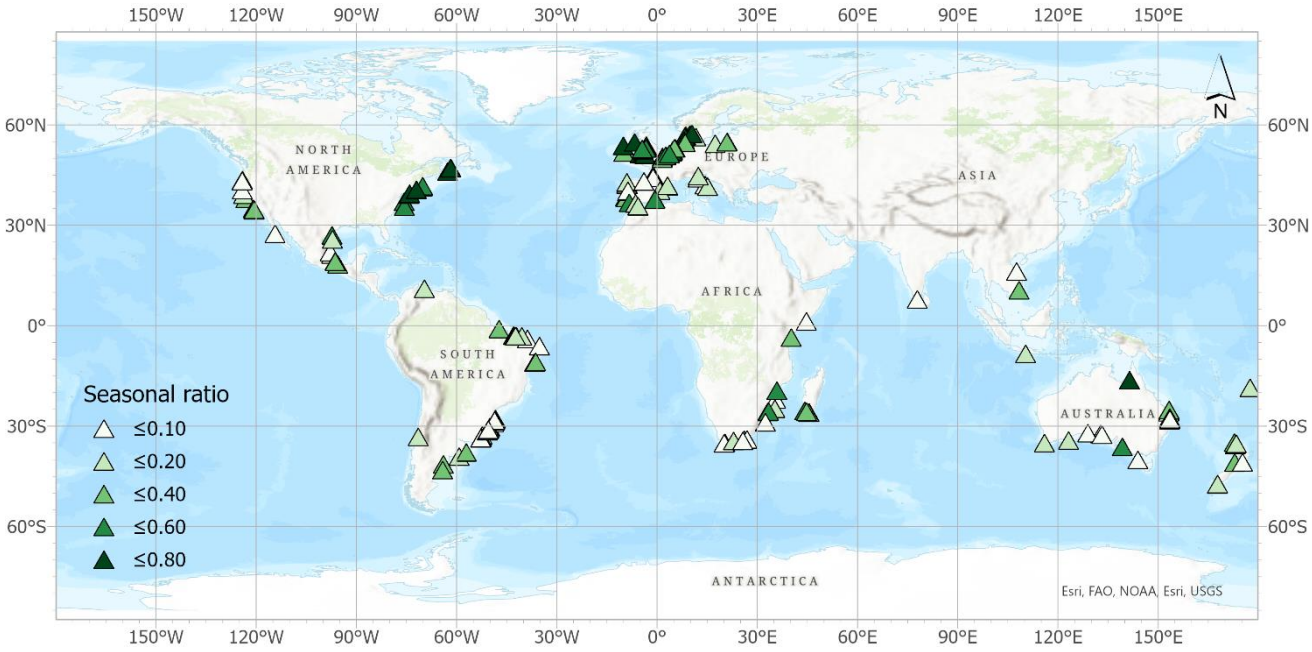

Figure 3.10. Contribution of seasonality to the variance of the area-averaged *NDVI* signal.

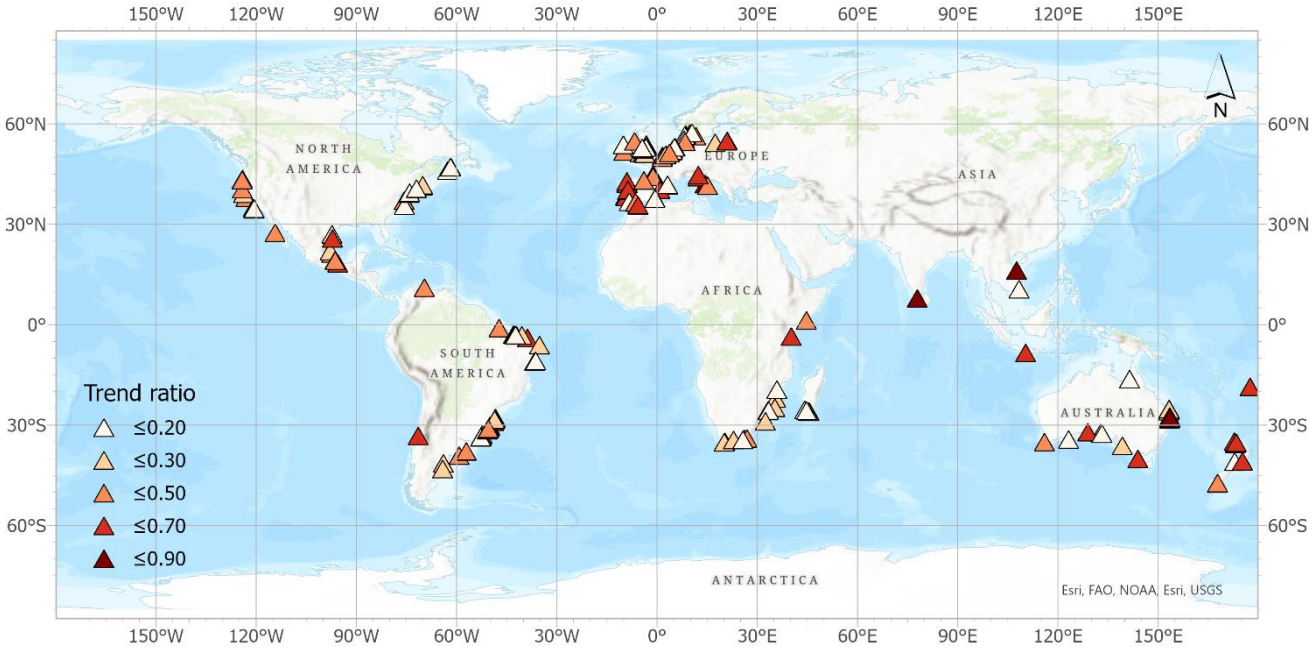

Figure 3.11. Contribution of the trend to the variance of the area-averaged *NDVI* signal.

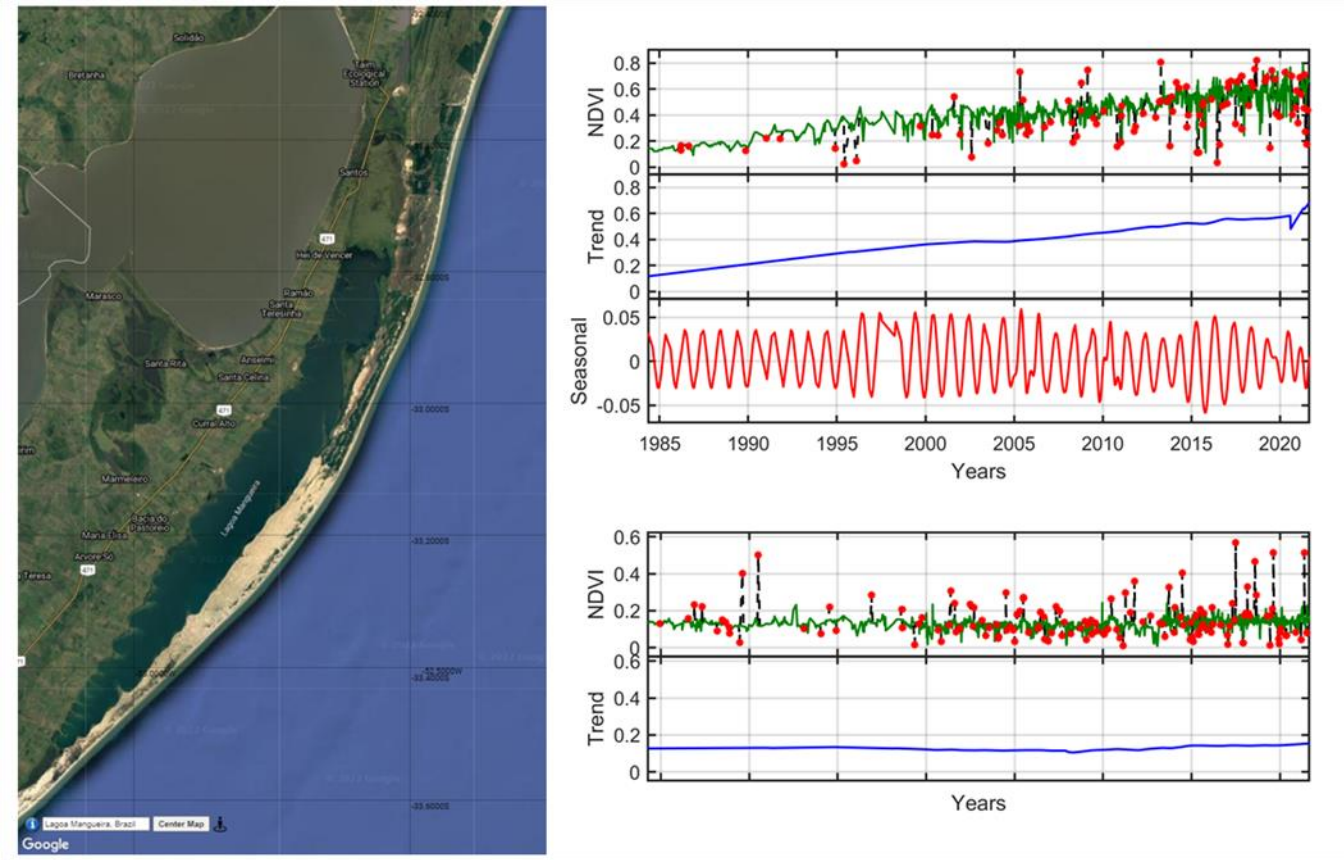

Figure 3.12. Comparison between the mobility trends of the neighbouring dunefields at Mangueira Lagoon, S Brazil: (upper right panel) afforested dunes; (lower right panel) naturally active dunes. *Source*: Google Earth Pro 7.3.4.8248.

The seasonal term of the *NDVI* signal can be further decomposed to find the scales at which different harmonic components contribute to the seasonal fluctuations of greening. This has been done using the Least Squares WAvelet decomposition method (LSWA) introduced by Ghaderpour and Pagiatakis (2017). The idea behind the wavelet analysis is to break the signal to different resolution scales in the time-frequency spectral domain. The proposed LSWA procedure returns the spectrogram of the decomposed signal and identifies statistically significant peaks at a chosen level of significance, in this case 1%. Signals indicating dense vegetation with clear seasonality due to phenological events exhibit a dominant annual component in the spectrogram, i.e. a peak of energy at 1 cycle/year. Figure 3.13 shows examples of spectrograms for the *NDVI* signals in the upper panels of each plot. The cyclic frequencies considered for the components of the seasonal signal, ω [cycle/year], fall in the range [0.1:0.1:4]. It is clearly seen in the plots that the annual energy peaks may contribute by more than 60% to the total variance. In addition, lower frequency constituents can also have contribution, though smaller, e.g., at half-year and 4-month temporal scales (Figure 3.13a, b, c).

One interesting result is the spectrogram for the Long Beach Island in Figure 3.13(d). It complements the results from the JUST decomposition in Figure 3.3(d), where a sudden jump in the trend, reflecting the consequences of the storm Sandy in 2012, has been detected. The destruction of vegetation cover is clearly distinguishable in the spectrogram, as well (Figure 3.13d). After the storm,

the percentage variance can be seen dropping from 80% to 30%, on the average. Figure 3.13(c, e, f) show spectrograms from different sites with Mediterranean type of climate. In particular, Figure 3.13(f) illustrates the case of the presently highly active and mobile Valdevaqueros dune in Spain. The drastic drop in the percentage variance after 2000 appears to be in agreement with reported increased rates of sand mobilisation (Navarro-Pons et al., 2016).

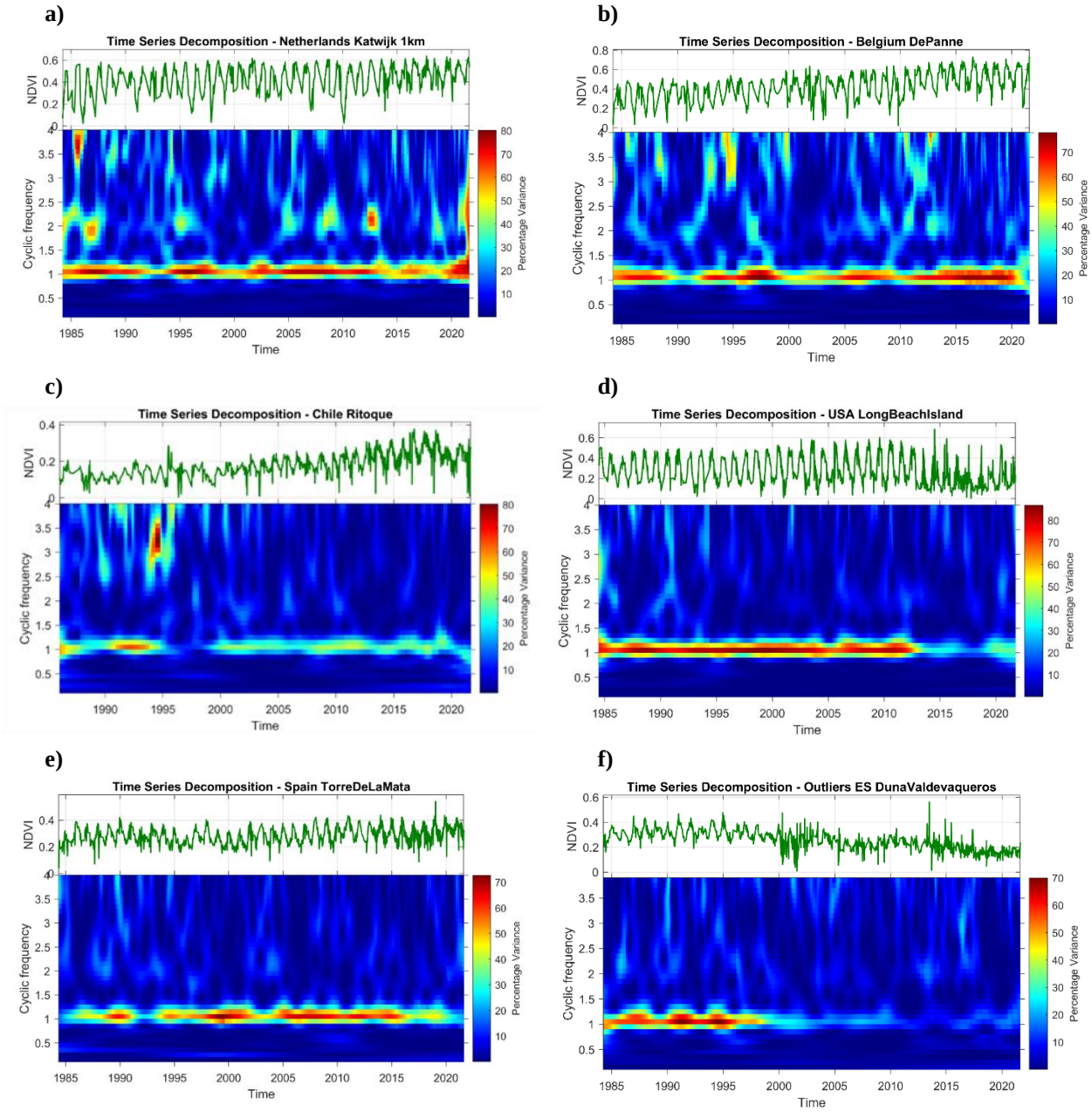

Figure 3.13. Contribution of the intra-annual (seasonal) component and its constituents to the area-averaged *NDVI* signal. (a) Katwijk, the Netherlands; (b) De Panne, Belgium; (c) Ritoque, Chile; (d) Long Beach Island, US; (e) Torre de la Mata, Spain; (f) Valdevaqueros, Spain.

At this stage, it can be said that the presented results delineate the general picture of long-term dune mobility between 1984 and 2021. On a global scale, greening appears to be the dominant dune mobility trend, which takes place regardless of density of vegetation cover (in terms of $\overline{NDVI}$) and magnitude of seasonal fluctuations (in terms of $\Delta NDVI$). However, on local and regional scales, the rate of greening (Q_{NDVI} [$\Delta NDVI$/year]) differs, depending on $\overline{NDVI}$ and on local climatological and environmental conditions. Therefore, before answering the first research question, it would be necessary to elaborate on the dependencies between the vegetation characteristics in Table 2.3, as this may allow to group dune sites with similar patterns of temporal vegetation dynamics.

In the following, the association between $\overline{NDVI}$ and Q_{NDVI} [$\Delta NDVI$/year] will be considered. By analogy with inland ecosystems, where $\overline{NDVI}$ = 0.3 sets the limit between bare soil and vegetated surfaces, the same value has been adopted here to distinguish sparse vegetation in sandier coastal ecosystems ($\overline{NDVI} \leq 0.3$) from largely vegetated dune areas ($\overline{NDVI} > 0.3$). These two classes contain 55% and 45% of all 162 greening dune sites, respectively. Therefore, the sampled dune areas appear to be slightly biased towards less vegetated conditions.

First, the frequency distribution of the Sen's slopes Q_{NDVI} (Figure 3.5) has been constructed conditional on the $\overline{NDVI}$, $p(Q_{NDVI} | \overline{NDVI})$. The distribution provides information on how the rate of multitemporal change relates to the mean level of vegetation cover. It has been constructed across 4 intervals for all dune cases with statistically significant greening ($Q_{NDVI} > 0$, Figure 3.14). The intervals roughly depict (1) slowly increasing vegetation cover ($Q_{NDVI} \leq 0.003$); (2) moderately increasing ($0.003 < Q_{NDVI} \leq 0.006$); (3) rapidly increasing ($0.006 < Q_{NDVI} \leq 0.009$), and (4) very strongly increasing ($Q_{NDVI} > 0.009$). It can be seen that 57% (= 51 out of 89) of the sampled dunes with less vegetation ($\overline{NDVI} \leq 0.3$) have some of the lowest trend slopes ($Q_{NDVI} < 0.003$). On the other hand, the rate of change for 58% (= 42 out of 73) of the well-vegetated dunes ($\overline{NDVI} > 0.3$) is moderately large, within the interval 0.003-0.006 *NDVI*/year.

However, there are also 11 dune sites which, although covered with sparse vegetation ($\overline{NDVI} < 0.3$), exhibit very strong greening trends. Their properties are specified in Table 3.1, where the first three rows correspond to the dune cases with the steepest Sen's slopes in Figure 3.14 ($Q_{NDVI} > 0.009$). Detailed description of these dunefields can be found in Appendix A. Some relevant properties are also specified in Table 3.1, from which it can be concluded that all trend ratios are constantly much higher than the seasonal ratios. This implies that for all 11 cases the trend is the dominant component of the vegetation signals. Some of the sites and the causes for greening will be discussed in Chapter 4. It will be only added here that in terms of geographical location, these dunefields belong to different climatic regions.

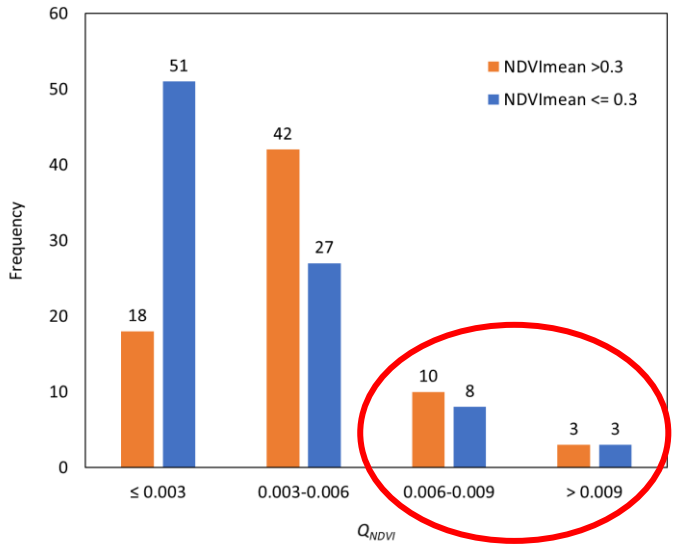

Figure 3.14. Sen's slope frequency distribution for the greening dunes, depending on $\overline{NDVI}$ (≤ 0.3 - sandy areas with sparse vegetation; > 0.3 - largely vegetated areas).

Table 3.1. Cases of identified greening dunes with relatively low $\overline{NDVI}$ but very strong trends.

Dunefield	***Long* [°]**	***Lat* [°]**	Q_{NDVI}	$\overline{NDVI}$	**ΔNDVI**	***Trend ratio***	***Seasonal ratio***
Ovari Beach, India	77.876	8.267	0.0198	0.263	0.046	0.808	0.021
Thua Thien, Vietnam	107.603	16.582	0.0102	0.237	0.049	0.848	0.029
South Stradbroke Island, Australia	153.428	-27.842	0.009	0.300	0.072	0.835	0.077
Guarda, Brazil	-48.615	-27.933	0.0070	0.248	0.070	0.535	0.132
Ahipara Dunes, New Zealand	173.092	-35.204	0.0067	0.212	0.026	0.425	0.039
Little Sandhill, Moreton Island, Australia	153.415	-27.303	0.0065	0.233	0.066	0.426	0.060
Porto Caleri, Italy	12.330	45.092	0.0064	0.288	0.085	0.583	0.131
Magisterio, Brazil	-50.269	-30.317	0.0061	0.281	0.061	0.547	0.070
Ghiomera, Italy	14.354	42.388	0.0067	0.171	0.025	0.777	0.027
Dunas Altas, Brasil	-50.344	-30.478	0.0062	0.188	0.039	0.619	0.043
Sigatoka River Dunes, Fiji	177.499	-18.170	0.0060	0.242	0.060	0.471	0.181

Next, a χ^2-test of independence has been performed to help find out whether the vegetation density in terms of $\overline{NDVI}$ affects the frequency distribution of the trend slope (Helsel et al., 2020). The null hypothesis of the test, H_0, assumes that the two variables are independent. First, the contingency table in Figure 3.15 (Contingency table/Observed (O)) has been used to calculate the expected frequencies for each cell in the table (the result is formulated as Contingency table/Expected (E)). Expected values are those for which the categories in the rows and columns are not associated, i.e. when H_0 is true and the same counts are returned in each cell of the table. The magnitudes of the normalized differences

(O-E)/E indicate that the highest associations between the rate of change Q_{NDVI} and $\overline{NDVI}$ exist for low and moderate Q_{NDVI}, thus they contribute most to the rejection of H_0. On the other hand, the lowest dependence appears for the largest slopes.

Contingency table/Observed (O)					
$\overline{NDVI}\backslash Q_{NDVI}$	≤ 0.003	0.003-0.006	0.006-0.009	> 0.009	**Total**
$\overline{NDVI}$ <= 0.3	51	27	8	3	**89**
$\overline{NDVI}$ > 0.3	18	42	10	3	**73**
Total	**69**	**69**	**18**	**6**	**162**

Contingency table/Expected (E)					
$\overline{NDVI}\backslash Q_{NDVI}$	≤ 0.003	0.003-0.006	0.006-0.009	> 0.009	**Total**
$\overline{NDVI}$ <= 0.3	37.907	37.907	9.889	3.296	**89**
$\overline{NDVI}$ > 0.3	31.093	31.093	8.111	2.704	**73**
Total	**69**	**69**	**18**	**6**	**162**

Contingency table/(O-E)^2/E					
$\overline{NDVI}\backslash Q_{NDVI}$	≤ 0.003	0.003-0.006	0.006-0.009	> 0.009	**Total**
$\overline{NDVI}$ <= 0.3	4.522	3.138	0.361	0.027	**89**
$\overline{NDVI}$ > 0.3	5.513	3.826	0.440	0.032	**73**
Total	**69**	**69**	**18**	**6**	**162**

Figure 3.15. Contingency tables for calculating the dependence of Q_{NDVI} on $\overline{NDVI}$.

To obtain the χ^2 statistics, the squared differences between each pair of observed and expected values are compared to the expected values and then summed, which in this case yields $\chi^2 = 17.860$. This value was subsequently compared with the critical values of χ^2 for levels of significance $\alpha = 0.01$ and 0.05 and degrees of freedom $dof = 3$. The corresponding critical values of χ^2 were retrieved from the χ^2 distribution table as $\chi^2_{0.99,\,3} = 11.345$ and $\chi^2_{0.95,\,3} = 7.815$. As the calculated χ^2 statistics is larger than the critical values, it has been concluded that the observed results are statistically significant for both $\alpha = 0.01$ and 0.05 which points to an existing relationship between the $\overline{NDVI}$ of the dune systems and the degree of greening. The same conclusion can be also drawn if using the *p*-value associated with $\chi^2 = 17.860$ and $dof = 3$. As the probability value $p = 0.00047$ is significantly small, H_0 has to be rejected.

Next, the distributions of the calculated $NDVI_{\min}$ (the lowest vegetation cover at a site) and $\Delta NDVI$ (the amplitude of the phenological variability), conditional on the $\overline{NDVI}$, can be seen plotted in Figure

3.16. As expected, when $\overline{NDVI}$ > 0.3 (Figure 3.16a), the majority of greening sites (75%) have the minimum *NDVI* (the orange bars) at the highest range of values ($NDVI_{min}$ > 0.3 *NDVI*;). At the same time, the seasonal amplitudes (the blue bars) are mostly relatively low (0.1-0.2 *NDVI*) or moderate (0.2-0.3 *NDVI*), but do not exceed 0.3 (except for one case). On the other hand, for low-vegetated areas ($\overline{NDVI} \leq 0.3$; Figure 3.16b), the minimum *NDVI* values are also lower, and the majority of dunes (76 cases, 85%) exhibit negligible seasonal fluctuations (≤ 0.1).

The relative amplitude of the phenological cycle with respect to $\overline{NDVI}$, formulated as $(\Delta NDVI/\overline{NDVI}) \cdot 100\%$, is illustrated in Figure 3.16(c, d). The plot corroborates the expectations that more vegetated dune areas would have more pronounced intra-annual variability that may dominate the trend, Figure 3.16(c). This situation is particularly relevant to highly stabilised or close to stabilisation dunes, e.g., the Greenwich dunes in Canada (Figure 3.17a, b), which have the largest amplitude for the phenological cycle ($\Delta NDVI\% = 103.55\%$). The opposite situation would take place if there is significantly less vegetation ($\overline{NDVI} \leq 0.3$), therefore the existing conditions facilitate aeolian activity. An example is the Ghiomera dune site, Italy, with seasonal fluctuations towards the other extreme, $\Delta NDVI\% = 14.58\%$ (Figure 3.17c, d). In this case, the trend component is dominant.

Finally, the results in Figure 3.18 and Figure 3.19 allow to group the dependence between dune dynamics and latitude, with latitude reflecting the regional variability of the climatic drivers, such as rainfall, temperature and wind regime (Lancaster and Helm, 2000; Delgado-Fernandez et al., 2019; Delgado-Fernandez and Davidson-Arnott, 2011). This approach was adopted by García-Romero et al. (2019) in order to associate the local climate with the type of foredune and vegetation along the south Australian shoreline. With respect to the rate of change Q_{NDVI}, Figure 3.18 reveals that a large percentage of dunefields from the temperate zone (defined here between 35º and 66.5º north/south latitudes) fall in the range of moderate slopes ($0.003 < Q_{NDVI} \leq 0.006$) and less in the lowest slope range (≤ 0.003). Dunes from the subtropics (between 23.5º and 35º north/south latitudes), on the other hand, appear to be associated to a large extent with low rates of change and to a lesser extent with moderate increases. Moreover, the 6 cases circled in red in the highest *Q*-range are from both tropical regions (India, Indonesia and Vietnam) and subtropical regions (Brazil and Australia) which are equally distributed between dunes with sparse vegetation and well-vegetated dunes (see also Figure 3.14).

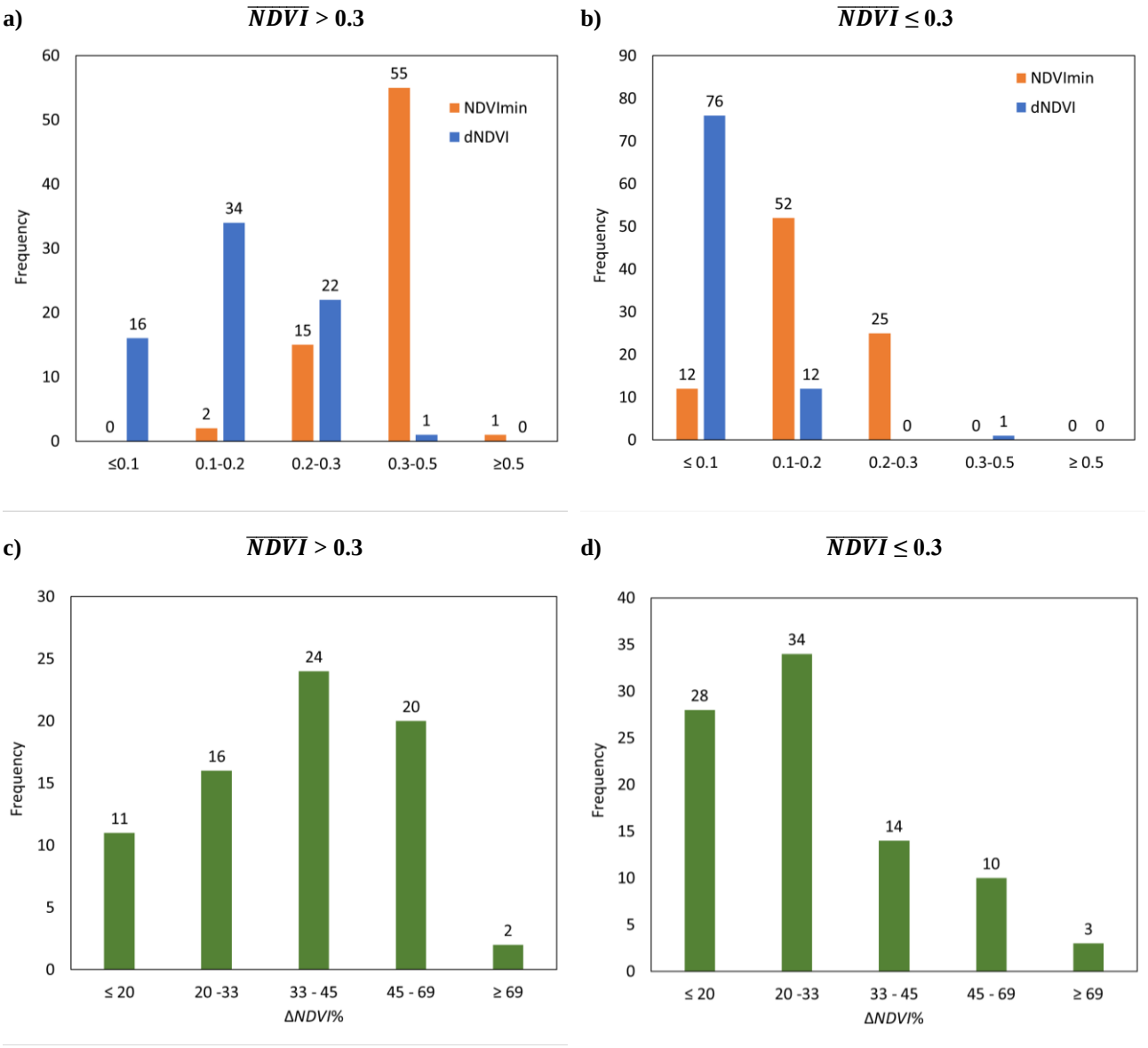

Figure 3.16. Frequency distributions of key vegetation features conditional on the mean level of vegetation at the dune site, $\overline{NDVI}$: (a, c) for well-vegetated dunes, $\overline{NDVI} > 0.3$; (b, d) for less vegetated dunes, $\overline{NDVI} \leq 0.3$.

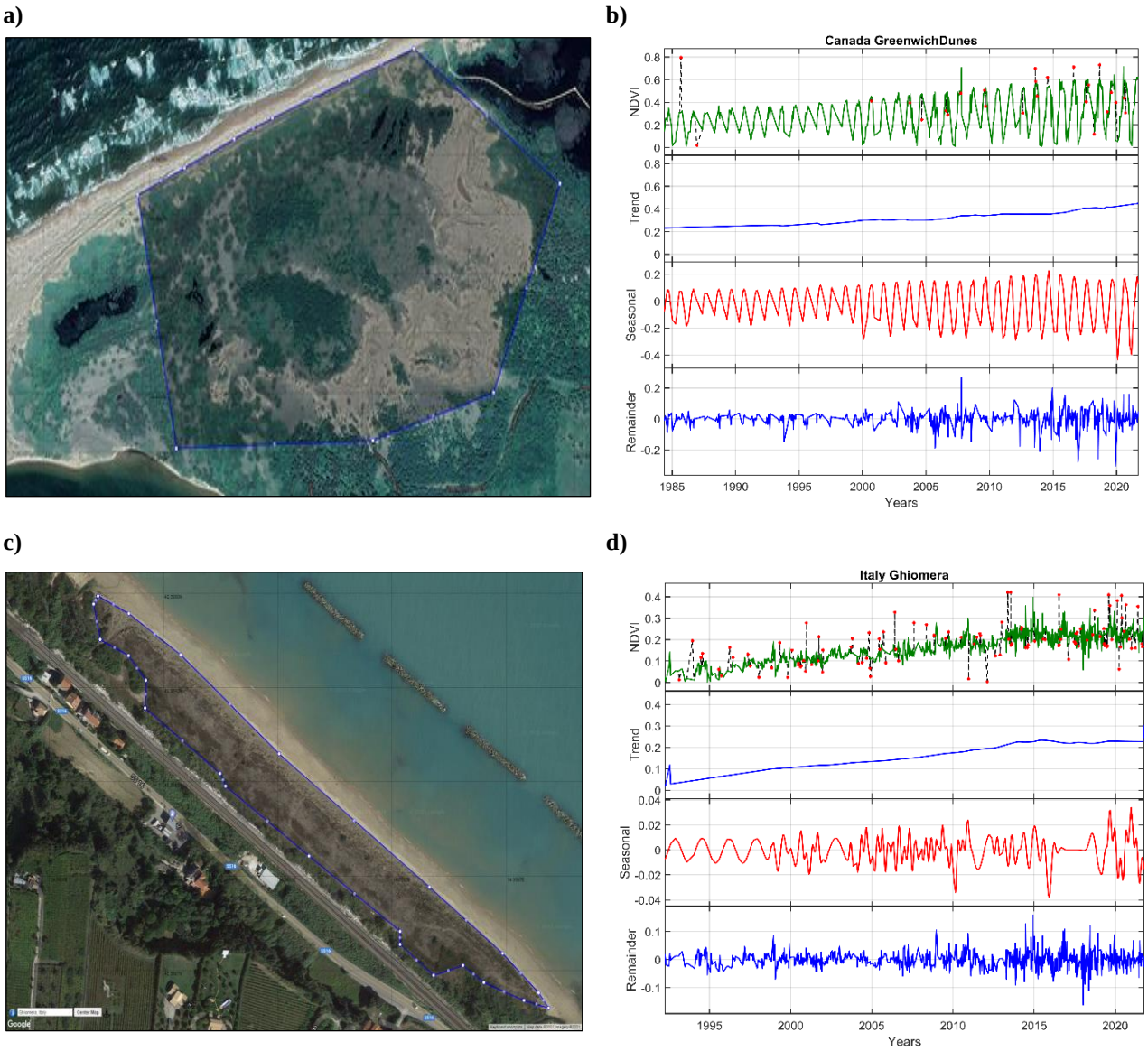

Figure 3.17. Examples of dune sites with different levels of vegetation cover affecting the seasonality pattern: (a, b) $\overline{NDVI} > 0.3$, $\Delta NDVI\% = 103.55\%$ (Greenwich dunes, Canada); (c, d) $\overline{NDVI} \leq 0.3$, $\Delta NDVI\% = 14.58\%$ (Ghiomera, Italy). *Source*: Google Earth Pro 7.3.4.8248.

As regards the change of the seasonal pattern with the latitude, the histogram representation in Figure 3.19 confirms that the largest fluctuations in the vegetation dynamics ($\Delta NDVI > 0.2$) are associated with temperate climates. In particular, the two cases with the largest $\Delta NDVI$ (in the red circle) correspond to the cases of the Greenwich dunes, Canada (Figure 3.17), and a site from the New Jersey barrier island, US (Nordstrom and Arens, 1998). All 22 cases in the range 0.2 – 0.3 *NDVI* belong to northern Europe, except for 2 of them, which are from the US coast (Hog island and Walking dunes).

The analysis of dunefields with increasing aeolian activity, on the other hand, shows average vegetation cover ranging from 0.092 *NDVI*, for the dune du Pilat, France (Tastet and Pontee, 1998; Clarke et al., 2002; Gabarrou et al., 2018) to 0.328 *NDVI*, for Rubjerg Knude dune, Denmark (Saye et al., 2006). Rubjerg Knude is the only dune from the group of largely mobile dunes here with

$\overline{NDVI}$ > 0.3. This could be due to the high *NDVI* values for the vegetated surfaces that have been buried over time by the sand of the dune which is migrating in agreement with the accelerated rate of coastal retreat (Navarro-Pons et al., 2016). It should be also noted that the majority of the mobilised dunes (~76%) have Q_{NDVI} > -0.003 *NDVI*/year. Therefore, for the whole period of 38 years, the negative change will be approximately -0.01 *NDVI*.

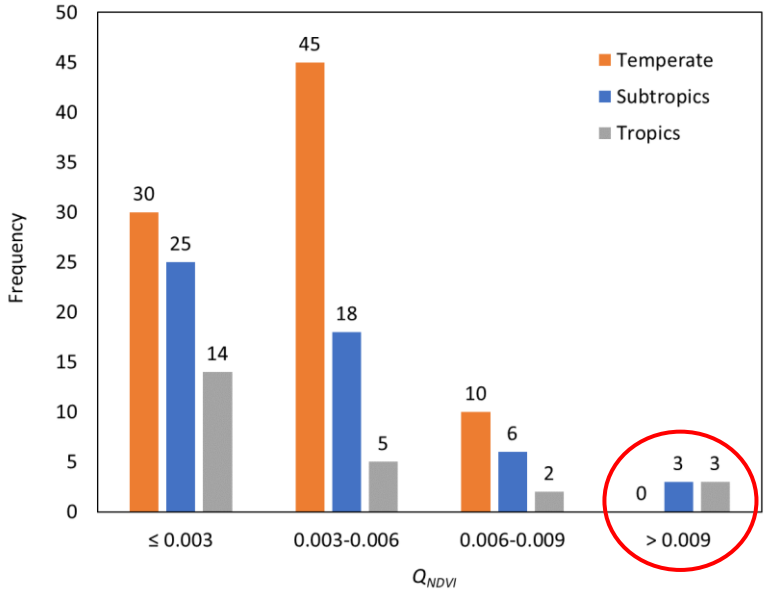

Figure 3.18. Comparison between dune mobility trends from temperate, subtropical and tropical zones in terms of Q_{NDVI}.

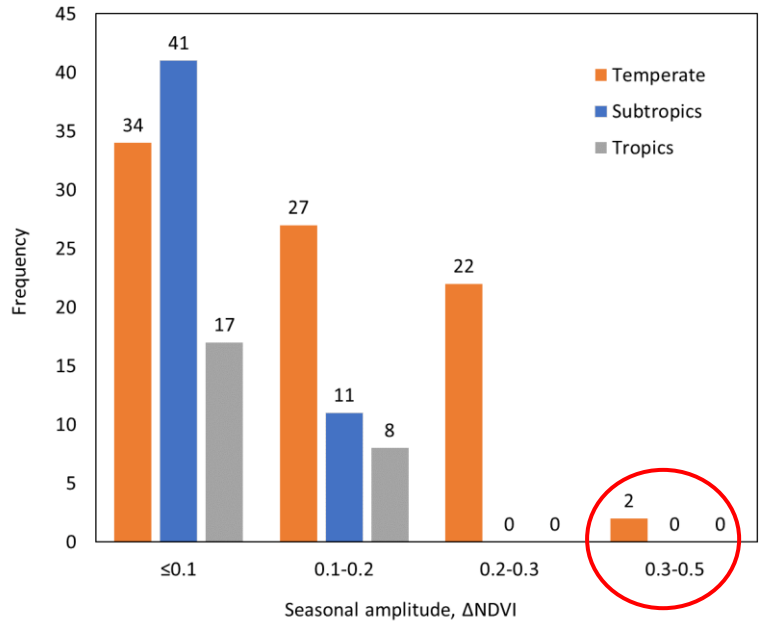

Figure 3.19. Comparison between dune mobility trends from temperate, subtropical and tropical zones in terms of amplitude of seasonal variations, Δ*NDVI*. Only sites with spatially increasing vegetation are considered (a total of 162 cases).

Further analysis of all greening and mobilising dunes includes comparison between the rates of dune cover change over two 20-year periods: the first counted from the beginning of the *NDVI* time series, and the second counted from the end. This approach results in a small overlap, since the study period is less than 40 years. Some of the records are shorter due to lacking observations over the first years of measurements, therefore those years had to be excluded from the conducted analysis. The shortest time series (only 6 cases), have approximately 20 years of data, thus 10-year periods have been calculated and compared (among them is Ovari Beach, India, see Figure A.1, Appendix A).

Comparison between the two trend slopes reveals that many dune sites have experienced an overall acceleration in the changes over the last years, irrespective of the initial direction of change (see Table B.1, Appendix B). In particular, from the total of 179 dune sites with statistically significant trends, 63% show acceleration over the last 20 years and 37% – deceleration (Table 3.2). The (+) and (–) signs in Table 3.2 define the direction of change. The positive (+) sign refers to greening ($Q_{NDVI} > 0$), and the negative (-) sign refers to an increase in the open sand areas with mobile sand ($Q_{NDVI} < 0$). The list of dune sites with accelerated vegetation growth for the four possible combinations of change (++, --, +-, -+) can be seen in Table B.1 (Appendix B). The sites in each class are ordered from the highest to the lowest absolute difference between the changes over the two considered periods.

Table 3.2. Dune cases for each combination of trend directions (Q_{NDVI}) over the first and the last 20 or 10 years of the study period. Only dune fields with statistically significant changes are considered, namely, a total of 179 cases of which 162 greening (~ 91%) and 17 (~ 9%) undergoing mobilisation.

First 20 years	*Last 20 years*	*Total*	*Accelerated*	*Decelerated*
Q(+)	*Q*(+)	132	86	47
Q(-)	*Q*(-)	8	2	6
Q(+)	*Q*(-)	7	2	5
Q(-)	*Q*(+)	32	23	8

Accelerated (++) trends are identified for 86 greening dune sites (Table 3.2 and Table B.1, Appendix B); about 24% of them (21 cases) belong to European coasts. Furthermore, the (--) and (+-) groups include only mobile dunes; the accelerated cases of (-+) greening are 23 and the Guerrero Negro dune site is among them. On the other hand, Table B.2 shows the dunefields with decelerated vegetation growth, where 32 cases (68%) of all decelerated greening (++) dune sites, shown in the first column of the table, also originate from Europe.

The acceleration/deceleration patterns are visualised in Figures B.1 – B.3 (Annex B) where the slopes for the two time intervals considered are plotted against each other for the following dune mobility groups: (1) vegetated, $\overline{NDVI} > 0.3$; (2) less vegetated, $\overline{NDVI} \leq 0.3$ and (3) mobile. In addition, the acceleration patterns can be associated with the climatic conditions of the main climatic zones (tropics, subtropics and temperate), also depicted in the plots. This representation is intended to

facilitate the choice of dune sites to be discussed in Chapter 4 with respect to regional climatic patterns that may have influenced their current mobility status.

On the basis of the presented results, the following conclusions could be drawn which answer the first research question:

- Positive (greening) trends appear to dominate on a global scale, as compared to a few dune areas with negative (mobilising) trends pointing to sand mobilisation or no change;
- The *NDVI* signals are mainly dominated by gradual (interannual) and seasonal (yearly) variations, while sudden jumps in the trends are rare;
- Greening takes place regardless of how dense the vegetation cover is, or how strong the seasonal pattern is. However, the rates of greening depend locally on the average vegetation cover in a way that stronger increases (larger Q_{NDVI}) are associated with larger $\overline{NDVI}$;
- The shape of the trendlines describes a nonlinear response to the driving factors. This can be also seen from the comparison of the trend slopes over two 20-year periods (from the beginning and from the end of the *NDVI* signals) which may differ;
- The differences in the trend slopes point to acceleration with time in the vegetation status in 63% of the dune sites, irrespective of the initial direction of the change (positive/negative).

In addition, it can be said that:

- The most marked seasonal patterns are associated with temperate climates, e.g., dunefields on the coasts of NW Europe (cool temperate moist) exhibit pronounced seasonal patterns and somewhat weaker trends. This is also the case for dune systems at the barrier islands on the east coast of US evolving under warm temperate moist conditions;
- With respect to the seasonal fluctuations in the *NDVI* signals, the least squares wavelet decomposition procedure (LSWA) by Ghaderpour and Pagiatakis (2017) returns statistically significant peaks in the spectrogram at different time scales, but mostly on a yearly scale, which is explained by the phenological cycle of the growing vegetation;
- For sparse vegetation canopies in arid and semi-arid tropical climates, where the vegetation status depends on precipitation, the range of seasonal fluctuations is low. In those conditions, vegetation is expected to respond directly to changes in the rainfall and trend may become dominant.

3.2. Research Question 2: Drivers of dune mobility

Trends in the time series of the main climatic variables: daily mean temperature (at 2 m height), T [ºC], daily mean wind speed (at 10 m height), W [m/s], and accumulated daily precipitation levels, P [mm/day], and their relationship with the coastal dune mobility are explored next (see also Chapter 2.3). The analysis is based on the assumption that natural dune mobility is controlled mainly by changes in the local climate (Lancaster and Helm, 2000). Therefore, if that is the case, it should be expected that dunefields classified as "greening" are correlated with favourable combinations of trends for the climatic variables, namely, warmer, wetter and less windy conditions (Clemmensen et al., 2014). The cases with increased aeolian activity, on the other hand, should couple with changes in the climate favouring sand transport. Arid to semi-arid locations are less vegetated and the coastal dunes there have higher mobility, as compared to dunes in wet conditions, such as those in tropical and temperate latitudes where vegetation colonisation and dune stabilisation take place (Hesp, 2013).

The first step in the analysis includes statistical testing for significant trends in the climatic time series for the 162 greening dune sites and 17 sites with prevailing aeolian activity discussed in Section 3.1. For the purpose, Mann-Kendall test has been applied to the whole time series (Mann, 1945; Kendall, 1975) followed by estimation of the Sen's slopes (Sen, 1968). The statistical analyses confirm significant changes over the past 38 years for all climatic variables at the 1% level of significance, as $p < 0.01$ (Table 3.3). In particular, the mean daily temperature has been increasing with time for both greening and sandier areas, with some exceptions. The total daily precipitation and the mean daily wind speed, on the other hand, reveal similar number of dune cases for increasing and decreasing statistically significant trends.

Table 3.3. Statistically significant MK test results ($p < 0.01$) for the daily mean climate variables.

Parameter	***# Significant Q > 0***	***# Significant Q < 0***	***# Non-Significant***
		Greening dunes (162)	
Average daily temperature, T [ºC]	158	1	3
Accumulated daily precipitation, P [mm/day]	67	63	32
Average daily wind speed, W [m/s]	59	63	40
		Mobilised dunes (17)	
Average daily temperature, T [ºC]	16	0	1
Accumulated daily precipitation, P [mm/day]	7	10	0
Average daily wind speed, W [m/s]	8	6	3

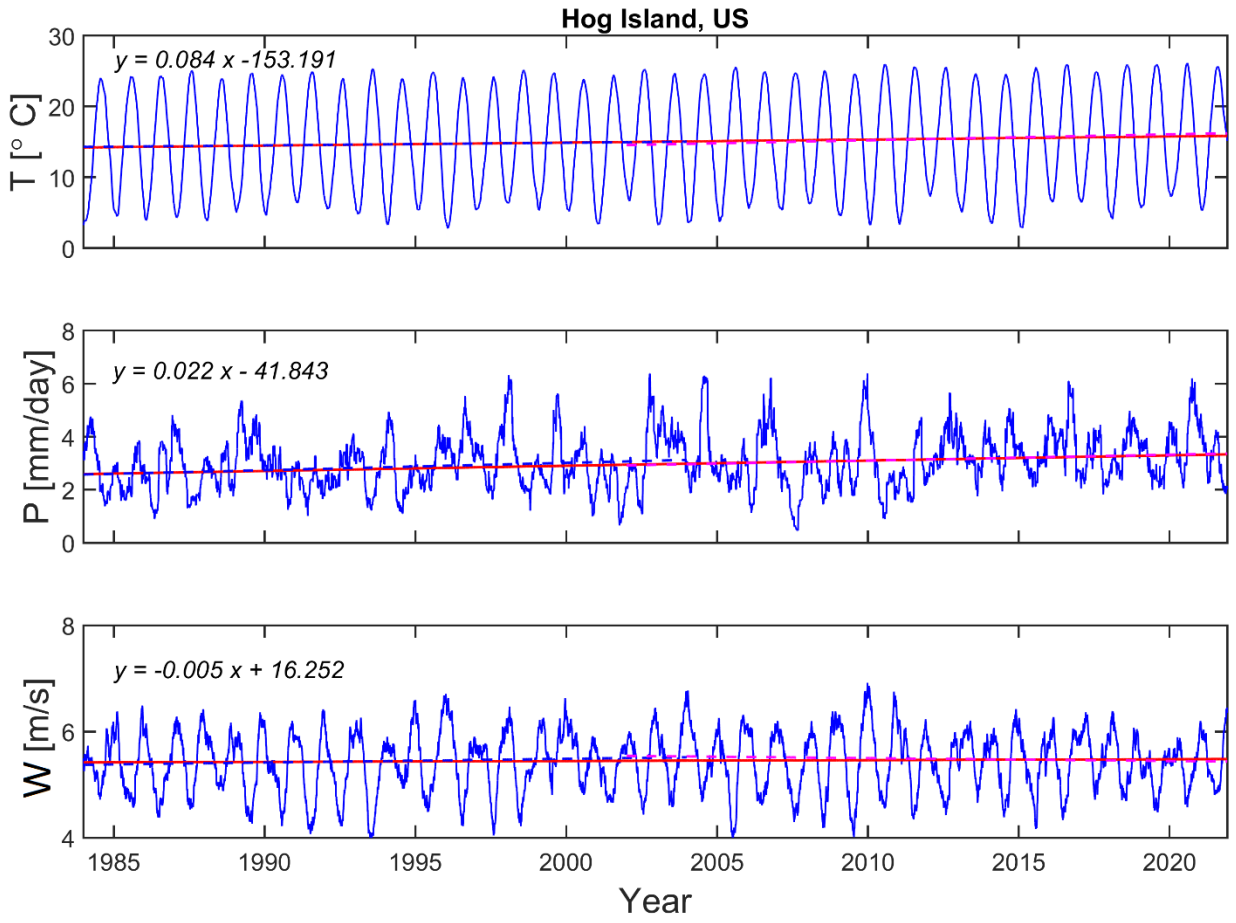

Figure 3.20. Climatological records for Hog Island, US, for the period 1984 – 2021: (a) Daily mean temperature, *T* [ºC]; (b) Daily accumulated precipitation, *P* [mm/day]; (c) Daily mean wind speed, *W* [m/s]. The red line is the identified trend based on the Mann-Kendall statistical test.

Figure 3.20 illustrates the requested climatic records for Hog Island, described by Huang et al. (2018) as suitable for studying the effects of global warming due to limited anthropogenic influence (see also Figure C.1, Appendix C). Statistically significant trends from the Mann-Kendall test and the trends over the two 20-year periods from the beginning and from the end of the time series are also shown in the figure, although not well distinguishable. In particular, the last 20 years point to tendencies favouring vegetation growth, including increasing temperature and precipitation and decreasing wind speed (Figure 3.20) which is in agreement with reported ongoing vegetation expansion (Huang et al., 2018).

The correlation between dune activity and regional climate is explored next. It has been chosen to base the correlation analysis on the long-term trends in the *NDVI*, i.e. Q_{NDVI} [*NDVI*/year], and the trends of the considered meteorological parameters (Q_T, Q_P and Q_W).

The dependence of Q_{NDVI} on the temperature rate of change Q_T [ºC/year] can be seen in the scatter plot in Figure 3.21. The calculated Sen's slope Q_T is always statistically significant, except for the

three cases plotted in orange which illustrate non-significant temperature changes. Two of these exceptions correspond to a temperature decrease over time. However, the data point of the largest identified temperature decrease, Q_T = -0.008 ºC/year, is statistically significant and describes the temperature trend at Ritoque, Chile. The plot reveals a weak dependence between the degree of change of *NDVI* and the daily temperature, such as the changes occur slowly, at 0.011 *NDVI*/ºC, and the estimated Pearson correlation coefficient is R = 0.067.

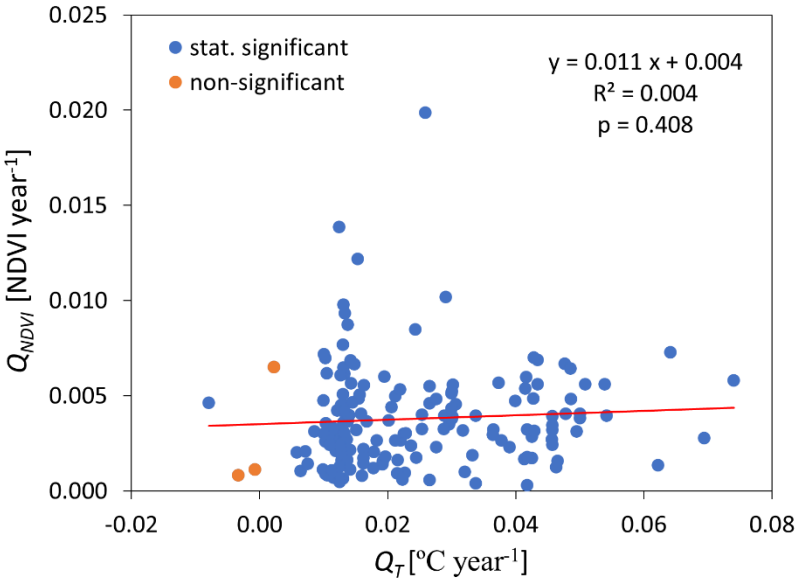

Figure 3.21. Scatter diagram between the *NDVI* and daily mean temperature trends for all greening dune sites. The cases of negative Q_T are plotted in orange. The largest negative Q_T is calculated for the dunes of Ritoque, Chile.

Next, Figure 3.22 illustrates how Q_{NDVI} [*NDVI*/year] correlates with the precipitation trend Q_P [mm day^{-1} year^{-1}], where Q_P is found to be statistically non-significant in 32 of the cases since $p > 0.01$ (for chosen 1% level of significance). Most of the non-significant cases show reduction of the daily total precipitation. Excluding them from the analysis, however, does not improve the overall dependence as the coefficient of determination R^2 increases only slightly, from 0.0193 to 0.0197. The R^2 values for temperature and precipitation indicate that the temperature increase does not explain the rates of dune stabilisation and the precipitation factor contributes by only 2% to the observed variability in Q_{NDVI}.

Figure 3.22 confirms that the vegetation expansion is governed by the climate in a way that locally increased rainfall would make the dune systems greener (da Silva and Hesp, 2013; Martinho et al., 2010). Increasing aridity would have the opposite effect, i.e., the rate of stabilisation is expected to decrease (Hugenholtz and Wolfe, 2005). The range of observed temperature variations (Figure 3.21), however, do not seem to play a particular role in the state of dune mobility. Moreover, warming can promote greening, but this is mainly relevant to cool climates.

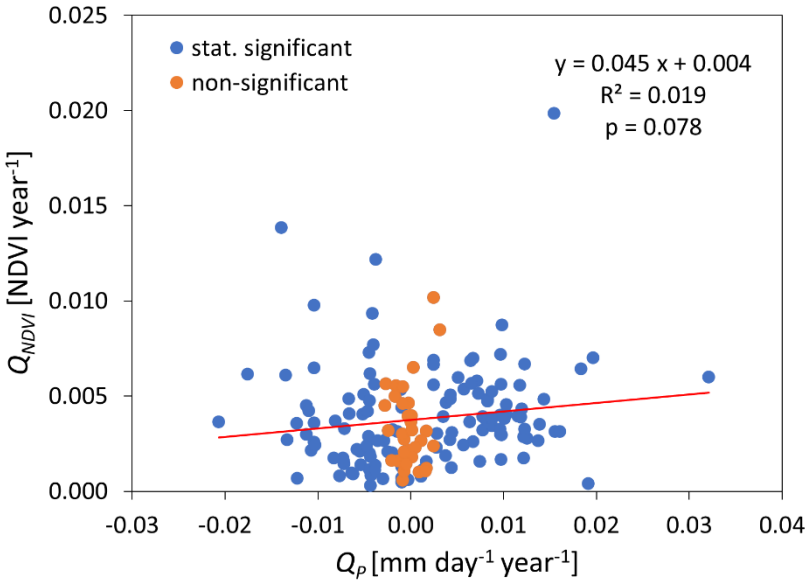

Figure 3.22. Scatter diagram between the *NDVI* and daily total precipitation trends for all greening dune sites. The cases of non-significant Q_P are plotted in orange.

In contrast to Figure 3.21 and Figure 3.22, Figure 3.23 illustrates a decreasing tendency between the rate of vegetation greening, Q_{NDVI} [*NDVI* year^{-1}], and the rate at which the wind speed varies with time, Q_W [m s^{-1} year^{-1}]. The sample of calculated slopes is nearly symmetrically distributed over the negative and positive range of values. The observed dependence is quantified by a negative slope -0.089 *NDVI* m^{-1} s^{-1}; therefore for each 1 m/s increase in the wind speed, there is a decrease of 0.089 *NDVI*. This may point to an increase of open dune areas within the system, although, given the inherent hysteretic response of dune mobility to vegetation (Tsoar, 2005), very strong winds would be necessary so that dune remobilisation occurs naturally.

On the other hand, at locations with wind stilling ($Q_W < 0$), which results in reduced potential of the wind to put the sediments into motion and transport them, the dune surface becomes more vegetated with time. Removing the non-significant cases, depicted in orange in Figure 3.23, leads to a slightly increased R^2, from 0.019 to 0.029. The R^2 value here shows again only 2% explained variability, similarly to the precipitation factor.

The results in Figure 3.21 – Figure 3.23 also suggest that greening takes place even when the changes in temperature, precipitation and wind are negligibly small. This could be explained by the fact that even if all climatic drivers are working together towards stabilisation, they will still have different contributions. In other words, while a particular factor is not contributing sufficiently to the change, other factors may be important. Therefore, on a regional and local scale, the relative contribution of the dune mobility drivers should be understood first, so that to explain the reason for the increase in vegetation.

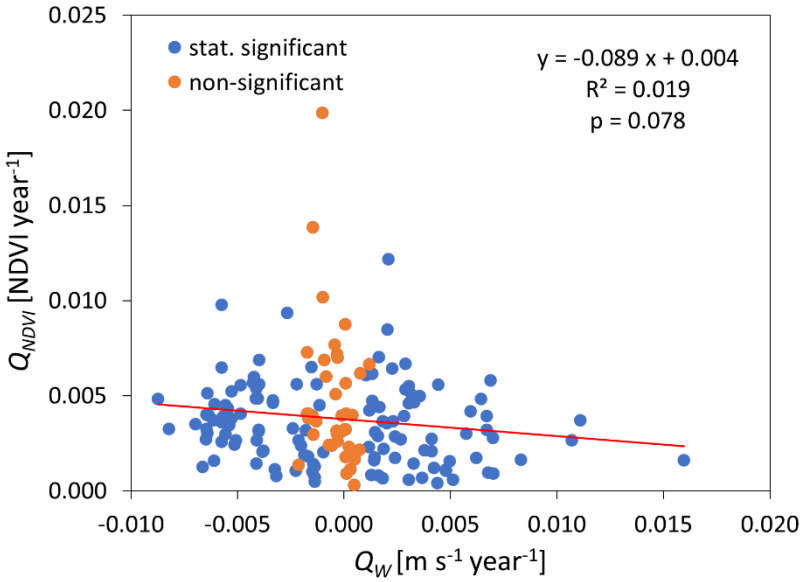

Figure 3.23. Scatter diagram between the *NDVI* and daily mean wind speed trends for all greening dune sites. The cases of non-significant Q_W are plotted in orange.

To further examine the relative importance of the climatic factors for dune greening, a multiple regression analysis has been also performed (Figure 3.24). The model of dependence shows a very low coefficient of determination R^2 which indicates that only 3.4% of the variability of Q_{NDVI} could be explained by the local climate. Furthermore, the ANOVA test results in Figure 3.24 show that the *p*-value of the multivariate model is non-significant, as $p = 0.142 >> 0.01$. Regarding the actual variables, the results show again lack of statistically significant dependence between Q_{NDVI} and the degree of change of any of the meteorological parameters (Q_T, Q_P and Q_W), as the returned *p*-values for each of them is much higher than the accepted 1% significance level, $p > 0.01$ (Figure 3.24). The coefficients in the bottom table corroborate further that for each unit change in Q_T, Q_P and Q_W, Q_{NDVI} indeed exhibits a negligible increase.

However, as the calculated *p*-values for the wind speed ($p = 0.18$) and precipitation ($p = 0.13$) are significantly smaller than the *p*-value for the temperature ($p = 0.95$), this could be used in support of the concept that the dune mobility is primarily driven by wind power and precipitation rates. This concept has been successfully implemented by Yizhaq et al. (2009) for modelling and prediction of vegetation cover under the effect of wind, precipitation and human activity, as well as for relating dune activity with different levels of vegetation spread.

The results from the multiple regression contradict the hypothesis made at the beginning of the analysis that further greening demands future change in the climatic conditions. Therefore, this hypothesis may not be true. In other words, the current climate possibly have reached a threshold of being sufficiently warm and wet which already makes the dunes greener anyway without dependence on ongoing changes in the climatic variables, particularly on temperature changes.

Regression Statistics	
Multiple *R*	0.184
R^2	0.034
Adjusted R^2	0.015
Standard Error	0.003

ANOVA

Source	***df***	***SS***	***MS***	***F***	***Significance F***
Regression	3	3.763E-05	1.254E-05	1.843E+00	1.416E-01
Residual	158	1.076E-03	6.807E-06		
Total	161	1.113E-03			

Term	***Coefficients***	***Standard Error***	***t stat***	***p-value***	***Lower 95%***	***Upper 95%***
Intercept	0.004	0.000	8.820	0.000	0.003	0.005
Q_P	0.040	0.030	1.346	0.180	-0.019	0.099
Q_T	-0.001	0.016	-0.065	0.948	-0.033	0.030
Q_W	-0.077	0.050	-1.537	0.126	-0.177	0.022

Figure 3.24. Results from the multiple regression analysis for the dependence of Q_{NDVI} on the combined action of the trends in the climatic variables (Q_T, Q_P and Q_W).

The next step includes finding out whether the degree of change of the climate variables correlates differently with the degree of change of vegetation over the first and the last 20 years of the study period. It has been kept in mind that it is not possible to relate changes in the dune mobility with simultaneous changes in the local climate variables, as the dune response is known to lag behind the climatic change (Hugenholtz and Wolfe, 2005). The obtained results are illustrated in Figure 3.25. The first period (Figure 3.25a, c, e) exhibits stronger dependencies between vegetation and local climate, where the correlation coefficient of the wind slope is the highest, although pointing again to a weak correlation, $R = 0.21$ (Figure 3.25e). Over the last 20 years, Q_{NDVI} shows very low association with the changes in the daily temperature and total precipitation (Figure 3.25b, d). In addition, the wind speed is found to be consistently reducing over both periods (Figure 3.25e and f) which is in agreement with the negative trend for the whole period 1984 – 2021 in Figure 3.23.

The dunefields showing sand mobilisation have been also analysed with respect to their response to the changes in the meteorological variables. The multiregression analysis showed again non-significant results, i.e., no relevance of climate to the current state of dune activity.

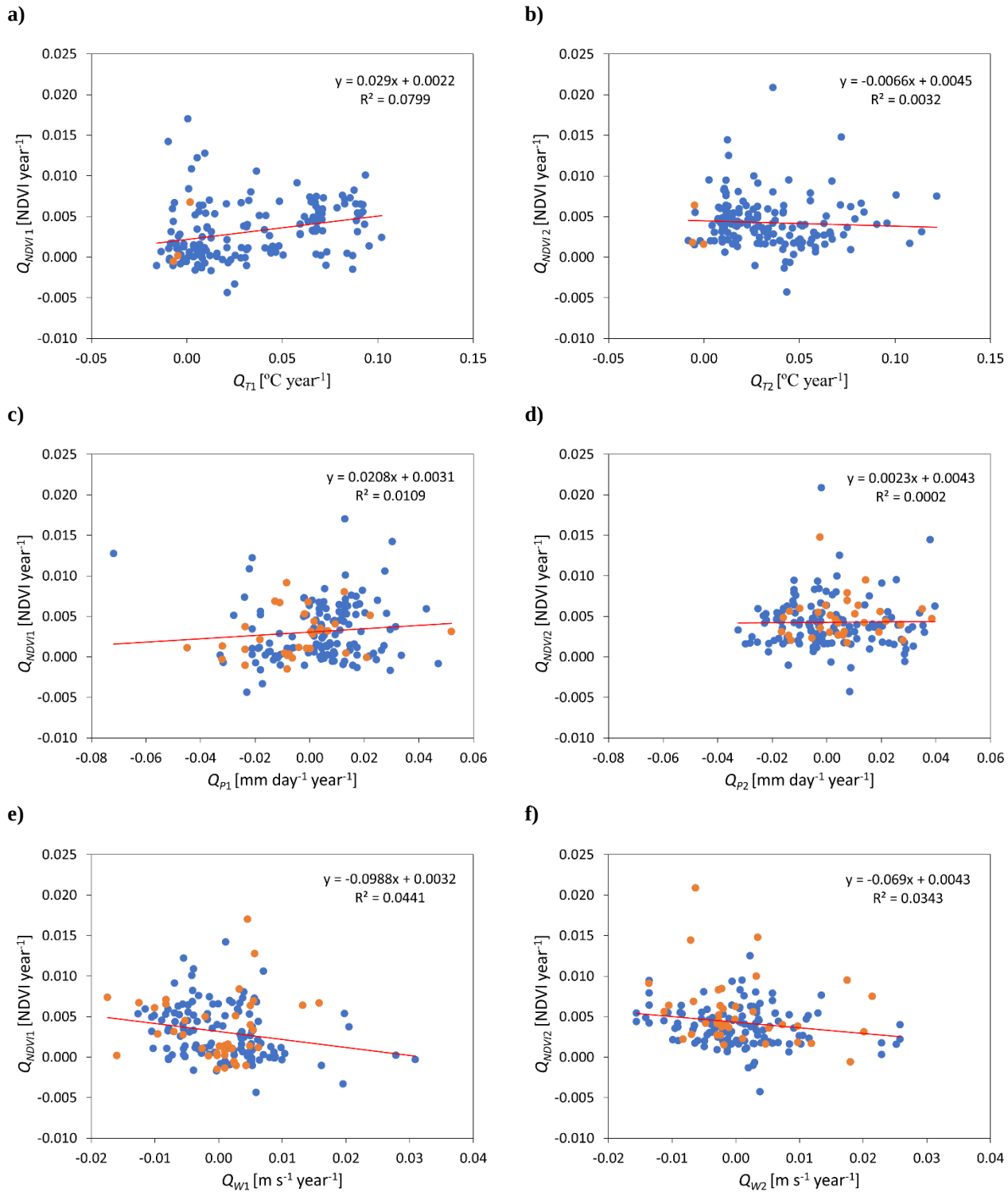

Figure 3.25. Correlation analysis over the two 20-year periods considered: (a, c, e) first 20 years; (b, d, f) last 20 years. The data points illustrate only the greening dunefields. The adopted legend is the same as in Figure 3.21 – Figure 3.23. The data points in orange illustrate statistically non-significant trends of the climatic variables.

The climatic time series show some general correlation patterns associated with the climatic zones in which the dunefields are evolving (Figure 2.3). They may provide an estimate of the favourable conditions for dune greening and mobilisation. Some statistical parameters for the correlation

coefficients of the greening dune sites are shown in Table 3.4 (estimated minimum, maximum and mean values). As can be seen, the range of values for the three pairs is similar, except for the average values. The spatial distribution of the correlation patterns can be seen in Figure 3.26 to Figure 3.28. The strength of correlation has been grouped as: (1) strong positive/negative ($0.6 < |R| \leq 0.9$); (2) moderate positive/negative ($0.3 < |R| \leq 0.6$); and low to no correlation ($-0.3 < R \leq 0.3$). The maps also share the same colour legend for ease of interpretation and comparison between the plots.

For example, the map in Figure 3.26 shows the mean daily temperature correlated with the daily total precipitation. Moderate to strong positive correlation exists between them under humid subtropical (warm and wet) conditions, which refer to southern Brazil, southeast Africa, as well as eastern Australia and the central part of the Mexican Gulf. On the other hand, strong negative association characterises the dune systems on coasts with Mediterranean type of climate (warm and dry) including large areas of the west coast of the US and the southern shoreline of Australia.

Table 3.4. Correlation statistics for each pair of climatic variables.

Correlation	R_{TP}	R_{PW}	R_{TW}
minimum	-0.809	-0.923	-0.887
maximum	0.703	0.770	0.789
average	-0.033	0.191	-0.238

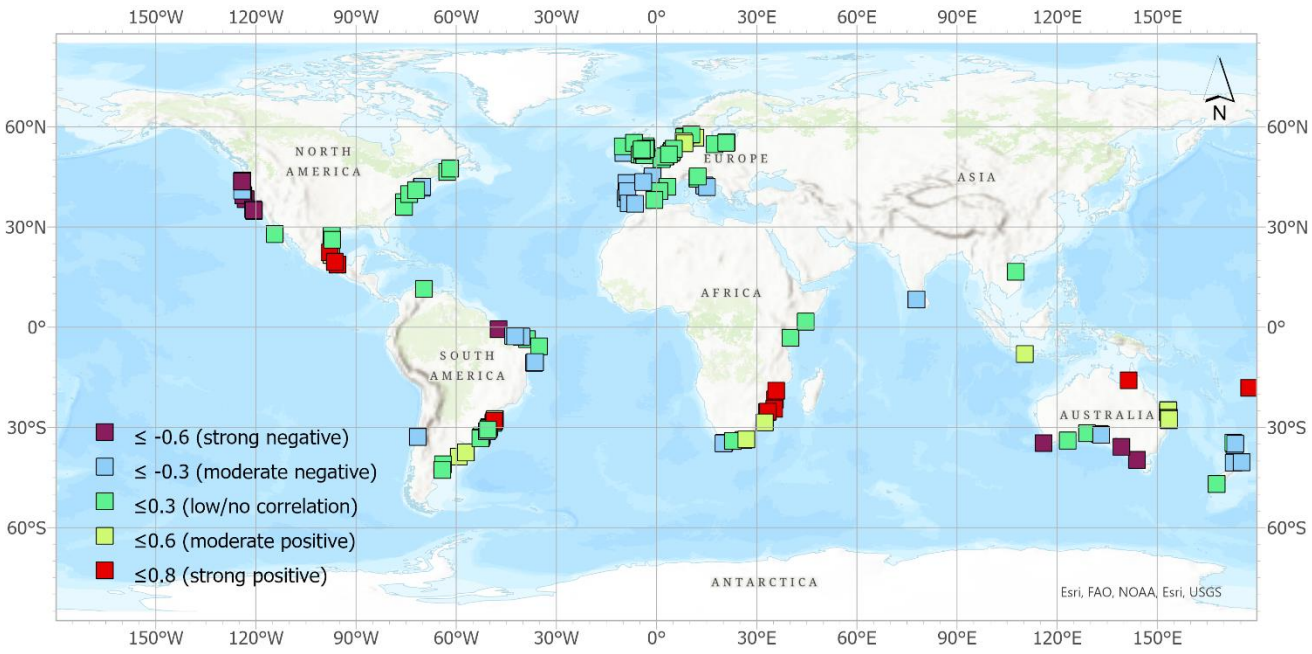

Figure 3.26. Greening dunes: spatial correlation patterns between mean daily temperature, T [ºC], and accumulated precipitation, P [mm/day].

It is also possible to identify a spatial pattern for the correlation between local precipitation rates and wind speed, as shown in Figure 3.27. In general, the strongest positive correlations can be identified in the temperate zones between 30º and 60º N/S, while the strongest negative dependencies are associated with the tropics.

Figure 3.28, on the other hand, illustrates the temperature variations correlated with the daily averaged wind speeds. The red markers on the map confirm the expectations that temperature and wind speed are positively correlated in Equatorial Brazil, at the central part of southern Australia and on the Fraser and Moreton islands, Australia. Strong negative correlation is identified in the temperate zone of the northern hemisphere (the east coast of US; the central, northern and NW Europe). The variables are negatively correlated on the Patagonian drylands, Argentina, as well. Moderate positive correlation dominates in the southern subtropics (Ritoque, Chile), while moderate negative – in the northern subtropics (e.g., Guerrero Negro, Mexico).

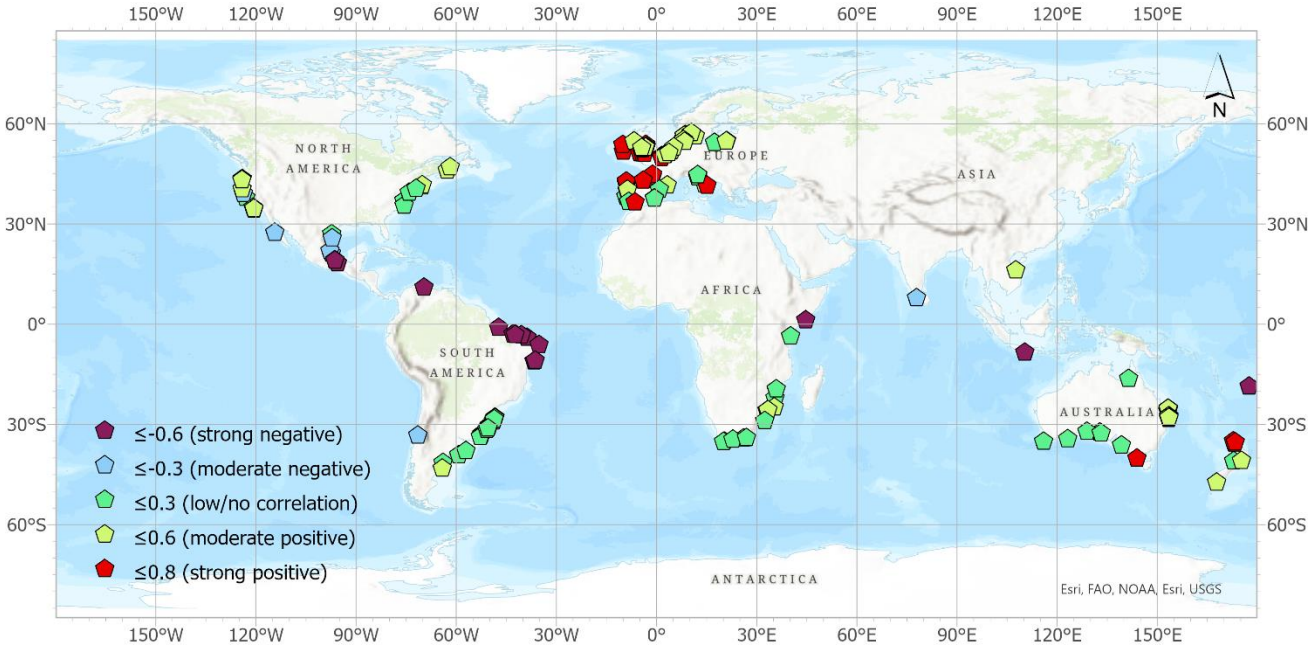

Figure 3.27. Greening dunes: spatial correlation patterns between mean daily accumulated precipitation, *P* [mm/day] and mean daily wind speed, *W* [m/s].

Finally, as both the performed correlation analysis and multiple regression analysis returned lack of statistical dependence between the changes in dune vegetation cover and those in the considered climatic variables, a different approach has been adopted next in order to decide on the causes for the observed greening or increase of open sand areas. This approach includes instead of quantifying statistical relationships, to look at whether greening happens always in the same classes of favourable combinations of local trends in the meteorological parameters (Q_T, Q_P and Q_W). In particular, the climatic conditions stimulating vegetation expansion are described in the most general case by: $T\uparrow$, $P\uparrow$

and $W\downarrow$. It should be noted that, for the period of study (1984 – 2021), the daily temperature has increased at all greening sites, except for three of them, as illustrated in Figure 3.21.

Other possible combinations of local meteorological conditions include: (1) $T\uparrow$, $P\uparrow$, $W\uparrow$ (warmer, wetter, windier; $Q_T > 0$, $Q_P > 0$, $Q_W > 0$); (2) $T\uparrow$, $P\downarrow$, $W\downarrow$ (warmer, drier, less windy; $Q_T > 0$, $Q_P < 0$, $Q_W < 0$); and (3) $T\uparrow$, $P\downarrow$, $W\uparrow$ (warmer, drier, windier; $Q_T > 0$, $Q_P < 0$, $Q_W > 0$). The last combination promotes aeolian activity, while the first two may eventually also lead to active aeolian transport, if the sand drift potential is high enough (Tsoar, 2005). As discussed by Delgado-Fernandez et al. (2019), lack of vegetation in arid to semi-arid areas would lead to coastal dunes with higher mobility, as opposed to the wet conditions in tropical or temperate settings which favour vegetation growth and therefore dune stabilisation (Hesp, 2013).

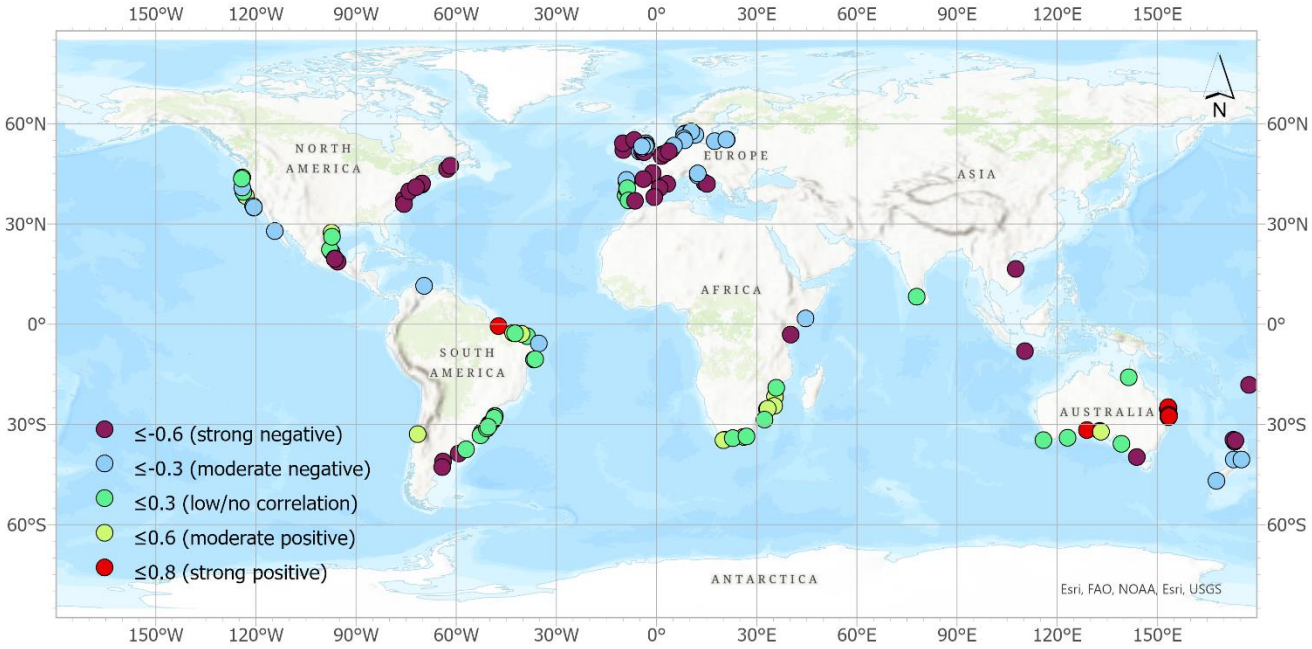

Figure 3.28. Greening dunes: spatial correlation patterns between mean daily temperature, T [ºC], and mean daily wind speed, W [m/s].

Table 3.5 shows the distribution of identified greening dune sites across the combinations of trends in the local meteorological parameters. Many cases of greening (approximately a third) are associated with the favourable combination of conditions ($T\uparrow$, $P\uparrow$, $W\downarrow$; Figure C.4, Appendix C). However, this is mainly true for dunes from temperate cool climates, such as vegetated dunes from northern Europe and across the Atlantic Ocean. On the other hand, most of the greening Danish dunes can be seen evolving over the recent decades under windier conditions which contradicts the reported decrease of storminess over northern Europe after the Little Ice Age (Clemmensen et al., 2014). In addition, negative temperature trends ($Q_T < 0$) have been identified for three greening dunefields: Ritoque, Chile; Alexandria and Port Alfred, South Africa. Table 3.5 also reveals that a substantial number of dunes (43 cases) classified as "greening" develop in climates facilitating aeolian transport: strong winds and

decreasing precipitation levels ($T\uparrow$, $P\downarrow$, $W\uparrow$), as illustrated by the dune cases in Figures C.3 and C.5 (Appendix C). These two cases, in particular, belong to extensive dunefields which are highly dynamic overall.

The same analysis has been applied to the dunes classified as mobilised here. Table 3.6 shows that for 7 of the highly mobile dunes (41%), the combination of temperature, precipitation and wind speed has indeed contributed to increased sand drift ($T\uparrow$, $P\downarrow$, $W\uparrow$). For example, very strong winds control the dynamics of the chevrons on Madagascar (Figure C.7, Appendix C) and the dunes in NE Brazil. However, the regional climatic settings for other dunes from the group, such as Dune du Pilat (Figure C.9, Appendix C), Terschelling and Long Beach Island, appear to favour the opposite process.

Furthermore, intermediate combinations of trends in the climatic variables may either cause local greening or mobilisation, depending on the relevant importance of the climatic factors (e.g., Figures C.1, C.2, C.8). There are also cases when the regional climate favours greening/mobility, but other local, non-climatological factors (sediment supply, dune management, variation in the populations of grazers) outweigh the expected climatic effect. Such cases include Dune du Pilat (Figure C.9, Appendix C), Rubjerg Knude (Figure C.8), the Younghusband Peninsula dunes (Figure C.6), the described case of Lagoa Mangueira dunes in Brazil (Figure 3.12), among others.

The dune examples in Table 3.5 and Table 3.6 will be discussed in Chapter 4.

Table 3.5. Greening dunefields: distribution across possible combinations of local trends in the meteorological variables. The temperature increase may be an important factor that contributes to greening primarily in temperate cool climates.

	Conditions	***# Cases***	***Trend***
1	$T\uparrow$, $P\uparrow$, $W\downarrow$	51	Greening (Figures C.4)
2	$T\uparrow$, $P\uparrow$, $W\uparrow$	30	Mobilisation/Greening (Figure C.1)
3	$T\uparrow$, $P\downarrow$, $W\downarrow$	35	Mobilisation/Greening (Figures C.2b, C.6)
4	$T\uparrow$, $P\downarrow$, $W\uparrow$	43	Mobilisation (Figures C.3, C.5)
	Total	**162**	**Stabilised**

Table 3.6. Active dunefields: distribution among possible combinations of local trends in the meteorological variables.

	Conditions	***# Cases***	***Trend***
1	$T\uparrow$, $P\uparrow$, $W\downarrow$	4	Greening (Figure C.9)
2	$T\uparrow$, $P\uparrow$, $W\uparrow$	3	Mobilisation/Greening (Figure C.8)
3	$T\uparrow$, $P\downarrow$, $W\downarrow$	3	Mobilisation/Greening (Figure C.2a)
4	$T\uparrow$, $P\downarrow$, $W\uparrow$	7	Mobilisation (Figure C.7)
	Total	**17**	**Mobilised**

The results from this chapter can be summarised to answer the second research question as follows:

- Approximately a third of the analysed greening dunes (51 out of 162) experience increase in the vegetation cover which could be attributed to local favourable combination of climate variables;
- As the assumed "favourable" conditions imply increasing temperature, combined with increasing precipitation levels and decreasing wind power ($T\uparrow$, $P\uparrow$, $W\downarrow$), the above dependence holds mainly for dune sites from cool temperate climates, among which northern Europe and the east coast of US;
- Some of the dune sites showing increase of bare sand (Dune du Pilat, France; Terschelling, the Netherlands; Long Beach Island, US) are found to evolve under climatic conditions favouring greening. This is possible, as far as their mobile character is due to other environmental and/or human-related disturbances, such as unlimited sediment supply, dune rejuvenation projects, or storm events eroding the coast and causing natural remobilisation of the dunes;
- Multiple regression analysis for the greening dunes has shown non-significant association between the levels of vegetation change and the changes in the climatic variables. This contradicts the hypothesis that changes in climate are needed to cause further dune greening. In other words, it is possible that the current climate has reached the threshold state of being sufficiently warm and wet which already makes the dune surfaces greener;
- Although the multiple regression analysis for the active dune systems also shows lack of dependence on the trends in the climatic drivers, these results should be interpreted with care, since the mobilisation trends have different major drivers. Nevertheless, wind power and precipitation rates continue to be of significance importance for the aeolian dynamics (Tsoar, 2005).

The conclusions for RQ1 (Section 3.1) and RQ2 (Section 3.2) will be discussed and validated in the next chapter for selected dune sites representing different mobility behaviour under the same mobility controls or, in other cases, similar mobility behaviour under different mobility controls (see Appendix C).

4. Discussion

4.1. *Dune greening*

Dune mobility has been studied here through a combination of different methods for statistical analysis and descriptive key parameters calculated from the components of the vegetation signal. Irrespective of the type of analysis applied, the main result – the confirmation of a global tendency for vegetation expansion, proves to be quite robust. Approximately 90% of the selected dunes worldwide became greener over the last decades (Figure 3.2 and Figure 3.4). Such result is in line with the findings by Jackson et al. (2019) who also base their analysis on *NDVI* data from Landsat imagery, although considering a limited number of relatively pristine dunefields. The present study, on the other hand, uses a much larger sample of dunefields and additionally corroborates through the key vegetation indices (Martinez and Gilabert, 2009) that the magnitudes and rates of long-term vegetation changes are to a great extent site-specific, something that has been suggested as likely by Jackson et al. (2019). The results here are also consistent with the literature review by Gao et al. (2020) for a broad range of geographically spread dune sites.

Well-vegetated dunes, distinguished by $\overline{NDVI} > 0.3$, are mainly associated with moderately steep trends (0.003 – 0.006 *NDVI*/year), while sites with permanently low vegetation cover ($\overline{NDVI} \leq 0.3$) – with some of the slowest temporal changes ($\leq$ 0.003 *NDVI*/year), as demonstrated by Figure 3.14. These results corroborate the conclusions of Martinez and Gilabert (2009) on observed landcover changes in Spain, where comparison is made between vegetated and dry regions. Furthermore, very large slopes (here, > 0.006 *NDVI*/year) could also be expected from naturally dense vegetation canopies. However, such results are exceptions for dunes with sparse vegetation in dry tropical and subtropical settings, and usually have non-climatic explanation (see Table 3.1 and Appendix A).

An important feature of the greening process at the selected dunefields is the observed acceleration over the last two decades of the studied time interval, irrespective of the initial direction of change (Table B.1; Appendix B). This simply points to a change in the set of driving forces, or in a particular factor, that may have caused such behaviour, particularly for the dune sites with exceptionally steep slopes not explained by the actual average vegetation cover (Table 3.1).

4.2.Causes for dune greening and mobility

4.2.1. Climatology

The regional climate, in terms of precipitation (Marcomini and Maidana, 2006), local winds (Levin, 2011; Levin et al., 2009; Tsoar, 2005), or both (da Silva et al., 2013; da Silva and Hesp, 2013; Martinho et al., 2010), could act as the main driver of natural dune mobility. Climate can also affect the vegetation cover in terms of decreased/increased storminess (Anthonsen et al., 1996; Clemmensen and Murray, 2006) and changes in the regional cyclonic activity (Levin, 2011).

To evaluate the importance of the climatic drivers on the temporal variations of dune vegetation cover (*NDVI*), time series of the main meteorological parameters (temperature, precipitation and wind speed) have been used in the present study, and the observed local rates of change of these variables have been correlated with the identified changes in the *NDVI*. The conducted assessment follows the conceptual model for mobile/vegetated sand dunes (Tsoar et al., 2009). According to the mobility concept for natural dunes, it is expected that vegetation expands with increasing precipitation, since higher moisture content suppresses the aeolian process by increasing the sand cohesion. Stronger winds promote aeolian transport and dune mobility, while weaker winds result in greening and dune stability since wind power controls the sand transport capacity (Yizhaq et al., 2009; Tsoar et al., 2009). However, in the present case, contrary to the conceptual expectations, neither the performed individual correlations, nor the multiple regression analysis returned statistically significant dependences on the climatic trends. In particular, the test statistics showed $p \sim 0.08$, for the daily averaged precipitation and wind, and $p \sim 0.41$, for the average daily temperature, assuming 1% level of significance (Figure 3.21 – Figure 3.23). These results made us reconsider the hypothesis about dependence between the degree of driver change and degree of change itself, and suggest as an explanation that the current climate has likely reached the state of warmth and moisture under which dunes are greening without necessity of further changes in the controlling climate factors. However, there is also a possibility that non-climatic drivers are responsible for the actual mobility trends.

Given the lack of statistical dependencies on the climatic variables, it has been decided here to classify combinations of climatic trends and verify whether particular dune mobility patterns occur always in the same classes. The optimal conditions for dune greening under climate warming has been defined as the combination of increased temperature and precipitation ($T\uparrow$, $P\uparrow$), and reduced wind speed ($W\downarrow$). On the other hand, the combination ($T\uparrow$, $P\downarrow$, $W\uparrow$) is viewed as facilitating the sand transport. As a result, it has been confirmed that many greening dune sites adhere to the climatological expectations, namely 51 out of 162 (31%), of which 36 (71%) are densely vegetated. It should be noted that a temperature increase would have larger effect on the greening in cooler climates (e.g., NW Europe). Such consideration is in agreement with Hugenholtz and Wolfe (2005) which find higher rates of natural sand dune stabilisation during cooler and wetter periods in the past. Warming, on the

other hand, is the current trend for the temperate zones of the northern and southern hemisphere (Clemmensen et al., 2014).

In the context of existing agreement between actual and expected dune mobility trends determined by the local climate, selected dunefields are discussed in the following, so that to conclude on the drivers of mobility. If the actual trend deviates from the climate-driven trend, it is necessary that non-climatic factors are investigated to find their relative importance for the coastal dune dynamics.

To start with, two greening dune systems from cool and warm temperate regions have been compared to explore the validity of the above considerations (Figures C.1 and C.4, Appendix C), as both of them show high average vegetation levels and relatively strong seasonality. In particular, Hog island, US (warm temperate climate; Figure C.1) has $\overline{NDVI}$ = 0.579 *NDVI*/year and $\Delta NDVI$ = 0.217 *NDVI*. The other dunefield, Sandscale Haws, UK, evolving in cool temperate climate, is characterised by $\overline{NDVI}$ = 0.517 *NDVI*/year and slightly higher range of seasonal fluctuations, $\Delta NDVI$ = 0.233. Both sites have limited human influence (cf. Huang et al., 2018; Pye et al., 2020), therefore it has been considered that the vegetation cover changes we are witnessing at present are mostly climate-related. Nevertheless, it should be kept in mind that increased atmospheric nitrogen deposition, which stimulates the vegetation growth, may be particularly relevant for the dune greening in NW Europe (Jackson et al., 2019; Pye and Blott, 2017). In addition, the present research confirmed the existence of a favourable combination of climatic conditions for Sandscale Haws, which agrees with the long-term climatic trends there discussed by Pye et al. (2020). On the other hand, the local warming on Hog Island, pointed out by Huang et al. (2018) as the reason for vegetation expansion, appears to be in line with the findings here of increasing temperature and precipitation over time ($T\uparrow$, $P\uparrow$, $W\uparrow$).

Among the climate variables, wind power plays a major role in maintaining the dunes active, provided that the local rainfall is enough to support vegetation growth (Tsoar, 2005). In this context, vast areas of highly active dune systems may develop in humid environments, e.g., in the humid tropics due to persistent strong winds during the dry season (Hesp, 2013). Such mobility pattern is clearly visible for the extensive Lençois Maranhenses dunefield in NE Brazil (Figure C.3, Appendix C). The regional climate, shaped by the position of the Intertropical Convergence Zone (ITCZ), is characterised by two seasons: wet (ITCZ at the southernmost position) and dry (ITCZ at the northernmost position). The trend of increasing wind speed which drives the dune mobility (cf. Hilbert et al., 2016) has been identified by the statistical analysis conducted in this study, and is additionally guaranteed by the estimated negative correlation between the daily wind speed and the total precipitation (Figure 3.27). The local climatic combination ($T\uparrow$, $P\downarrow$, $W\uparrow$) agrees with the overall highly mobile state of the dunefield, while disagreeing with the identified greening trend. Nevertheless, the *NDVI* values are very small ($\overline{NDVI} << 0.3$), thus pointing to bare sand. A similar combination of climatic conditions may explain the dune mobility at Maputo-Gaza barrier lagoon system in southern Mozambique (Miguel and Castro, 2018), where the climate is also determined by the position of the ITCZ (Figure C.2, Appendix C). The two transgressive dunefields divided by the border between the two provinces

(Maputo and Gaza) exhibit different levels of mobility: active and semi-active dunes are common to the south, and mostly vegetated dunes – to the north. While the climatic time series of both dune sites reveal a trend of wind reduction, the reduction is smaller for the southern, more active dunefield. This agrees with Miguel and Castro (2018), which found that wind has the major contribution to the mobility and significant migration of the Maputo dunes. On the other hand, the northern site is less exposed to wind due to the headland between the dune systems, therefore it is naturally more vegetated.

The present study also considers cases of active dunefields as they are commonly perceived: large transgressive dune formations evolving in arid and semi-arid climates, where low rainfall and high temperatures favour fast drying of sand while hindering plant growth. Lack of vegetation implies mobility through the direct availability of the sand. Among typical climates supporting mobile dunes are the dry subtropical settings of Guerrero Negro, Mexico (Figure C.5, Appendix C). The estimated $\overline{NDVI}$ is extremely low (= 0.049 *NDVI*), corresponding to areas of bare sand. The climatic conditions of Guerrero Negro, described by the combination ($T\uparrow$, $P\downarrow$, $W\uparrow$) favour an overall tendency of increased mobility, particularly due to strong summer winds promoting active aeolian transport. Nevertheless, the dune area has been classified here as "greening", because of the presence of numerous nebkha dunes.

For 7 of the active dune systems, the enhanced mobility is in line with the local meteorological conditions. The latter facilitate aeolian transport, mainly in terms of strong wind (high sand drift potential) and decreased precipitation ($T\uparrow$, $P\downarrow$, $W\uparrow$). This is the case of the chevrons on Madagascar and worldwide, represented by the Fenambosy chevron in Figure C.7.

4.2.2. Sediment supply

Apart from climate, sediment supply is the other important environmental factor relevant to the dune mobility (Navarro-Pons et al., 2016; Tastet and Pontee, 1998). Abundant sand available for transportation increases the possibility for vegetation burial and dune migration (Hesp, 2013; Aagaard et al., 2007). The main source of sand is commonly the beach as a result of wave action and coastal erosion, although fluvial sediments also frequently feed nearby coastal areas. Among those areas are the dunefields on the SE coast of Mozambique, fed by Limpopo and Incomati rivers (Figure C.2, Appendix C), and various dunes from western Europe fed by La Gironde (France), Douro (Portugal) and the Segura River (Spain).

A few of the investigated dune cases here demonstrate substantial mobility due to excessive sand supplies combined with strong local winds. The sand has either local origin (e.g., Rubjerg Knude dune, Denmark, see Figure C.8, Appendix C; dunes on Isle de Madeleine, Canada), or is brought to the dune site through longshore drift (the Maranhão dunefields, NE Brazil). Furthermore, the dunes on the east coast of Isle de Madeleine are more dynamic than those on the west coast due to higher levels of marine erosion as a result of more energetic waves. Higher sediment supply in the recent years is responsible for maintaining mobile the Aquitaine dune system in France which hosts Dune du Pilat – the largest

active dune in Europe (Figure C.9, Appendix C; Gabarrou et al., 2018). The abundant sediment supply in this case outweighs the effect of local climate, which has been found here to favour greening ($T\uparrow$, $P\uparrow$, $W\downarrow$). For the case of the Rubjerg Knude dune, on the other hand, the local climate may support either mobilisation or stabilisation, depending on the relative importance of wind and precipitation ($T\uparrow$, $P\uparrow$, $W\uparrow$). Gabarrou et al. (2018), however, confirm that strong local winds are responsible for active transportation of the abundant sand eroded from the cliff and the migration of the dune landward. Unlimited sediment supply, combined with drier conditions and very strong winds, drive the identified here mobilisation of Bolonia and Valdevaqueros dune systems (SW Spain), and of Duna de Cresmina (Portugal).

An increased presence of nebkha dunes in arid conditions indicates reduced sediment supply (Hesp et al., 2021; Garcia-Romero et al., 2019). This has been confirmed for the selected Guerrero Negro area, where the sparse nebkha vegetation is reflected in the slowly greening trend (Figure C.5, Appendix C). Reduced sediment supply and negative sediment balance, on the other hand, may explain cases of coastal erosion, such as the beach and dune erosion of Guardamar del Segura coast in Spain, caused by channelisation of the Segura River (Pagán et al., 2017).

4.2.3. Anthropogenic factors

Deviations from the naturally expected changes in the dune mobility detected during this study may be qualitatively explained by anthropogenic influences. The anthropogenic activities may impact significantly the dune vegetation cover and the dune dynamics, with certain human activities intended for stabilisation (e.g., planting, afforestation; Provoost et al., 2011; Arens et al., 2007; Pye et al., 2020), and others leading to sand mobilisation (e.g., introduction of grazers; Pye and Blott, 2017; del Valle et al., 2008; dune rejuvenation programs; Pye and Blott, 2020; Ruessink et al., 2018). In general, previous management practices included widespread stabilisation to protect the coast from flooding, with marram grass planting and afforestation to stop migrating sand initiated in Europe (Provoost et al., 2011; Arens et al., 2007; Pye et al., 2020). Indeed, the present study corroborated that some of the largest key indices describing dense dune vegetation with marked seasonality ($\overline{NDVI}$ and $\Delta NDVI$) correspond to dune sites from N and NW Europe, particularly from Wales and England (Pye et al., 2014). Moreover, trends of warming temperatures and declining wind speeds, which support the stabilisation process, have already been reported for N and NW Europe (Pye et al., 2020; Clemmensen et al., 2017).

Currently, the dune management adopts a more dynamic approach aiming at restoration of the dune mobility and the biodiversity of the dune habitats. Particular cases of mobile dunes here correspond to management attempts to reactivate the foredunes by removing the vegetation cover. An example is the Wadden Island of Terschelling, where a nearly complete remobilisation of the foredune and significant sand burial of the area behind it have been achieved between 1995 and 2000 (Arens et al., 2013). This result has been detected in the trend of the analysed *NDVI* time series here. The restoration proved to

be successful, irrespective of the local climate which promotes greening (as concluded from the meteorological time series). Another successful example is the dynamic restoration at South Kennemerland, where three inland parabolic dunes were reactivated by removal of vegetation and soil, and five notches were excavated through the foredune in 2012 – 2013 (Ruessink et al., 2018), see also Figure 2.5. Restoration projects in the inner dunes, however, demonstrate that simple removal of vegetation may not be enough to remobilise the dunes on a large scale, or at least is not an immediate, long-term solution, as discussed by Hilton and Konlechner (2010), regarding the slow process of marram grass removal and dune restoration on Stewart Island (New Zealand). An example when the greening trend became dominant as a result of drastically reduced population of rabbits (initially introduced to maintain the dune areas open) is the Younghusband Peninsula (Australia), Figure C.6 (Appendix C).

Anthropogenic influence in the dune evolution is apparent for the dune sites in Table 3.1. Common feature between those sites is that the local sparse vegetation cover (quantified through the $\overline{NDVI}$) supports steep vegetation trends, which is against the expectations and the results for the majority of the dune cases here. Some of the dune exceptions show moreover significantly accelerated greening trends over the last decades (Ovari Beach, Thua Thien and Guarda dunes, Figures A.1 – A.2, Appendix A). Evidences that the acceleration is due to stabilisation measures can be found in the literature (Bar and McKenzie, 1976; Mujabar and Chandrasekar, 2012; Nehren et al., 2016). Artificial stabilisation should be considered responsible for excess of greening when dune sites subjected to the same climatic conditions show notably different vegetation patterns, as illustrated in Figure 3.12 for the Mangueira Lagoon dunefields in Brazil.

Finally, Duna de Cresmina (Portugal) can be used as an example of indirect human-induced negative effect on the dune dynamics (Rebêlo et al., 2002). In this case, the infrastructure creates a corridor where wind accelerates. This results in sand accumulation away from the beach and beach erosion. A natural corridor of strong winds also exists for the highly active Valdevaqueros dune system in Spain (Navarro-Pons et al., 2016).

4.3. Uncertainties and limitations of the current study

This study has added to the insight in the trends of stabilisation of the coastal dunes worldwide by confirming that regional and local weather patterns and environmental settings may explain features of the dune dynamics. The obtained results, however, imply uncertainties related on first place with the fact that many of the selected dune systems have experienced human interventions to a different extent. Therefore, the changes that we observe do not reflect dune system responses to only natural forcing which would allow to use the calculated vegetation indices to predict further changes.

In addition, data uncertainties should be taken into account particularly with respect to the *NDVI* time series. Missing data, outliers and errors due to cloudy weather, mainly at sites with humid climates,

may affect the trend estimates. Although this is partially resolved by using non-parametric trend detection method and data pre-processing, it could hinder the identification of jumps by the JUST routine. This is especially true when data are missing around the time of the potential jump, which could be the case in Figure 2.6. Eventually, uncertainties may be introduced through the Sen's slope estimates, which have been used when correlating the dune greening with the main climatic drivers of dune mobility. It has been demonstrated that the Sen's slope uncertainty largely diminishes after reducing the dispersion in the data sample by using the trend of the decomposed *NDVI* signal instead of the signal itself. The comparison between the calculated slopes is illustrated in Figure 3.6.

Finally, limitation of the presented research is that it focuses on quantification of the effects of regional climate on the dune mobility, while providing only a qualitative estimate of the disturbances due to other environmental and anthropogenic factors. Therefore, the study here could be extended to quantify also the magnitude of the non-climatic disturbances. This, as discussed by Delgado-Fernandez et al. (2019), would allow to evaluate what would be the direction of change in the dune system if the artificial disturbances are removed which is important for management practices aiming at restoration of the dune systems to their natural state.

4.4. Management implications

An important result to be taken into consideration for dune management is that under the current climate dunes will continue greening without necessity of further changes in the climatic variables, particularly in the temperature. Moreover, since greening occurs primarily as a response to the regional climate, the coastal management practices should take this into account for successful long-term solutions.

The above also implies that greening is currently naturally occurring, even if it was facilitated by management programs in the past. This refers particularly to dunes evolving in humid settings. Therefore, if the dunes are already fixed (or show stabilisation trends) under the current environmental conditions, attempts for their mobilisation would be equal to disturbance, followed by an attempt for recovery of the system.

When the concern is about loss of natural habitats and biodiversity in the fixed dunes, rejuvenation measures might become a preferred choice for dune management. However, we should also agree with Delgado-Fernandez et al. (2019) that if the aim of dune management is to protect and preserve the natural processes in the dune environments, the dunes should be allowed to recover by natural means. At the same time, restrictions should be imposed to minimise the human-induced stresses.

From the perspective of global warming, it should be also considered that over the last approximately 30 years, the typical flora, at least in Europe, have shown signs of vulnerability to the increasing temperatures. Therefore, what was natural for the dunes 70 years ago, may not adapt to the current conditions if the attempt would be to restore the native species of the dune ecosystems.

5. Conclusions

Based on multitemporal *NDVI* time series retrieved from Landsat imagery at the Climate Engine App (http://climateengine.org/), the first important conclusion from the study is that ongoing dune greening is the dominant trend in the dune evolution worldwide. From all selected dunefields, 87.1% are greening, in contrast to only 9.1% which are either naturally dynamic, or have been remobilised due to management activities to rejuvenate the sandy dune landscapes and ecosystems.

While greening is a global trend, the degree of greening is locally dependent on the average vegetation cover. Faster greening (high Q_{NDVI}) is associated with denser vegetation which explains why this pattern holds typically for dunes from temperate climates (Q_{NDVI} between 0.003 and 0.006 *NDVI*/year). Temperate climates also tend to have the most pronounced seasonality in *NDVI*, due to vegetation phenology.

The second important outcome illustrating the nonlinearity of dune responses to disturbances over time is the observed acceleration in the trends, particularly in the greening trends. A total of 63% of all statistically significant positive and negative trends show acceleration over the second half of the study period, regardless of the initial direction of change. Such acceleration is mainly associated with dunefields from the subtropics and tropics with sparse vegetation canopies.

Another conclusion refers to the link between the expected degree of change in the climatic conditions and the magnitude of vegetation response. Greening shows lack of association with the trends in the climatic variables, since $p > 0.01$ at 1% level of significance. The two possible suggested explanations of this result are: (1) the current climate has already reached temperature and precipitation thresholds so that dunes continue greening irrespective of further changes in the meteorological variables; (2) it is not the climate variables that stimulate vegetation growth, but other natural and/or human-induced factors, such as increased levels of CO_2 and nutrients in the atmosphere, or land use changes.

Greening, however, agrees largely with classes of favourable climatic combinations. About a third of all greening dune sites are linked to combinations of trends in the climatic variables which promote vegetation growth. This result agrees with the hypothesis of Jackson et al. (2019) that dunes are becoming naturally greener in response to climate change and regional climate variability.

In the case of non-greening dunes, it has been inferred that local environmental factors, namely abundant sediment supply along with frequent strong winds, can explain the observed dune mobility, as opposed to situations of limited sediment supply or hindered littoral drift, commonly due to

constructed dams inland or engineering structures for flood protection of the coast which result in dune stabilisation.

Finally, the results from this study suggest that the anthropogenic impact on the vegetation cover and long-term dune dynamics can be significant, including planting and conversely, vegetation removal that stimulates the dune dynamics. In short, their relative importance can be so significant that could outweigh the role of the local climate and other local environmental factors such as sediment supply.

References

Aagaard, T., Orford, J., & Murray, A. S. (2007). Environmental controls on coastal dune formation; Skallingen Spit, Denmark. Geomorphology, 83(1–2), 29–47. https://doi.org/10.1016/j.geomorph.2006.06.007

Abbott, D., Gusiakov, V., Rambolamanana, G., Breger, D., Mazumder, R., & Galinskaya, K. (2016). What are the origins of v-shaped (chevron) dunes in Madagascar? The case for their deposition by a holocene megatsunami. In Sediment Provenance: Influences on Compositional Change from Source to Sink. Elsevier Inc. https://doi.org/10.1016/B978-0-12-803386-9.00008-3

Ajedegba, J. O., Perotto-Baldivieso, H. L., & Jones, K. D. (2019). Coastal Dune Vegetation Resilience on South Padre Island, Texas: A Spatiotemporal Evaluation of the Landscape Structure. Journal of Coastal Research, 35(3), 534–544. https://doi.org/10.2112/JCOASTRES-D-18-00034.1

Anthonsen, K. L., Clemmensen, L. B., & Jensen, J. H. (1996). Evolution of a dune from crescentic to parabolic form in response to short-term climatic changes: Råbjerg Mile, Skagen Odde, Denmark. Geomorphology, 17(1-3 SPEC. ISS.), 63–77. https://doi.org/10.1016/0169-555x(95)00091-i

Arens, S. M., & Geelen, L. H. W. T. (2006). Dune landscape rejuvenation by intended destabilisation in the Amsterdam water supply dunes. Journal of Coastal Research, 22(5), 1094–1107. https://doi.org/10.2112/04-0238.1

Arens, S. M., Mulder, J. P. M., Slings, Q. L., Geelen, L. H. W. T., & Damsma, P. (2013). Dynamic dune management, integrating objectives of nature development and coastal safety: Examples from the Netherlands. Geomorphology, 199, 205–213. https://doi.org/10.1016/j.geomorph.2012.10.034

Arens, S. M, Slings, Q. L., Geelen, L. H. W. T., & Van der Hagen, H. G. J. M. (2007). Implications of environmental change for dune mobility in the Netherlands. International Conference on Management and Restoration of Coastal Dunes, Minist. de Medio Ambiente, Santander, Spain., January 2007, 3–5.

Avis, A. M. (1989). A review of coastal dune stabilisation in the Cape Province of South Africa. Landscape and Urban Planning, 18(1), 55–68. https://doi.org/10.1016/0169-2046(89)90055-8

Awty-Carroll, K., Bunting, P., Hardy, A., & Bell, G. (2019). An evaluation and comparison of four dense time series change detection methods using simulated data. Remote Sensing, 11(23). https://doi.org/10.3390/rs11232779

Barbosa, L. M., & Dominguez, J. M. L. (2004). Coastal dune fields at the São Francisco River strandplain, northeastern Brazil: Morphology and environmental controls. Earth Surface Processes and Landforms, 29(4), 443–456. https://doi.org/10.1002/esp.1040

Barr, D. A., & McKenzie, J. B. (1976). Dune stabilisation in Queensland, Australia, using vegetation and mulches. International Journal of Biometeorology, 20(1), 1–8. https://doi.org/10.1007/BF01553165

Botha, G. A., Bristow, C. S., Porat, N., Duller, G., Armitage, S. J., Roberts, H. M., Clarke, B. M., Kota, M. W., & Schoeman, P. (2003). Evidence for dune reactivation from GPR profiles on the Maputaland coastal plain, South Africa. Geological Society Special Publication, 211(July 2014), 29–46. https://doi.org/10.1144/GSL.SP.2001.211.01.03

Buynevich, I. V., Filho, P. W. M. S., & Asp, N. E. (2010). Dune advance into a coastal forest, equatorial Brazil: A subsurface perspective. Aeolian Research, 2(1), 27–32. https://doi.org/10.1016/j.aeolia.2009.11.001

Clarke, M., Rendell, H., Tastet, J. P., Clave, B., & Masse, L. (2002). Late-Holocene sand invasion and North Atlantic storminess along the Aquitaine coast, southwest France. Holocene, 12(2), 231–238. https://doi.org/10.1191/0959683602hl539rr

Claudino-Sales, V., Wang, P., & Horwitz, M. H. (2008). Factors controlling the survival of coastal dunes during multiple hurricane impacts in 2004 and 2005: Santa Rosa barrier island, Florida. Geomorphology, 95(3–4), 295–315. https://doi.org/10.1016/j.geomorph.2007.06.004

Clemmensen, L. B., Hansen, K. W. T., & Kroon, A. (2014). Storminess variation at Skagen, northern Denmark since AD 1860: Relations to climate change and implications for coastal dunes. Aeolian Research, 15, 101–112. https://doi.org/10.1016/j.aeolia.2014.09.001

Clemmensen, L. B., & Murray, A. (2006). The termination of the last major phase of aeolian sand movement, coastal dunefields, Denmark. Earth Surface Processes and Landforms, 31(7), 795–808. https://doi.org/10.1002/esp.1283

Cooper, J. A. G., & Pilkey, O. H. (2002). The Barrier Islands of Southern Mozambique. Journal of Coastal Research, 36(36), 164–172. https://doi.org/10.2112/1551-5036-36.sp1.164

Costas, S., Naughton, F., Goble, R., & Renssen, H. (2016). Windiness spells in SW Europe since the last glacial maximum. Earth and Planetary Science Letters, 436, 82–92. https://doi.org/10.1016/j.epsl.2015.12.023

da Silva, G. M., & Hesp, P. A. (2013). Increasing rainfall, decreasing winds, and historical changes in Santa Catarina dunefields, southern Brazil. Earth Surface Processes and Landforms, 38(9), 1036–1045. https://doi.org/10.1002/esp.3390

da Silva, G. M., Martinho, C. T., Hesp, P., Keim, B. D., & Ferligoj, Y. (2013). Changes in dunefield geomorphology and vegetation cover as a response to local and regional climate variations. Journal of Coastal Research, 165, 1307–1312. https://doi.org/10.2112/si65-221.1

Davidson-Arnott, R. G. D., & Law, M. N. (1996). Measurement and prediction of long-term sediment supply to coastal foredunes. Journal of Coastal Research, 12(3), 654–663.

Davidson-Arnott, R., Hesp, P., Ollerhead, J., Walker, I., Bauer, B., Delgado-Fernandez, I., & Smyth, T. (2018). Sediment budget controls on foredune height: Comparing simulation model results with field data. Earth Surface Processes and Landforms, 43(9), 1798–1810. https://doi.org/10.1002/esp.4354

de Jong, R., de Bruin, S., de Wit, A., Schaepman, M. E., & Dent, D. L. (2011). Analysis of monotonic greening and browning trends from global NDVI time-series. Remote Sensing of Environment, 115(2), 692–702. https://doi.org/10.1016/j.rse.2010.10.011

de Jong, R., Verbesselt, J., Schaepman, M. E., & de Bruin, S. (2012). Trend changes in global greening and browning: Contribution of short-term trends to longer-term change. Global Change Biology, 18(2), 642–655. https://doi.org/10.1111/j.1365-2486.2011.02578.x

de Jong, R., Verbesselt, J., Zeileis, A., & Schaepman, M. E. (2013). Shifts in global vegetation activity trends. Remote Sensing, 5(3), 1117–1133. https://doi.org/10.3390/rs5031117

del Valle, H. F., Rostagno, C. M., Coronato, F. R., Bouza, P. J., & Blanco, P. D. (2008). Sand dune activity in north-eastern Patagonia. Journal of Arid Environments, 72(4), 411–422. https://doi.org/10.1016/j.jaridenv.2007.07.011

Delgado-Fernandez, I., & Davidson-Arnott, R. (2011). Meso-scale aeolian sediment input to coastal dunes: The nature of aeolian transport events. Geomorphology, 126(1–2), 217–232. https://doi.org/10.1016/j.geomorph.2010.11.005

Delgado-Fernandez, I., O'Keeffe, N., & Davidson-Arnott, R. G. D. (2019). Natural and human controls on dune vegetation cover and disturbance. Science of the Total Environment, 672, 643–656. https://doi.org/10.1016/j.scitotenv.2019.03.494

Esteves, L. S., Brown, J. M., Williams, J. J., & Lymbery, G. (2012). Quantifying thresholds for significant dune erosion along the Sefton Coast, Northwest England. Geomorphology, 143–144, 52–61. https://doi.org/10.1016/j.geomorph.2011.02.029

Evans, J., & Geerken, R. (2004). Discrimination between climate and human-induced dryland degradation. Journal of Arid Environments, 57(4), 535–554. https://doi.org/10.1016/S0140-1963(03)00121-6

Everard, M., Jones, L., & Watts, B. (2010). Have we neglected the societal importance of sand dunes? An ecosystem services perspective. Aquatic Conservation: Marine and Freshwater Ecosystems, 20(4), 476–487. https://doi.org/10.1002/aqc.1114

Ewing, R. C., & Kocurek, G. (2010). Aeolian dune-field pattern boundary conditions. Geomorphology, 114(3), 175–187. https://doi.org/10.1016/j.geomorph.2009.06.015

Feagin, Rusty A., Figlus, J., Zinnert, J. C., Sigren, J., Martínez, M. L., Silva, R., Smith, W. K., Cox, D., Young, D. R., & Carter, G. (2015). Going with the flow or against the grain? The promise of vegetation for protecting beaches, dunes, and barrier islands from erosion. Frontiers in Ecology and the Environment, 13(4), 203–210. https://doi.org/10.1890/140218

Forkel, M., Carvalhais, N., Verbesselt, J., Mahecha, M. D., Neigh, C. S. R., & Reichstein, M. (2013). Trend Change detection in NDVI time series: Effects of inter-annual variability and methodology. Remote Sensing, 5(5), 2113–2144. https://doi.org/10.3390/rs5052113

Reckendorf, D. L., Robert Baum, J. C. (2019). Stabilisation of Sand Dunes in Oregon Author (s): Frank Reckendorf , Don Leach , Robert Baum and Jack Carlson Source : Agricultural History , Vol . 59 , No . 2 , The History of Soil and Water Conservation : A Symposium (Apr ., 1985), pp . 260-268 Publ. 59(2), 260–268.

Fryberger, S. G., Krystinik, L. F., & Schenk, C. J. (1990). Tidally flooded back-barrier dunefield, Guerrero Negro area, Baja California, Mexico. Sedimentology, 37(1), 23–43. https://doi.org/10.1111/j.1365-3091.1990.tb01981.x

Gabarrou, S., Le Cozannet, G., Parteli, E. J. R., Pedreros, R., Guerber, E., Millescamps, B., Mallet, C., & Oliveros, C. (2018). Modelling the Retreat of a Coastal Dune under Changing Winds. Journal of Coastal Research, 85(85), 166–170. https://doi.org/10.2112/SI85-034.1

Gao, J., Kennedy, D. M., & Konlechner, T. M. (2020). Coastal dune mobility over the past century: A global review. Progress in Physical Geography, 44(6), 814–836. https://doi.org/10.1177/0309133320919612

Garcia-Lozano, C., Pintó, J., & Daunis-i-Estadella, P. (2018). Changes in coastal dune systems on the Catalan shoreline (Spain, NW Mediterranean Sea). Comparing dune landscapes between 1890 and 1960 with their current status. Estuarine, Coastal and Shelf Science, 208(December 2016), 235–247. https://doi.org/10.1016/j.ecss.2018.05.004

García-Romero, L., Delgado-Fernández, I., Hesp, P. A., Hernández-Calvento, L., Hernández-Cordero, A. I., & Viera-Pérez, M. (2019). Biogeomorphological processes in an arid transgressive dunefield as indicators of human impact by urbanization. Science of the Total Environment, 650, 73–86. https://doi.org/10.1016/j.scitotenv.2018.08.429

García-Romero, L., Delgado-Fernández, I., Hesp, P. A., Hernández-Calvento, L., Viera-Pérez, M., Hernández-Cordero, A. I., Cabrera-Gámez, J., & Domínguez-Brito, A. C. (2019a). Airflow dynamics, vegetation and aeolian erosive processes in a shadow zone leeward of a resort in an arid transgressive dune system. Aeolian Research, 38(March), 48–59. https://doi.org/10.1016/j.aeolia.2019.03.006

García-Romero, L., Delgado-Fernández, I., Hesp, P. A., Hernández-Calvento, L., Viera-Pérez, M., Hernández-Cordero, A. I., Cabrera-Gámez, J., & Domínguez-Brito, A. C. (2019b). Airflow dynamics, vegetation and aeolian erosive processes in a shadow zone leeward of a resort in an arid transgressive dune system. Aeolian Research, 38(April), 48–59. https://doi.org/10.1016/j.aeolia.2019.03.006

García-Romero, L., Hesp, P. A., Peña-Alonso, C., Miot da Silva, G., & Hernández-Calvento, L. (2019). Climate as a control on foredune mode in Southern Australia. Science of the Total Environment, 694, 133768. https://doi.org/10.1016/j.scitotenv.2019.133768

Gaspar de Freitas, J. (2021). Dune (s): Fiction, history, and science on the Oregon coast . The Anthropocene Review, 205301962110568. https://doi.org/10.1177/20530196211056814

Ghaderpour, E. (2021). JUST: MATLAB and python software for change detection and time series analysis. GPS Solutions, 25(3), 1–7. https://doi.org/10.1007/s10291-021-01118-x

Ghaderpour, E., & Pagiatakis, S. D. (2017). Least squares wavelet analysis of unequally spaced and non-stationary time series and its applications. Math Geosciences, 49(7), 819-844.

Ghaderpour, E., & Vujadinovic, T. (2020). Change detection within remotely sensed satellite image time series via spectral analysis. Remote Sensing, 12(23), 1–27. https://doi.org/10.3390/rs12234001

Girardi, J. D., & Davis, D. M. (2010). Parabolic dune reactivation and migration at Napeague, NY, USA: Insights from aerial and GPR imagery. Geomorphology, 114(4), 530–541. https://doi.org/10.1016/j.geomorph.2009.08.011

Gocic, M., & Trajkovic, S. (2013). Analysis of changes in meteorological variables using Mann-Kendall and Sen's slope estimator statistical tests in Serbia. Global and Planetary Change, 100, 172–182. https://doi.org/10.1016/j.gloplacha.2012.10.014

Goḿez-Pina, G., Muñoz-Ṕerez, J. J., Ramírez, J. L., & Ley, C. (2002). Sand dune management problems and techniques, Spain. Journal of Coastal Research, SPEC. ISSUE 36, 325–332. https://doi.org/10.2112/1551-5036-36.sp1.325

Harris, L., Nel, R., & Schoeman, D. (2011). Mapping beach morphodynamics remotely: A novel application tested on South African sandy shores. Estuarine, Coastal and Shelf Science, 92(1), 78–89. https://doi.org/10.1016/j.ecss.2010.12.013

Harvey, N. (2006). Holocene coastal evolution: Barriers, beach ridges, and tidal flats of South Australia. Journal of Coastal Research, 22(1), 90–99. https://doi.org/10.2112/05A-0008.1

Hawinkel, P., Swinnen, E., Lhermitte, S., Verbist, B., Van Orshoven, J., & Muys, B. (2015). A time series processing tool to extract climate-driven interannual vegetation dynamics using Ensemble Empirical Mode Decomposition (EEMD). Remote Sensing of Environment, 169, 375–389. https://doi.org/10.1016/j.rse.2015.08.024

Helsel, D. R., Hirsch, R. M., Ryberg, K. R., Archfield, S. A., & Gilroy, E. J. (2020). Statistical Methods in Water Resources Techniques and Methods 4 – A3. USGS Techniques and Methods.

Héquette, A., Ruz, M., Zemmour, A., Marin, D., Sipka, V., Héquette, A., Ruz, M., Zemmour, A., Marin, D., & Cartier, A. (2021). Alongshore Variability in Coastal Dune Erosion and Post-Storm Recovery , Northern Coast of France Source : Journal of Coastal Research , Special Issue No . 88 : Coastal Evolution under Climate Linked references are available on JSTOR for this article : Al.

Hernández-Calvento, L., Jackson, D. W. T., Medina, R., Hernández-Cordero, A. I., Cruz, N., & Requejo, S. (2014). Downwind effects on an arid dunefield from an evolving urbanised area. Aeolian Research, 15, 301–309. https://doi.org/10.1016/j.aeolia.2014.06.007

Hernández-Cordero, A. I., Hernández-Calvento, L., Hesp, P. A., & Pérez-Chacón, E. (2018). Geomorphological changes in an arid transgressive coastal dune field due to natural processes and human impacts. Earth Surface Processes and Landforms, 43(10), 2167–2180. https://doi.org/10.1002/esp.4382

Hesp, P. (2002). Foredunes and blowouts: initiation, geomorphology and dynamics. Geomorphology, 48(1–3), 245–268. https://doi.org/10.1016/S0169-555X(02)00184-8

Hesp, P. A., Hernández-Calvento, L., Gallego-Fernández, J. B., Miot da Silva, G., Hernández-Cordero, A. I., Ruz, M. H., & Romero, L. G. (2021). Nebkha or not? -Climate control on foredune mode. Journal of Arid Environments, 187(January). https://doi.org/10.1016/j.jaridenv.2021.104444

Hesp, P. (2013). Conceptual models of the evolution of transgressive dune field systems. Geomorphology, 199, 138–149. https://doi.org/10.1016/j.geomorph.2013.05.014

Hilbert, N. N., Guedes, C. C. F., & Giannini, P. C. F. (2016). Morphologic and sedimentologic patterns of active aeolian dune-fields on the east coast of Maranhão, northeast Brazil. Earth Surface Processes and Landforms, 41(1), 87–97. https://doi.org/10.1002/esp.3786

Hilton, M., Harvey, N., Hart, A., James, K., & Arbuckle, C. (2006). The impact of exotic dune grass species on foredune development in Australia and New Zealand: A case study of Ammophila arenaria and Thinopyrum junceiforme. Australian Geographer, 37(3), 313–334. https://doi.org/10.1080/00049180600954765

Hilton, M. J., & Konlechner, T. M. (2010). A review of the marram grass eradication Programme (1999 – 2009), Stewart Island, New Zealand. The New Zealand Plant Protection Society Inc. and the Council of Australasian Weed Societies Inc. - 17th Australasian Weeds Conference, 26-30 Sept(i), 386–389.

Hinkel, J., Nicholls, R. J., Tol, R. S. J., Wang, Z. B., Hamilton, J. M., Boot, G., Vafeidis, A. T., McFadden, L., Ganopolski, A., & Klein, R. J. T. (2013). A global analysis of erosion of sandy beaches and sea-level rise: An application of DIVA. Global and Planetary Change, 111, 150–158. https://doi.org/10.1016/j.gloplacha.2013.09.002

Houser, C., Hapke, C., & Hamilton, S. (2008). Controls on coastal dune morphology, shoreline erosion and barrier island response to extreme storms. Geomorphology, 100(3–4), 223–240. https://doi.org/10.1016/j.geomorph.2007.12.007

Houser, C., Wernette, P., Rentschlar, E., Jones, H., Hammond, B., & Trimble, S. (2015). Post-storm beach and dune recovery: Implications for barrier island resilience. Geomorphology, 234, 54–63. https://doi.org/10.1016/j.geomorph.2014.12.044

Huang, H., Zinnert, J. C., Wood, L. K., Young, D. R., & D'Odorico, P. (2018). Non-linear shift from grassland to shrubland in temperate barrier islands. Ecology, 99(7), 1671–1681. https://doi.org/10.1002/ecy.2383

Hugenholtz, C. H., & Wolfe, S. A. (2005). Recent stabilisation of active sand dunes on the Canadian prairies and relation to recent climate variations. Geomorphology, 68(1–2), 131–147. https://doi.org/10.1016/j.geomorph.2004.04.009

Huntington, J. L., Hegewisch, K. C., Daudert, B., Morton, C. G., Abatzoglou, J. T., McEvoy, D. J., & Erickson, T. (2017). Climate engine: Cloud computing and visualization of climate and remote sensing data for advanced natural resource monitoring and process understanding. Bulletin of the American Meteorological Society, 98(11), 2397–2409. https://doi.org/10.1175/BAMS-D-15-00324.1

Irish, J. L., Lynett, P. J., Weiss, R., Smallegan, S. M., & Cheng, W. (2013). Buried relic seawall mitigates Hurricane Sandy's impacts. Coastal Engineering, 80, 79–82. https://doi.org/10.1016/j.coastaleng.2013.06.001

Jackson, D. W.T., & Cooper, J. A. G. (2011). Coastal dune fields in Ireland: Rapid regional response to climatic change. Journal of Coastal Research, SPEC. ISSUE 64, 293–297.

Jackson, Derek W.T., Costas, S., González-Villanueva, R., & Cooper, A. (2019). A global 'greening' of coastal dunes: An integrated consequence of climate change? Global and Planetary Change, 182(June), 103026. https://doi.org/10.1016/j.gloplacha.2019.103026

Jackson, N. L., & Nordstrom, K. F. (2011). Aeolian sediment transport and landforms in managed coastal systems: A review. Aeolian Research, 3(2), 181–196. https://doi.org/10.1016/j.aeolia.2011.03.011

Jewell, M., Houser, C., & Trimble, S. (2014). Initiation and evolution of blowouts within Padre Island National Seashore, Texas. Ocean and Coastal Management, 95, 156–164. https://doi.org/10.1016/j.ocecoaman.2014.04.019

Jimenez, J. A., Maia, L. P., Serra, J., & Morais, J. (1999). Aeolian dune migration along the Cearâ coast, north-eastern Brazil. Sedimentology, 46(4), 689–701. https://doi.org/10.1046/j.1365-3091.1999.00240.x

Kirkpatrick, J. B., & Hassall, D. C. (1981). Vegetation of the Sigatoka sand dunes, fiji. New Zealand Journal of Botany, 19(3), 285–297. https://doi.org/10.1080/0028825X.1981.10426381

Konlechner, T. M., Ryu, W., Hilton, M. J., & Sherman, D. J. (2015). Evolution of foredune texture following dynamic restoration, Doughboy Bay, Stewart Island, New Zealand. Aeolian Research, 19, 203–214. https://doi.org/10.1016/j.aeolia.2015.06.003

Lancaster, N., & Helm, P. (2000). A test of a climatic index of dune mobility using measurements from the southwestern United States. Earth Surface Processes and Landforms, 25(2), 197–207. https://doi.org/10.1002/(SICI)1096-9837(200002)25:2<197::AID-ESP82>3.0.CO;2-H

Levin, N. (2011). Climate-driven changes in tropical cyclone intensity shape dune activity on Earth's largest sand island. Geomorphology, 125(1), 239–252. https://doi.org/10.1016/j.geomorph.2010.09.021

Levin, N., Jablon, P. E., Phinn, S., & Collins, K. (2017). Coastal dune activity and foredune formation on Moreton Island, Australia, 1944–2015. Aeolian Research, 25, 107–121. https://doi.org/10.1016/j.aeolia.2017.03.005

Levin, N., Tsoar, H., Herrmann, H. J., Maia, L. P., & Claudino-Sales, V. (2009). Modelling the formation of residual dune ridges behind barchan dunes in north-east Brazil. Sedimentology, 56(6), 1623–1641. https://doi.org/10.1111/j.1365-3091.2009.01048.x

Luisa Martínez, M., Mendoza-González, G., Silva-Casarín, R., & Mendoza-Baldwin, E. (2014). Land use changes and sea level rise may induce a "coastal squeeze" on the coasts of Veracruz, Mexico. Global Environmental Change, 29, 180–188. https://doi.org/10.1016/j.gloenvcha.2014.09.009

Maia, L. P., Freire, G. S. S., & Lacerda, L. D. (2005). Accelerated dune migration and aeolian transport during El Niño events along the NE Brazilian coast. Journal of Coastal Research, 21(6), 1121–1126. https://doi.org/10.2112/03-702A.1

Mann, H. B. (1945). Non-Parametric Test Against Trend. Econometrica, 13(3), 245–259. http://www.economist.com/node/18330371?story%7B_%7Did=18330371

Marcomini, S. C., & Maidana, N. (2006). Response of Eolian Ecosystems To Minor Climatic Changes. Journal of Coastal Research, 2004(39), 204–208.

Martínez, B., & Gilabert, M. A. (2009). Vegetation dynamics from NDVI time series analysis using the wavelet transform. Remote Sensing of Environment, 113(9), 1823–1842. https://doi.org/10.1016/j.rse.2009.04.016

Martínez, M. L., Landgrave, R., Silva, R., & Hesp, P. (2019). Shoreline Dynamics and Coastal Dune Stabilisation in Response to Changes in Infrastructure and Climate. Journal of Coastal Research, 92(sp1), 6. https://doi.org/10.2112/si92-002.1

Martinho, C. T., Hesp, P. A., & Dillenburg, S. R. (2010). Morphological and temporal variations of transgressive dunefields of the northern and mid-littoral Rio Grande do Sul coast, Southern Brazil. Geomorphology, 117(1–2), 14–32. https://doi.org/10.1016/j.geomorph.2009.11.002

Mathew, S., Davidson-Arnott, R. G. D., & Ollerhead, J. (2010). Evolution of a beach-dune system following a catastrophic storm overwash event: Greenwich Dunes, Prince Edward Island, 1936-2005. Canadian Journal of Earth Sciences, 47(3), 273–290. https://doi.org/10.1139/E09-078

Mendes, V. R., & Giannini, P. C. F. (2015). Coastal dunefields of south Brazil as a record of climatic changes in the South American Monsoon System. Geomorphology, 246, 22–34. https://doi.org/10.1016/j.geomorph.2015.05.034

Miccadei, E., Mascioli, F., Piacentini, T., & Ricci, F. (2011). Geomorphological features of coastal dunes along the central adriatic coast (Abruzzo, Italy). Journal of Coastal Research, 27(6), 1122–1136. https://doi.org/10.2112/JCOASTRES-D-10-00161.1

Miguel, L. L. A. J., & Castro, J. W. A. (2018). Aeolian dynamics of transgressive dunefields on the southern Mozambique coast, Africa. Earth Surface Processes and Landforms, 43(12), 2533–2546. https://doi.org/10.1002/esp.4413

Miguel, L. L. A. J., Nehama, F. P. J., & Castro, J. W. A. (2019). Lagoon-barrier system response to recent climate conditions and sea level rise, Mozambique, Africa. Estuarine, Coastal and Shelf Science, 216, 71–86. https://doi.org/10.1016/j.ecss.2017.12.013

Miot da Silva, G., & Hesp, P. (2010). Coastline orientation, aeolian sediment transport and foredune and dunefield dynamics of Moçambique Beach, Southern Brazil. Geomorphology, 120(3–4), 258–278. https://doi.org/10.1016/j.geomorph.2010.03.039

Moulton, M. A. B., Hesp, P. A., Miot da Silva, G., Bouchez, C., Lavy, M., & Fernandez, G. B. (2019). Changes in vegetation cover on the Younghusband Peninsula transgressive dunefields (Australia) 1949–2017. Earth Surface Processes and Landforms, 44(2), 459–470. https://doi.org/10.1002/esp.4508

Mujabar, P. S., & Chandrasekar, N. (2012). Dynamics of coastal landform features along the southern Tamil Nadu of India by using remote sensing and Geographic Information System. Geocarto International, 27(4), 347–370. https://doi.org/10.1080/10106049.2011.638988

Muñoz-Reinoso, J. C. (2018). Doñana mobile dunes: what is the vegetation pattern telling us? Journal of Coastal Conservation, 22(4), 605–614. https://doi.org/10.1007/s11852-018-0594-0

Myneni, R. B., Hall, F. G., Sellers, P. J., & Marshak, A. L. (1995). Interpretation of spectral vegetation indexes. IEEE Transactions on Geoscience and Remote Sensing, 33(2), 481–486. https://doi.org/10.1109/36.377948

Navarro-Pons, M., Muñoz-Pérez, J. J., Román-Sierra, J., & García, S. (2016). Evidencias del incremento en la movilidad de dunas costeras en el último medio siglo como respuesta a la intervención humana. Scientia Marina, 80(2), 261–272. https://doi.org/10.3989/scimar.04336.16A

Nehren, U., Thai, H. H. D., Marfai, M. A., Raedig, C., Alfonso, S., Sartohadi, J., & Castro, C. (2016). Ecosystem services of coastal dune systems for hazard mitigation: Case studies from Vietnam, Indonesia, and Chile. In Advances in Natural and Technological Hazards Research (Vol. 42). https://doi.org/10.1007/978-3-319-43633-3_18

Nicholls, R. J., & De La Vega-Leinert, A. C. (2008). Implications of sea-level rise for Europe's coasts: An introduction. Journal of Coastal Research, 24(2), 285–287. https://doi.org/10.2112/07A-0002.1

Nordstrom, K. F., & Arens, S. M. (1998). The role of human actions in evolution and management of foredunes in The Netherlands and New Jersey, USA. Journal of Coastal Conservation, 4(2), 169–180. https://doi.org/10.1007/BF02806509

Nordstrom, Karl F., Lampe, R., & Vandemark, L. M. (2000). Reestablishing naturally functioning dunes on developed coasts. Environmental Management, 25(1), 37–51. https://doi.org/10.1007/s002679910004

Osswald, F., Dolch, T., & Reise, K. (2019). Remobilising stabilized island dunes for keeping up with sea level rise? Journal of Coastal Conservation, 23(3), 675–687. https://doi.org/10.1007/s11852-019-00697-9

Pagán, J. I., López, I., Aragonés, L., & Garcia-Barba, J. (2017). The effects of the anthropic actions on the sandy beaches of Guardamar del Segura, Spain. Science of the Total Environment, 601–602, 1364–1377. https://doi.org/10.1016/j.scitotenv.2017.05.272

Peyrat, J., Braun, M., Dolnik, C., Isermann, M., & Roweck, H. (2009). Vegetation dynamics on the Łeba Bar/Poland: A comparison of the vegetation in 1932 and 2006 with special regard to endangered habitats. Journal of Coastal Conservation, 13(4), 235–246. https://doi.org/10.1007/s11852-009-0073-8

Pickart, A. J., & Hesp, P. A. (2019). Spatio-temporal geomorphological and ecological evolution of a transgressive dunefield system, Northern California, USA. Global and Planetary Change, 172(September 2018), 88–103. https://doi.org/10.1016/j.gloplacha.2018.09.012

Provoost, S., Jones, M. L. M., & Edmondson, S. E. (2011). Changes in landscape and vegetation of coastal dunes in northwest Europe: A review. Journal of Coastal Conservation, 15(1), 207–226. https://doi.org/10.1007/s11852-009-0068-5

Psuty, N. P., & Silveira, T. M. (2010). Global climate change: An opportunity for coastal dunes?? Journal of Coastal Conservation, 14(2), 153–160. https://doi.org/10.1007/s11852-010-0089-0

Pye, K., & Blott, S. J. (2017). Evolution of a sediment-starved, over-stabilised dunefield: Kenfig Burrows, South Wales, UK. Journal of Coastal Conservation, 21(5), 685–717. https://doi.org/10.1007/s11852-017-0506-8

Pye, Kenneth, & Blott, S. J. (2020). Is 're-mobilisation' nature restoration or nature destruction? A commentary. Discussion. Journal of Coastal Conservation, 24(1), 2–5. https://doi.org/10.1007/s11852-020-00730-2

Rebêlo, L. P., Brito, P. O., & Monteiro, J. H. (2002). Monitoring the Cresmina dune evolution (Portugal) using differential GPS. Journal of Coastal Research, 36(36), 591–604. https://doi.org/10.2112/1551-5036-36.sp1.591

Rodríguez-Ramírez, A., Morales, J. A., Delgado, I., & Cantano, M. (2008). The impact of man on the morphodynamics of the Huelva coast (SW Spain). Journal of Iberian Geology, 34(2), 73–108. https://doi.org/10.5209/JIGE.33895

Ruessink, B. G., Arens, S. M., Kuipers, M., & Donker, J. J. A. (2018). Coastal dune dynamics in response to excavated foredune notches. Aeolian Research, 31, 3–17. https://doi.org/10.1016/j.aeolia.2017.07.002

Saye, S. E., Pye, K., & Clemmensen, L. B. (2006). Development of a cliff-top dune indicated by particle size and geochemical characteristics: Rubjerg Knude, Denmark. Sedimentology, 53(1), 1–21. https://doi.org/10.1111/j.1365-3091.2005.00749.x

Sayre, R., Karagulle, D., Frye, C., Boucher, T., Wolff, N. H., Breyer, S., Wright, D., Martin, M., Butler, K., Van Graafeiland, K., Touval, J., Sotomayor, L., McGowan, J., Game, E. T., & Possingham, H. (2020). An assessment of the representation of ecosystems in global protected areas using new maps of World Climate Regions and World Ecosystems. Global Ecology and Conservation, 21, e00860. https://doi.org/10.1016/j.gecco.2019.e00860

Schlacher, T. A., Dugan, J., Schoeman, D. S., Lastra, M., Jones, A., Scapini, F., McLachlan, A., & Defeo, O. (2007). Sandy beaches at the brink. Diversity and Distributions, 13(5), 556–560. https://doi.org/10.1111/j.1472-4642.2007.00363.x

Sen, P. K. (1968). Estimates of the Regression Coefficient Based on Kendall ' s Tau Author (s): Pranab Kumar Sen Source : Journal of the American Statistical Association , Vol . 63 , No . 324 (Dec ., 1968), pp . Published by : Taylor & Francis , Ltd . on behalf of the A. Journal of the American Statistical Association, 63(324), 1379–1389. https://www.jstor.org/stable/2285891

Sytnik, O., & Stecchi, F. (2015). Disappearing coastal dunes: tourism development and future challenges, a case-study from Ravenna, Italy. Journal of Coastal Conservation, 19(5), 715–727. https://doi.org/10.1007/s11852-014-0353-9

Syvitski, J. P. M., Vörösmarty, C. J., Kettner, A. J., & Green, P. (2005). Impact of humans on the flux of terrestrial sediment to the global coastal ocean. Science, 308(5720), 376–380. https://doi.org/10.1126/science.1109454

Taminskas, J., Šimanauskienė, R., Linkevičienė, R., Volungevičius, J., Slavinskienė, G., Povilanskas, R., & Satkūnas, J. (2020). Impact of hydro-climatic changes on coastal dunes landscape according to normalized difference vegetation index (The case study of curonian spit). Water (Switzerland), 12(11), 1–18. https://doi.org/10.3390/w12113234

Tastet, J. P., & Pontee, N. I. (1998). Morpho=chronology of coastal dunes in Medoc. A new interpretation of Holocene dunes in southwestern France. Geomorphology, 25(1–2), 93–109. https://doi.org/10.1016/S0169-555X(98)00035-X

Tribe, H. M., & Kennedy, D. M. (2010). The geomorphology and evolution of a large barrier spit: Farewell Spit, New Zealand. Earth Surface Processes and Landforms, 35(15), 1751–1762. https://doi.org/10.1002/esp.2009

Tsoar, H. (2005). Sand dunes mobility and stability in relation to climate. Physica A: Statistical Mechanics and Its Applications, 357(1), 50–56. https://doi.org/10.1016/j.physa.2005.05.067

Tsoar, Haim, Levin, N., Porat, N., Maia, L. P., Herrmann, H. J., Tatumi, S. H., & Claudino-Sales, V. (2009). The effect of climate change on the mobility and stability of coastal sand dunes in Ceará State (NE Brazil). Quaternary Research, 71(2), 217–226. https://doi.org/10.1016/j.yqres.2008.12.001

Tucker, C. J. (1979). Red and photographic infrared linear combinations for monitoring vegetation. Remote Sensing of Environment, 8(2), 127–150. https://doi.org/10.1016/0034-4257(79)90013-0

van der Biest, K., De Nocker, L., Provoost, S., Boerema, A., Staes, J., & Meire, P. (2017). Dune dynamics safeguard ecosystem services. Ocean and Coastal Management, 149, 148–158. https://doi.org/10.1016/j.ocecoaman.2017.10.005

van der Meulen, F., van der Valk, B., Baars, L., Schoor, E., & van Woerden, H. (2014). Development of new dunes in the Dutch Delta: nature compensation and 'building with nature.' Journal of Coastal Conservation, 18(5), 505–513. https://doi.org/10.1007/s11852-014-0315-2

Verbesselt, J., Hyndman, R., Newnham, G., & Culvenor, D. (2010). Detecting trend and seasonal changes in satellite image time series. Remote Sensing of Environment, 114(1), 106–115. https://doi.org/10.1016/j.rse.2009.08.014

Verbesselt, J., Hyndman, R., Zeileis, A., & Culvenor, D. (2010). Phenological change detection while accounting for abrupt and gradual trends in satellite image time series. Remote Sensing of Environment, 114(12), 2970–2980. https://doi.org/10.1016/j.rse.2010.08.003

Vimpere, L., Kindler, P., & Castelltort, S. (2019). Chevrons: Origin and relevance for the reconstruction of past wind regimes. Earth-Science Reviews, 193(April), 317–332. https://doi.org/10.1016/j.earscirev.2019.04.005

Wilson, P., Orford, J. D., Knight, J., Braley, S. M., & Wintle, A. G. (2001). Late-Holocene (post-4000. 2, 215–229.

Yan, N., & Baas, A. C. W. (2015). Parabolic dunes and their transformations under environmental and climatic changes: Towards a conceptual framework for understanding and prediction. Global and Planetary Change, 124, 123–148. https://doi.org/10.1016/j.gloplacha.2014.11.010

Young, D. R., Brantley, S. T., Zinnert, J. C., & Vick, J. K. (2011). Landscape position and habitat polygons in a dynamic coastal environment. Ecosphere, 2(6), art71. https://doi.org/10.1890/es10-00186.1

Zazo, C., Mercier, N., Silva, P. G., Dabrio, C. J., Goy, J. L., Roquero, E., Soler, V., Borja, F., Lario, J., Polo, D., & de Luque, L. (2005). Landscape evolution and geodynamic controls in the Gulf of Cadiz (Huelva coast, SW Spain) during the Late Quaternary. Geomorphology, 68(3–4), 269–290. https://doi.org/10.1016/j.geomorph.2004.11.022

Appendix A. Steep greening trends associated with low vegetation cover

This Appendix gives a detailed description of the four dunefields with the largest identified trend slopes (see Table 3.1).

Figure A.1(a) presents the Ovari beach dunefield, which is located on the coast of SE India in tropical savannah climate. Mujabar and Chandrasekar (2012) report significant aeolian activity at the coast and dunes of up to 40 m and higher. However, they also report that due to both natural factors and human interventions (among which intensive sand mining), between 1999 and 2006 the coast has suffered severe erosion and reduction of sandy areas. These changes are detectable in the trend in Figure A.1(c) as a small decrease in the values of *NDVI*. It must be noted that the beginning of the study period for the Ovari beach dunes is characterised by very low *NDVI* values pointing to an area of initially bare sand. However, according to Mujabar and Chandrasekar (2012), by 2006 around 6 km^2 of sand dunes became covered with vegetation. The tendency of increasingly vegetated dunes since then is confirmed by the satellite imagery in Google Earth Pro 7.3.4.8248.

The Thua Thien dunes in Central Vietnam (Figure A.1b) are quite narrow and shaped by the tropical monsoon climate (Nehren et al., 2016). The average height of the dunes is between 10 and 15 m, and reaches a maximum of 30 m. The total annual precipitation of 2800-3300 mm is expected to promote greening. As can be seen in Figure A.1(d), the area was almost bare of vegetation at the beginning of the study period, as compared to the shrubs and exotic tree species at present. Nehren et al. (2016) report a start in plantation of fast growing, salt tolerant exotic tree species around 1997 which reportedly replaced the native coastal forests. Therefore, the steep slope over the second half of the period possibly reflects the result from the process of dune stabilisation (Figure A.1d).

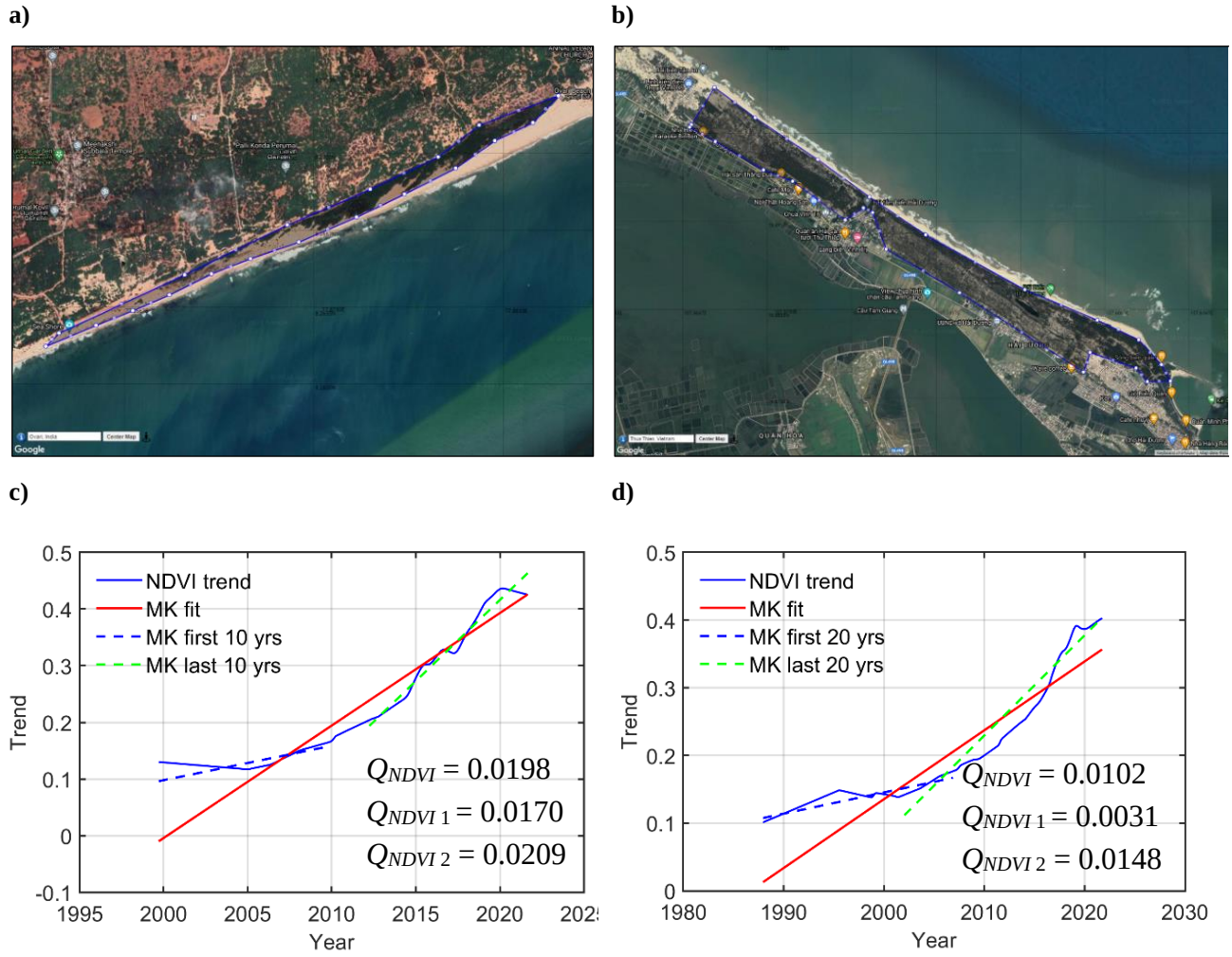

Figure A.1. (a) Ovari Beach, India (tropical dry; Mujabar and Chandrasecar, 2012); (b) Thua Thien, Vietnam (tropical monsoon; Nehren et al., 2016); (c) *NDVI* trend at Ovari Beach with fitted MK trend versus the two 10-year trends; (d) *NDVI* trend at Thua Thien with fitted MK trend versus the two 20-year trends. The estimated overall and partial *NDVI* trend slopes are included in the plots for reference. *Source*: Google Earth Pro 7.3.4.8248.

Figure A.2(a) illustrates the Guarda dunefield in southern Brazil, characterised by humid subtropical climate with hot summers, cool winters and no dry season (Mendez and Giannini, 2015). Therefore, the two important climatic drivers for dune formation and mobility are the wind and rainfall regimes. The overall stabilisation of the dunes from this region is attributed to adverse conditions for aeolian transport, i.e., increased rainfall and reduced sand drift potential (Mendez and Giannini, 2015; Martinho et al., 2010). Considering the relatively small size of the dunefield (~1.6 km^2), a factor for stabilisation could also be the elevated water table in response to rainfall which floods the interdune valleys where vegetation can spread. However, the observed sharp change in the slope in Figure A.2(c), although the *NDVI* remains for most of the time below 0.3 (the adopted limit to distinguish sparse vegetation from largely vegetated dune areas), points to human interventions, such as planting, to be involved in the greening.

The last dune site to be exemplified here is a fixed foredune on the coast of South Stradbroke Island, Australia (Barr and McKenzie, 1976), Figure A.2(b). The change between the trend slopes for the two 20-year periods is quite small (Figure A.2d). The climatic conditions (humid subtropical climate with hot and humid summers, and cool to mild winters) are favourable for vegetation development. In addition, as part of dune stabilisation work to counteract coastal erosion, planting of pioneering grass species and other related measures have been introduced since the 1970s (Barr and McKenzie, 1976). It can be therefore considered that the steep trend in Figure A.2(d) reflects results from the applied management techniques, since similarly to the other cases presented, the *NDVI* grows consistently from ~0.1 (bare sand) to nearly 0.5 (shrubs and grassland).

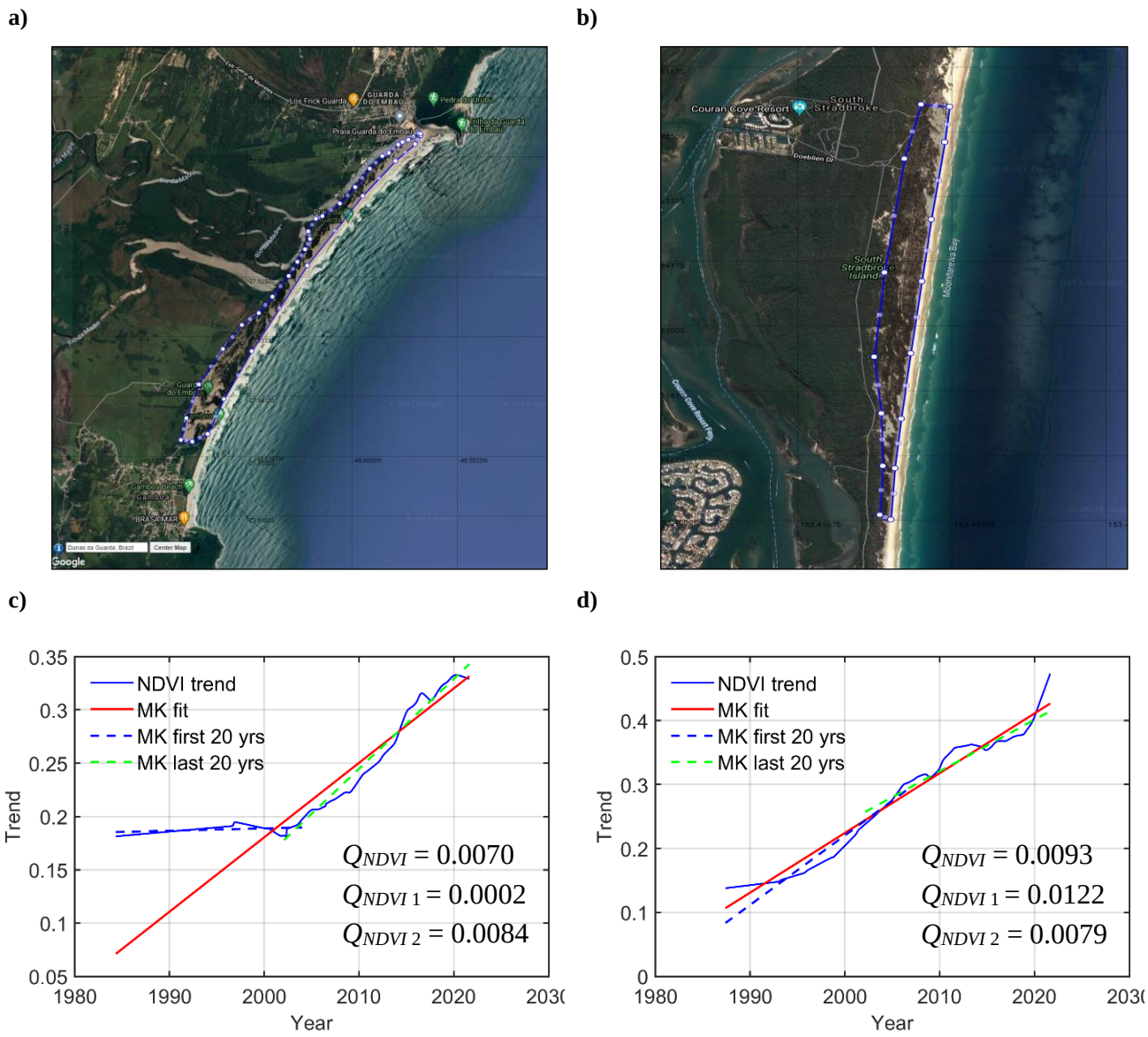

Figure A.2. (a) Guarda, Brazil (subtropical moist; Mendes and Giannini, 2015); (b) Stradbroke Island, Australia (humid subtropical; Barr and McKenzie, 1976); (c) *NDVI* trend at Guarda with fitted MK trend versus the two 20-year trends; (d) *NDVI* trend at Stradbroke Island with fitted MK trend versus the two 20-year trends. The estimated overall and partial *NDVI* trend slopes are included in the plots for reference. *Source*: Google Earth Pro 7.3.4.8248.

Appendix B. Acceleration and deceleration in the *NDVI* trends

Table B.1. Accelerated vegetation growth over the last 20 years. The cases of mobilised dunes are presented in red.

	accelerated (++)	**accelerated (--)**	**accelerated (+-)**	**accelerated (-+)**
1	Vietnam_Thua Thien Dunes	Spain_Valdevaqueros	Denmark Rubjerg Knude	Australia_FraserIsland_poly2
2	Australia_King Island_Parabolics	Spain_Bolonia	USA_LongBeachIsland	Mozambique_PraiaDoBilene
3	Brasil_Guarda			Australia_MoretonIsland_CapeMoreton
4	Mexico_Chakalacas			Mozambique_MaputoDunes_Lagoon
5	Italy_Marina Di Ravena			Brasil_Siriu
6	Brasil_Ouvidor			Brasil_Genipabu
7	Brasil_DunasAltas			Brasil_Jericoacoara
8	Australia_Moreton Island_LittleSandhill			USA_DunesCity
9	Portugal_Dunas_Sao Jacinto			Brasil_LencoisMaranhenses
10	Brasil_Ingleses			Somalia_MercaDunes
11	Brasil_Cauipe and Pecem			USA_MorroBayDunes
12	Australia_Moreton Island_The Desert			Spain_BaixTerBay_Mouth (Gola del Ter)
13	Mexico_El Farallon Dunefield			USA_WilliamTugmanParkDunes_ActiveDunes
14	Brasil_Garopaba Do Sul_Praia Figueirinha			Australia_PointBell
15	Australia_Fraser Island_Kirrar Dunefield			Brasil_RioSaoFrancisco_Updrift
16	Brasil_Solidao			SouthAfrica_PortAlfred
17	Brasil_AtlantidaSul			Spain_TorreDeLaMata
18	Australia_FraserIsland_poly1			Brasil_LagoaMangueira_South
19	Mexico_DunasDoradas_Tampico			Mozambique_BazarutoSouth
20	Argentina_ArroioZabalaNatureReserve			SouthAfrica_GoehlertDunes
21	Brasil_Mostardas			Mexico_GuerreroNegro
22	Brasil_Atalaia			Venezuela_MedanosDeCoro
23	Spain_GuardamarDelSegura			Spain_RosesBay
24	Brasil_Joaquina			
25	Australia_MoretonIsland_BIgSandhill			
26	India_OvariBeachDunes			
27	Brasil_Ibiraquera_Whole			
28	Canada_GreenwichDunes			
29	USA_LanphereDunes			
30	USA_CapeCod_BayDunes			
31	Canada_IlesDeMadeleine_West			
32	Mexico_PlayaLosAmarillos			
33	Brasil_Magisterio			
34	Brasil_JardimDoEden			
35	Russia_EfaDune			
36	Australia_FraserIsland_LakeWabbyDunefield			
37	USA_CapeCod_Provincetown			
38	Mexico_PlayaDeOlvidada			
39	Spain_LiencresSpit			
40	Brasil_RioSaoFrancisco_Downdrift			
41	USA_BodegaBayDunes_WholeArea			
42	USA_NewJersey Larger Polygon			
43	Australia_NassauDelta_DuneRidges			

Table B.1 (cont.). Accelerated vegetation growth over the last 20 years. The cases of mobilised dunes are presented in red.

	accelerated (++)	accelerated (--)	accelerated (+-)	accelerated (-+)
44	Belgium_dePanne			
45	USA_SouthPadreIsland			
46	USA_Oregon_TenmileDunes			
47	Chile_Ritoque			
48	UnitedKIngdom_Wales_MorfaHarlech			
49	Spain_GuardamarDeLaMarina			
50	Spain_Donhana			
51	Argentina_FaroQuerandi			
52	Poland_LebaBar			
53	Australia_NorthYoungHusbandPeninsula			
54	Australia_ChadingaConservationPark			
55	Indonesia_Parangritis			
56	SouthAfrica_DeMondDunes			
57	Mozambique_MarromeuDunes			
58	France_DesMaraisDHourtin			
59	Portugal_Dunas_CostaDaCaparica			
60	USA_InglenookFenDunes and 10 miles dunes			
61	SouthAfrica_Alexandria			
62	France_DunesDEcault			
63	Galicia_DunasDeTraba			
64	UnitedKIngdom_Wales_BroomhillBurrows			
65	UnitedKIngdom_Wales_TywynAberffraw			
66	USA_CallenderDunes			
67	UnitedKIngdom_NIR_Portstewart			
68	Portugal_Gale			
69	Australia_CapeArid_Larger			
70	NewZealand_FarewellSpitDunes			
71	NewZealand_ManawatuDunefield			
72	Mozambique_DunesDeDovela			
73	USA_MusselRockDunes			
74	Australia_Eucla_BilbunyaDunes			
75	UnitedKIngdom_Wales_Hillend			
76	NewZealand_AhiparaDunes			
77	NewZealand_AupouriDunes_Lower			
78	UnitedKIngdom_Wales_MorfaDyffryn			
79	Mexico_DunasCaboRojo_WholeArea			
80	Galicia_DunasDeCorrubedo			
81	Argentina_PozoSalado_2000			
82	Brasil_IslaDoCaju			
83	Argentina_ValdezPeninsula			
84	Lithuania_ParnidisKopa			
85	USA_WalkingDunes_ActiveArea			
86	USA_MinutemanDunes			

Table B.2. Decelerated vegetation growth over the last 20 years. The cases of mobilised duns are presented in red.

	decelerated (++)	decelerated (--)	decelerated (+-)	decelerated (-+)
1	Ireland_Newtown	Madagascar_FauxCapChevrons2	Denmark_Lodbjerge	France_DuneDuPilat
2	Denmark_Anholt_Isle	Madagascar_FauxCapChevrons1	Netherlands_Westenschouwen_Blowou	Brasil_TutoiaDunefield
3	France_DunesDeLaSlack	Madagascar_AmpalazaChevrons	SouthAfrica_GoukammaDunes	Madagascar_FenambosyChevrons
4	Denmark_VejersDunes	SouthAfrica_PortElizabeth	Netherlands_Schoorl	Netherlands_Terschelling_Active
5	USA_HogIsland	NewZealand_DoughboyBay_Central	Netherlands_SouthKennemerland_1km	Canada_IlesDeMadeleine_East
6	France_DunesDuMarquenterre	Portugal_Duna_deCresmina		Vietnam_PhanThietDunes
7	Denmark_Holmsland dunes			Brasil_PequenosLencoisMaranhenses
8	Australia_StadbrokeIsland_polygon1			USA_JockeyRidge
9	UnitedKIngdom_EN_SandscaleHaws			
10	UnitedKIngdom_Wales_Spit_TalacreWarren			
11	Portugal_Dunas_deMira			
12	Denmark_Hvidbjerge			
13	Denmark_SkagenActiveBlowouts			
14	Denmark_HanstholmPoly2_Reduced			
15	Australia_SouthStadbrokeIsland_fixedforedune			
16	Spain_EbroDelta			
17	Denmark_BorsmoseDunes			
18	Ireland_InchBeach			
19	SouthAfrica_ArnistonDunes			
20	Netherlands_Katwijk_1km			
21	Netherlands_Terschelling_Cap			
22	France_Reserve De La Dune			
23	Brasil_Cassino			
24	Galicia_ALanzada			
25	Italy_MoliseCoast			
26	Brasil_LagoaMangueira_North			
27	UnitedKIngdom_EN_SeftonDunes_LargerArea			
28	UnitedKIngdom_Wales_KenfigBurrows			
29	UnitedKIngdom_Wales_MerthyrMawr			
30	UnitedKIngdom_Wales_NewboroughWarren			
31	Australia_FraserIsland_IndianHead			
32	Belgium_Groenendijk			
33	Italy_Ghiomera			
34	Italy_PortoCaleri			
35	Australia_MoretonIsland_EastCoast			
36	Denmark_RabjergMile			
37	Germany_Listland			
38	UnitedKIngdom_Wales_LaugharnePendine Burrows			
39	Australia_WindyHarbour			
40	NewZealand_MasonBay			
41	USA_SantaMariaDunes			
42	France_CapFerret			
43	Fiji_SigatokaRiver			
44	UnitedKIngdom_Wales_BrownsladeLinneyBurrows			
45	NewZealand_KarikariBeach			
46	USA_PadreIslandNationalSeashore			
47	Kenya_MalindiDunes			

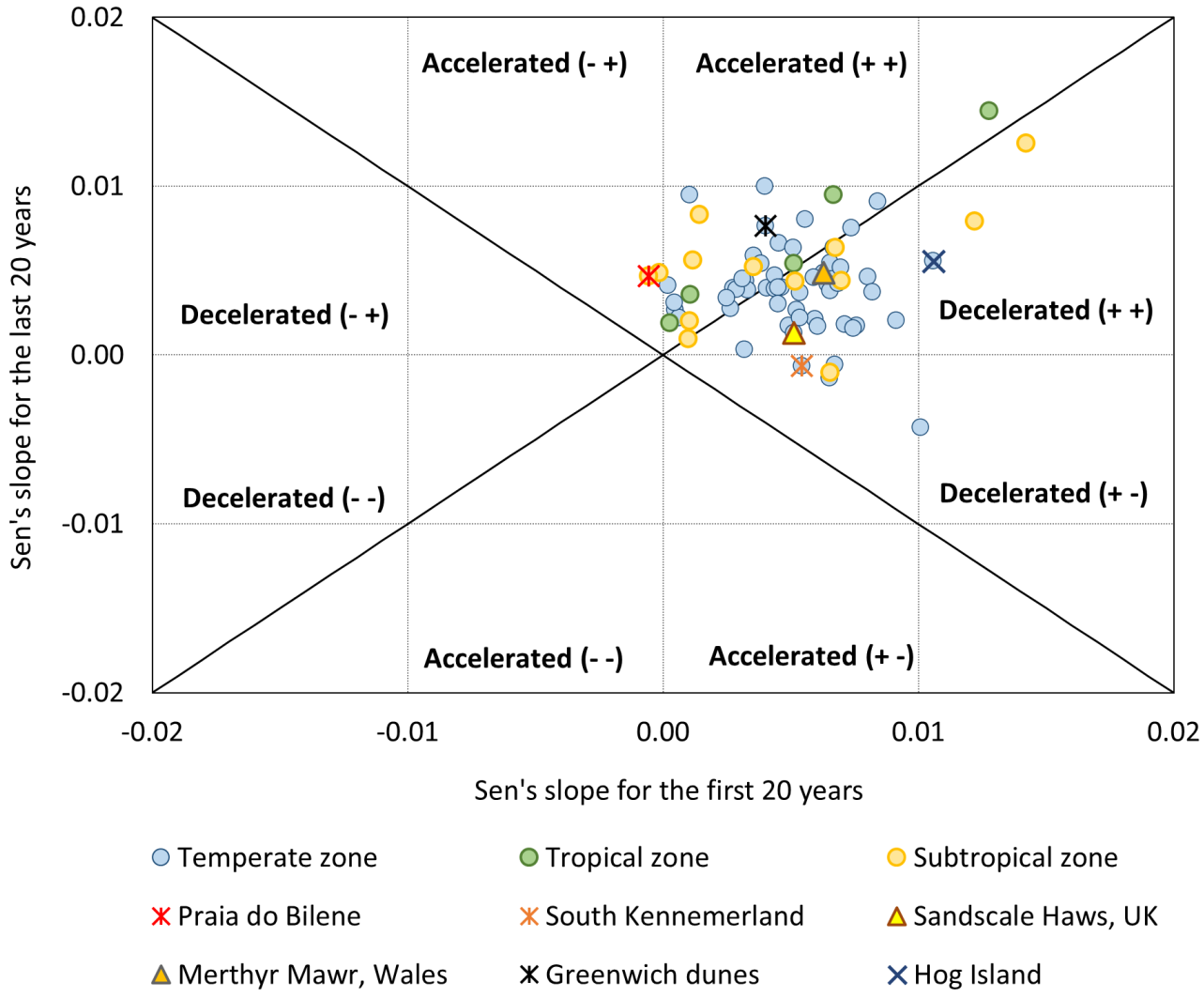

Figure B.1. Vegetated dunes ($\overline{NDVI}$ > 0.3): Change in the trend slope between the first and the last 20 years of the study period. Dunes selected for discussion in Chapter 4 which fall in this group are visualised in the plot (see Appendix C). The dune cases are superimposed on the main climatic regions.

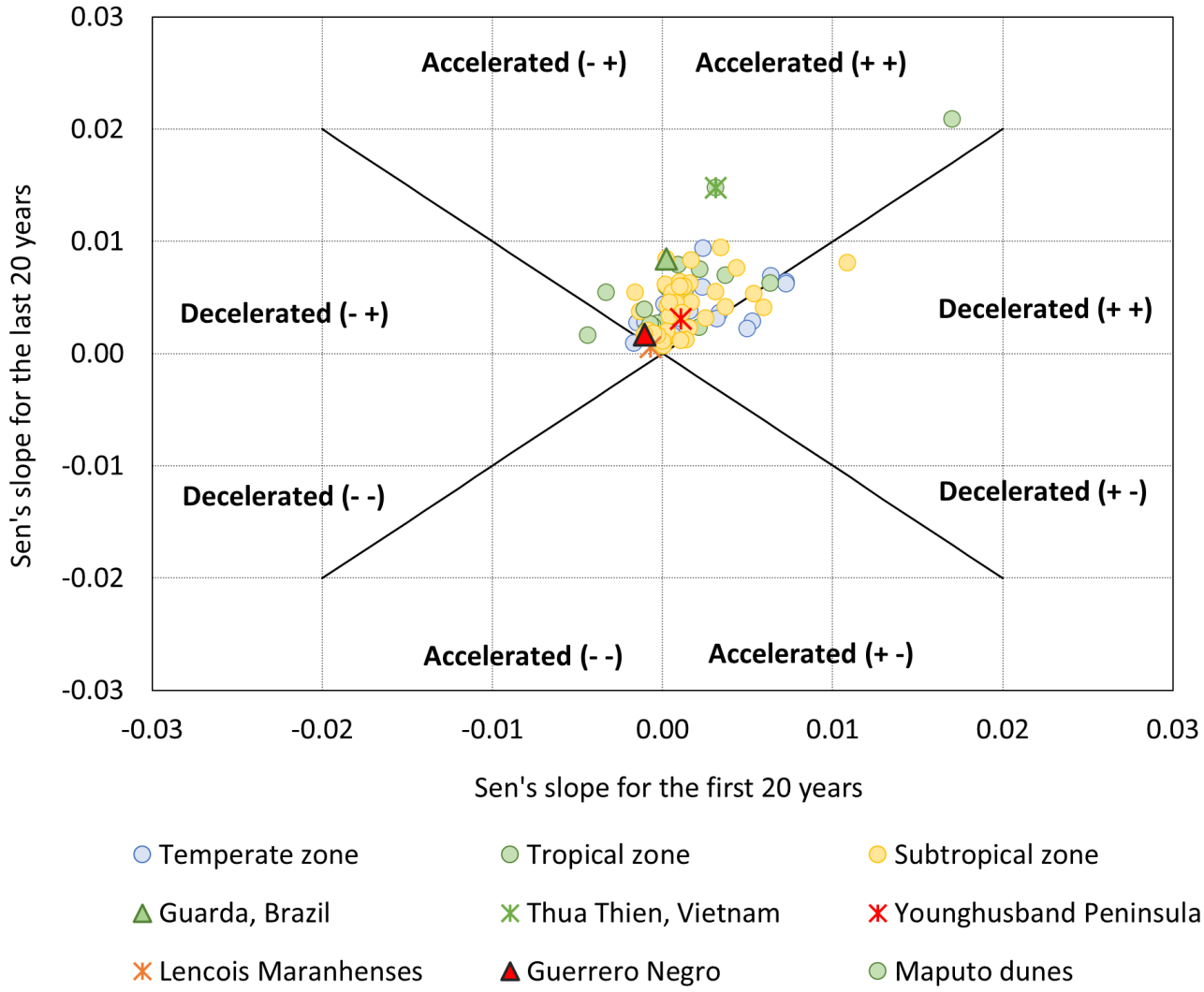

Figure B.2. Less vegetated dunes ($\overline{NDVI} \leq 0.3$): Change in the trend slope between the first and the last 20 years of the study period. Dunes selected for discussion in Chapter 4 which fall in this group are visualised in the plot (see Appendix C). The dune cases are superimposed on the main climatic regions.

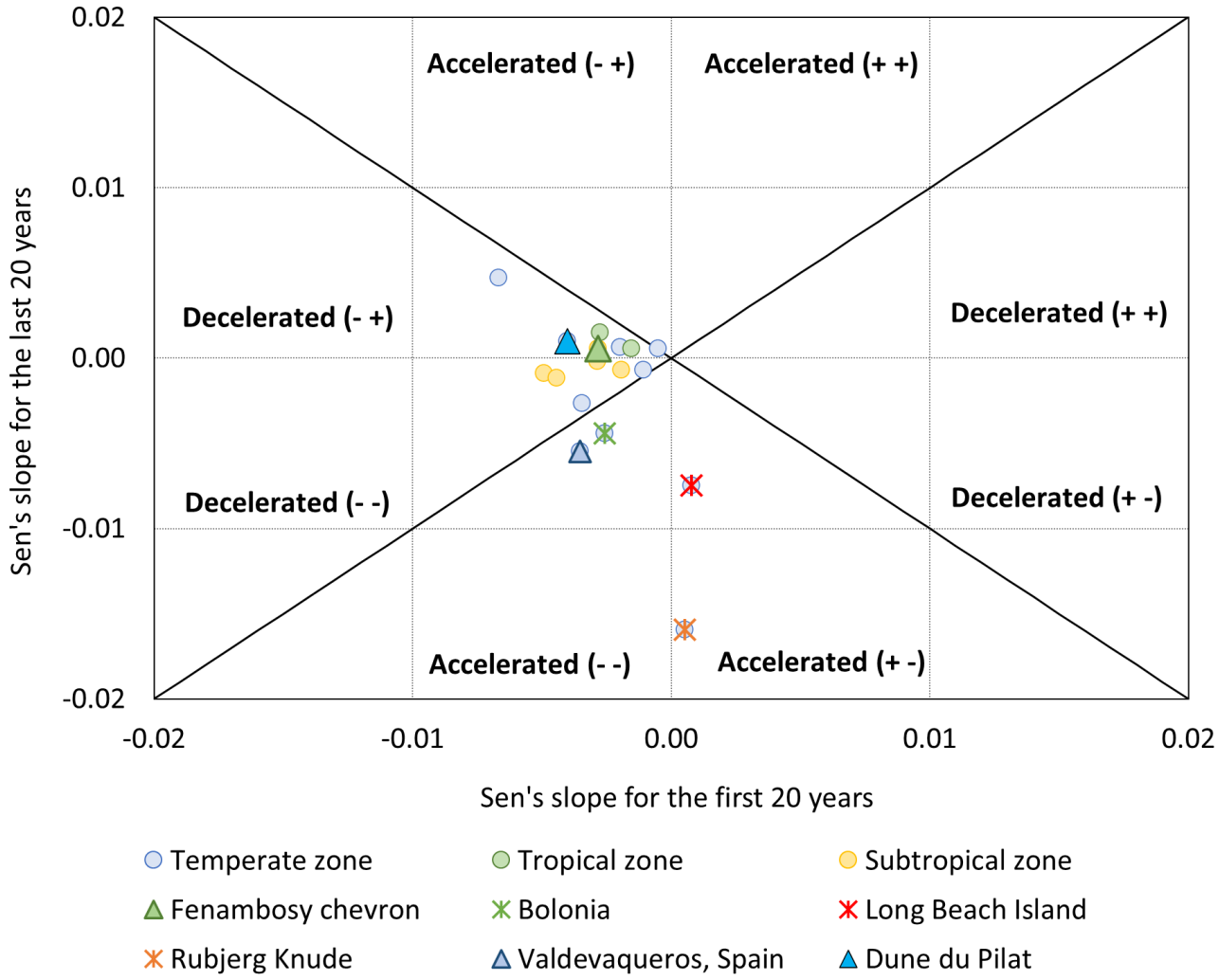

Figure B.3. Active dunes ($Q_{NDVI} < 0$): Change in the trend slope between the first and the last 20 years of the study period. Dunes selected for discussion in Chapter 4 which fall in this group are visualised in the plot (see Appendix C). The dune cases are superimposed on the main climatic regions.

Appendix C. Selected dune sites

The dune sites presented next exemplify different types of association between dune mobility and trends in the main climatic parameters. They show that (1) different climatological regimes may result in the same type of change (greening/mobilisation), and (2) while some dune sites adhere to the climatological expectations, others do not. The latter implies that factors different from climatic variability control the dune mobility at those sites. Such factors can be ample sand supply or human-related direct and indirect disturbances.

C.1. Hog Island, Virginia Coast, US (Greening trend, $\overline{NDVI} > 0.3$ / Warm temperate climate / $T\uparrow$, $P\uparrow$, $W\uparrow$)

Hog island is a warm temperate barrier island (Figure C.1a) which makes part of the Virginia Coast Reserve (Huang et al., 2018; Young et al., 2011). It is considered a suitable location for studying the effects of the warming climate and its local variations, since it is free of human interventions (Huang et al., 2018).

The island has an area of 12 km^2, with 10 km length and 2.5 km width at the widest point. Over the period 1984 – 2016, a loss of bare sand to shrub encroachment occurred on the island and was associated with a local increase in the mean winter temperature. The mean annual temperature varies between 11.9ºC and 14.7 ºC, and the mean annual rainfall – between 1065 and 1167 mm/year (Huang et al., 2018).

The reported greening has been also confirmed by the present analysis of the *NDVI* time series. The JUST decomposition in Figure C.1(b) reveals dense vegetation cover ($\overline{NDVI}$ = 0.58 *NDVI*) and a well-defined seasonal pattern ($\Delta NDVI$ = 0.217). Moreover, Hog island is one of the two non-European dune sites with most pronounced seasonality (Figure 3.19). The other case, the Walking Dunes, is also located on the east coast of US. Comparison between the trends for the first and last 20 years of the study period shows deceleration, although the trend remains positive overall.

Finally, the analysis of the associated climatic series demonstrates that the local climate has indeed changed to warmer and wetter over the last decades ($Q_T > 0$, $Q_P > 0$), but also became windier ($Q_W > 0$). Such combination of climatic trends ($T\uparrow$, $P\uparrow$, $W\uparrow$) may explain the continuous greening with time, although at a lower pace over the last two decades.

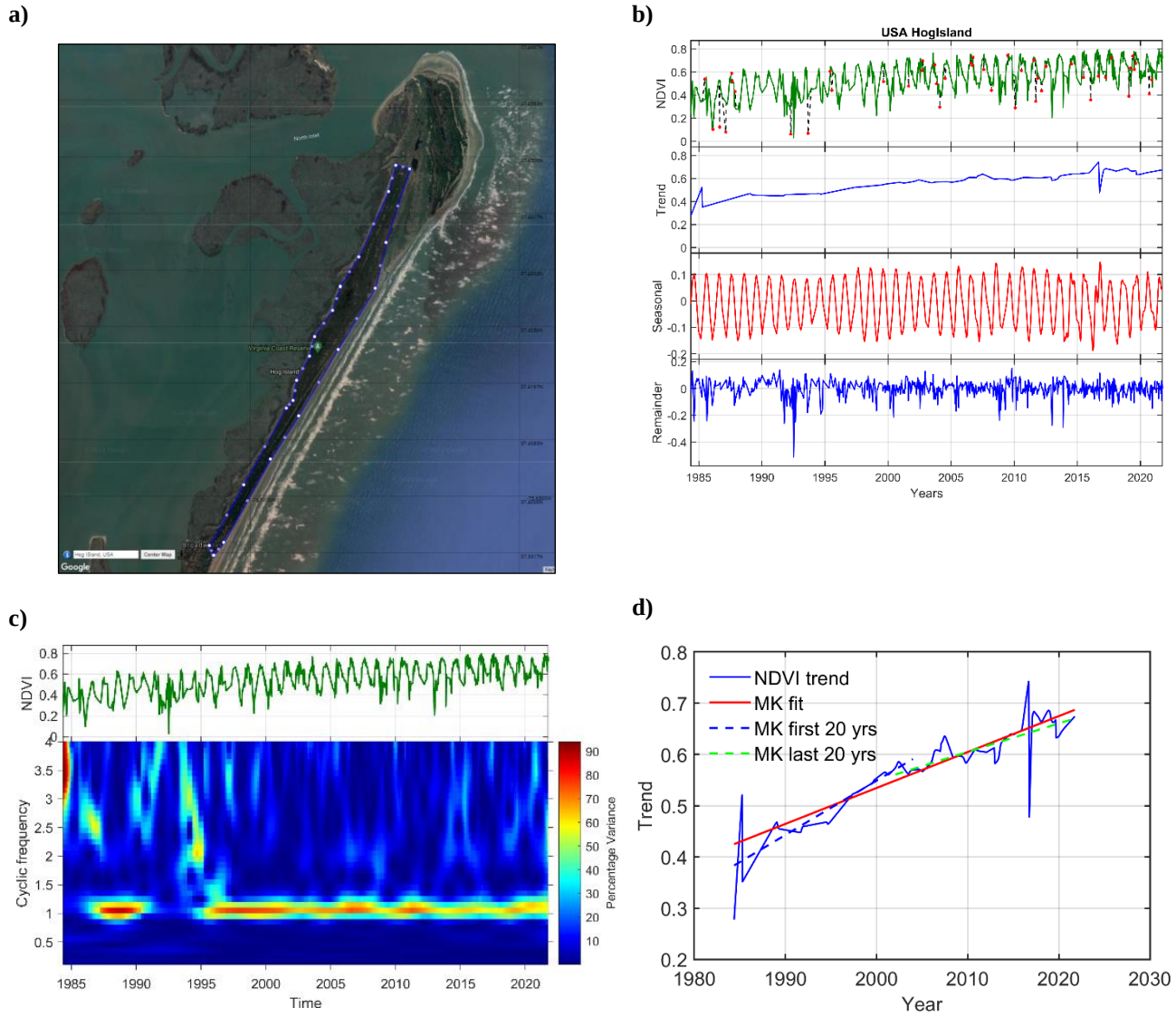

Figure C.1. (a) Hog Island dunefield, US (*Source*: Google Earth Pro 7.3.4.8248); (b) JUST decomposition (Ghaderpour and Vujanovic, 2020); (c) Spectrogram (LSWA; Ghaderpour and Pagiatakis, 2017); (d) Mann-Kendall test performed on the *NDVI* trend component with the two 20-year line fits also illustrated.

C.2. Praia do Bilene and Maputo dunes, southern Mozambique, Africa (Greening trend, $\overline{NDVI} > 0.3$ and $\overline{NDVI} \leq 0.3$, resp. / Tropical moist climate / T↑, P↓, W↓)

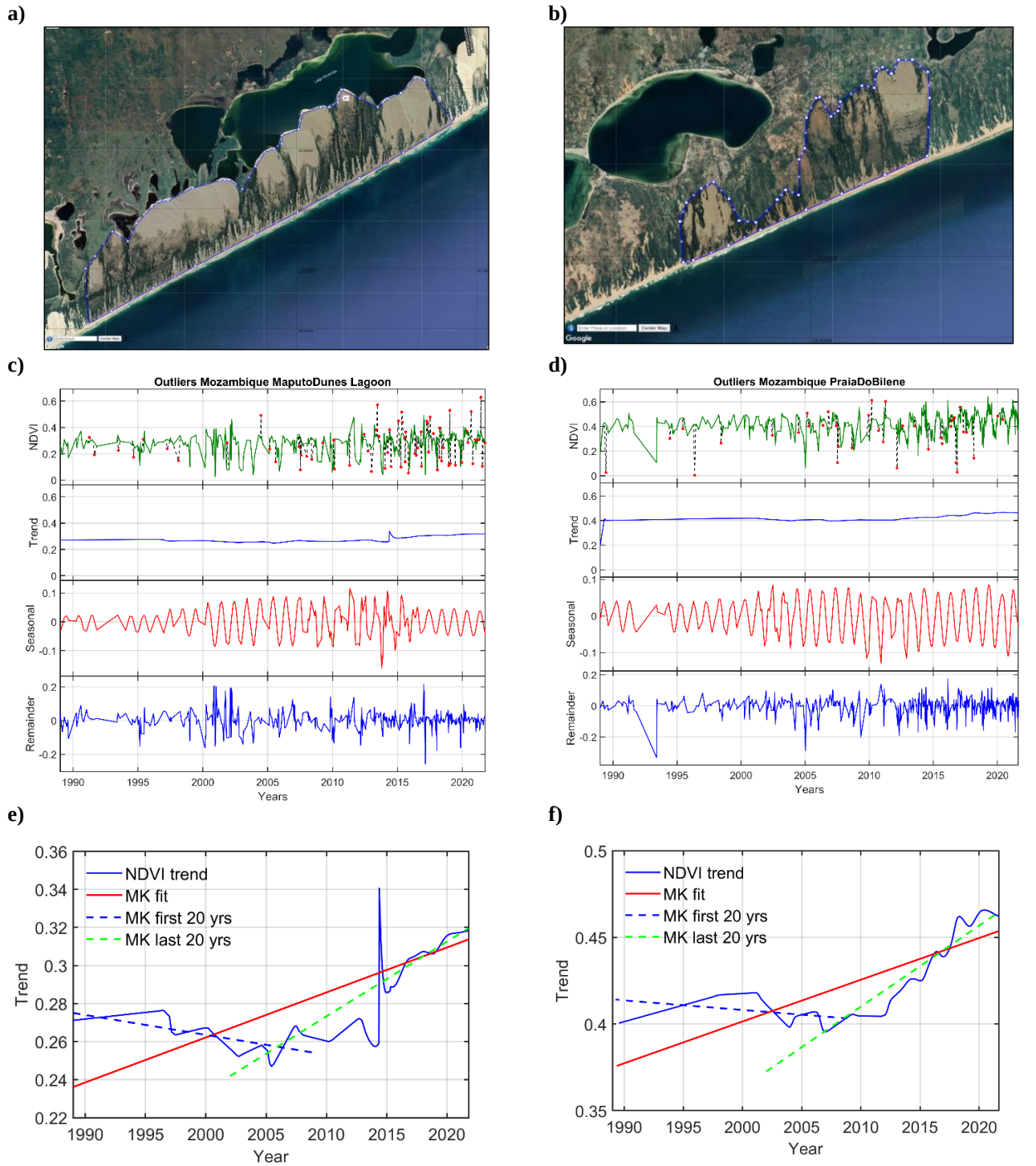

Figure C.2. (a) Maputo dunes (south, *NDVI* ≤ 0.3); (b) Praia do Bilene dunes (north, *NDVI* > 0.3) (*Source*: Google Earth Pro 7.3.4.8248); (c, d) JUST decomposition (Ghaderpour and Vujanovic, 2020); (e, f) Mann-Kendall test performed on the *NDVI* trend component with the two 20-year line fits also illustrated.

These two neighbouring transgressive dunefields belong to a barrier-lagoon system in southern Mozambique (Figure C.2a, b). They are located between Maputo and Gaza provinces and face the Indian Ocean to the east (Botha et al., 2003; Cooper and Pilkey, 2002).

The regional climate is tropical moist, according to the Köppen-Geiger classification (Miguel and Castro, 2018). Two seasons can be identified: summer (between October and March) and winter (from April to September). The mean annual precipitation is ~1300 mm/year, with maximum rainfall between December and March, associated with the southernmost position of ITCZ. Furthermore, the annual average temperature is ~23º and the monthly wind speed is high, occasionally reaching 11 m/s (Værat et al., 2012).

The two dunefields exhibit different degrees of mobility. The southern dune site (Maputo dunes) is characterised by mobile and semi-vegetated dunes with high levels of yearly migration (23 m/year; Miguel and Castro, 2018). The vegetation cover is less than 30%. On the other hand, the northern dunefield (Praia do Bilene) consists primarily (~70%) of vegetated (stabilised) dunes together with semi-vegetated dunes.

The aeolian activity is driven by strong winds during the dry season. Over the last 40 years, the average monthly wind speeds are seen to exceed the threshold for aeolian transport (6 m/s; cf. Fryberger, 1979). A maximum speed of 22 m/s has been reported for the same period between the months of July and October which results in instantaneous sand transport, as opposed to the low sand transport during the rainy summer season (October – March). High rainfall combined with an average monthly temperature of ~23ºC promotes vegetation growth and dune fixation (Miguel and Castro, 2018). On the other hand, significant evaporation during the dry winter season (Vaerat et al., 2012) supports active aeolian sand transport and dune migration.

The two neighbouring rivers Limpopo and Incomati are sources of large sediment supply reworked by waves. Maputo dunes receive larger sediment supply, which results in lower, continuous, dune ridge, in contrast to the dunes of Praia do Bilene which receive less sand and are less exposed to wind action, therefore they are more vegetated and higher.

Analysis of the *NDVI* multitemporal series returned $\overline{NDVI}$ = 0.24 and $\Delta NDVI$ = 0.113, for Maputo dunes, and $\overline{NDVI}$ = 0.45, $\Delta NDVI$ = 0.139, for Praia do Bilene dunes (Figure C.2c, d). Due to lack of data in the years at the beginning of the study period, those years were excluded from the analysis. Contrary to Praia do Bilene, Maputo dunes show lower seasonality in *NDVI*, since the open sand area is larger. Both areas demonstrate accelerated levels of vegetation growth over the last 20 years (Figure C.2e and f; see also Table B.1; Appendix B). Acceleration from a negative trend over the first 20 years to a positive trend over the last 20 years can be explained by local conditions favouring stabilisation. In terms of local climate, the dune systems reveal $T\uparrow$, $P\downarrow$, $W\downarrow$. Such combination may lead to either mobilisation or greening. In this particular case, the dunefields show different extent of greening due to other local environmental factors.

C.3. Lençois Maranhenses, NE Brazil (Greening trend, $\overline{NDVI}$ << 0.3 / Tropical moist climate / T↑, P↓, W↑)

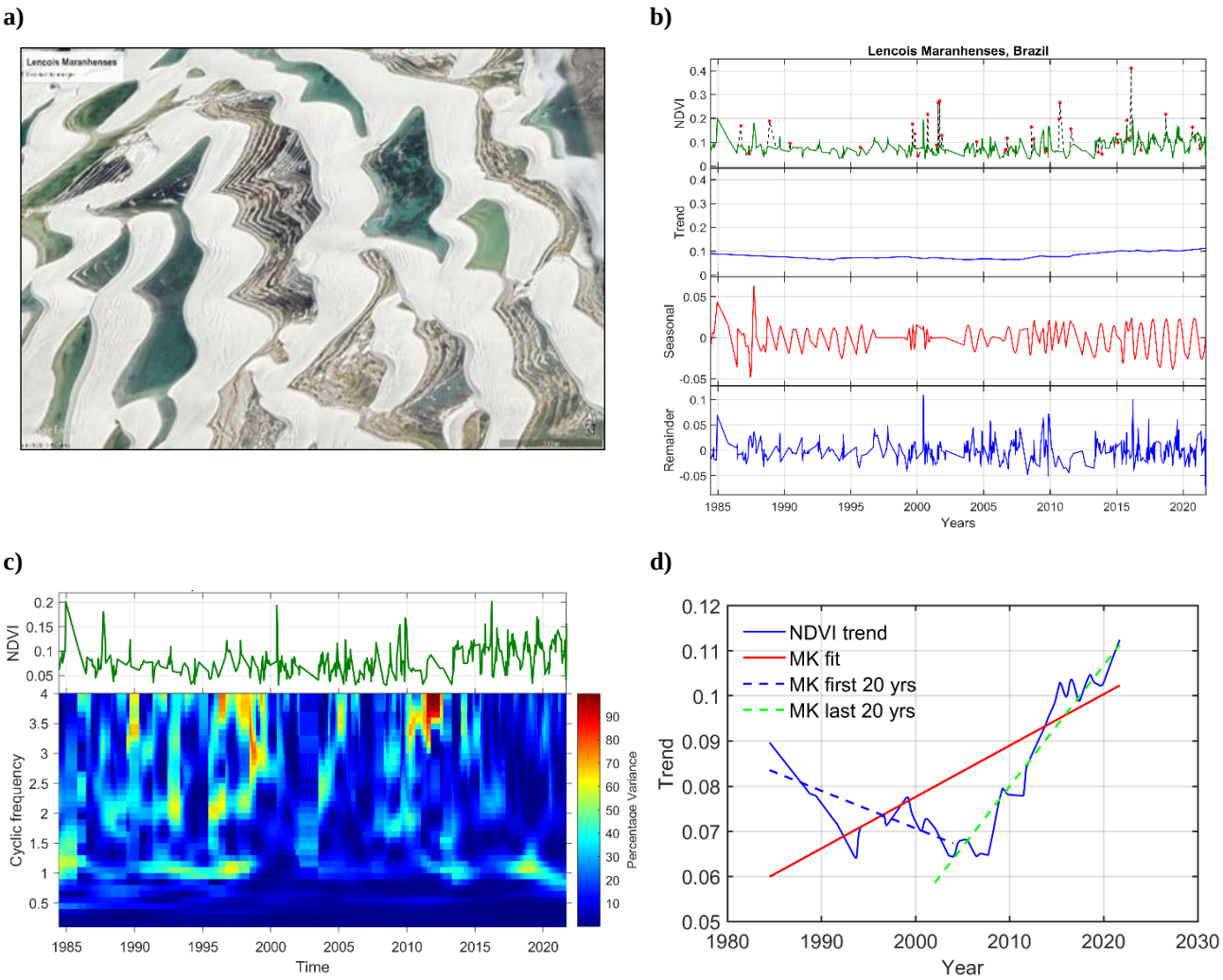

Figure C.3. (a) Fragment of Lençois Maranhenses dunefield, NE Brazil (*Source*: Google Earth Pro 7.3.4.8248); (b) JUST decomposition (Ghaderpour and Vujanovic, 2020); (c) Spectrogram (LSWA; Ghaderpour and Pagiatakis, 2017); (d) Mann-Kendall test performed on the *NDVI* trend component with the two 20-year line fits also illustrated.

Lençois Maranhenses is an extensive transgressive dunefield developed in the tropical moist settings of the Maranhão coast, NE Brazil (Hilbert et al., 2016; Maia et al., 2005; Dillenburg and Hesp, 2009; de Luna et al., 2011). It is the largest dunefield in Brazil and in the world. Typical climatic features are the high annual average temperature (27ºC), a four to six months dry period and torrential rains during the wet season in the first half of the year. The wind pattern is governed by the strong easterly trade winds. The wind regime and rainfall are determined by the position of ITCZ, such as the wet season is associated with ITCZ located farthest to the south, and the dry season – with ITCZ shifted farthest to the north (Levin et al., 2009).

The total area of the dunefield is roughly estimated as 1000 km^2 (Hilbert et al., 2016; Levin et al., 2009). The dunefield reaches ~31 km at its widest, eastern part (Dillenburg and Hesp, 2009). During

the wet season, the interdune valleys are flooded, making the sand non-available for aeolian transport. Nevertheless, the flooded sand is being reworked by the multiple drainages and subsequently accumulated in the interdune spaces. Those spaces become the secondary (internal) source of sediments during the dry period. The vegetated areas of the dunefield represent older dune phases in the form of transverse dunes, deflation plains dominated by gegenwalle ridges (Figure C.3a) and trailing ridges, or a combination of both (bistable regime, Figure 1.3a; Yizhaq et al., 2009).

The analysis conducted here confirmed the low levels of vegetation cover at Lençois Maranhenses ($\overline{NDVI}$ = 0.08), due to the predominantly mobile character of the dunefield, as well as the lack of seasonal pattern. However, the LSWA routine returned energetic seasonal artefacts at a yearly and less than a year scales, which probably reflect phenological changes in the vegetation growing on the partially flooded residual ridges (Figure C.3c).

On the other hand, considering the results for the trends of the main meteorological variables, namely, $Q_T > 0$, $Q_P < 0$, $Q_W > 0$, it can be concluded that they support high mobility which disagrees with the identified greening trend at the selected area. Nevertheless, it should be kept in mind that the magnitude of greening is very low. In this particular case, the dominant force that maintains the dunes active is the power of the wind. Finally, the *NDVI* signal shows an acceleration in the rate of change, from negative (mobilisation) to positive (greening), as can be seen in Figure C.3(d).

C.4. Sandscale Haws, UK (Greening trend, $\overline{NDVI}$ > 0.3 / Cool temperate moist climate / T↑, P↑, W↓)

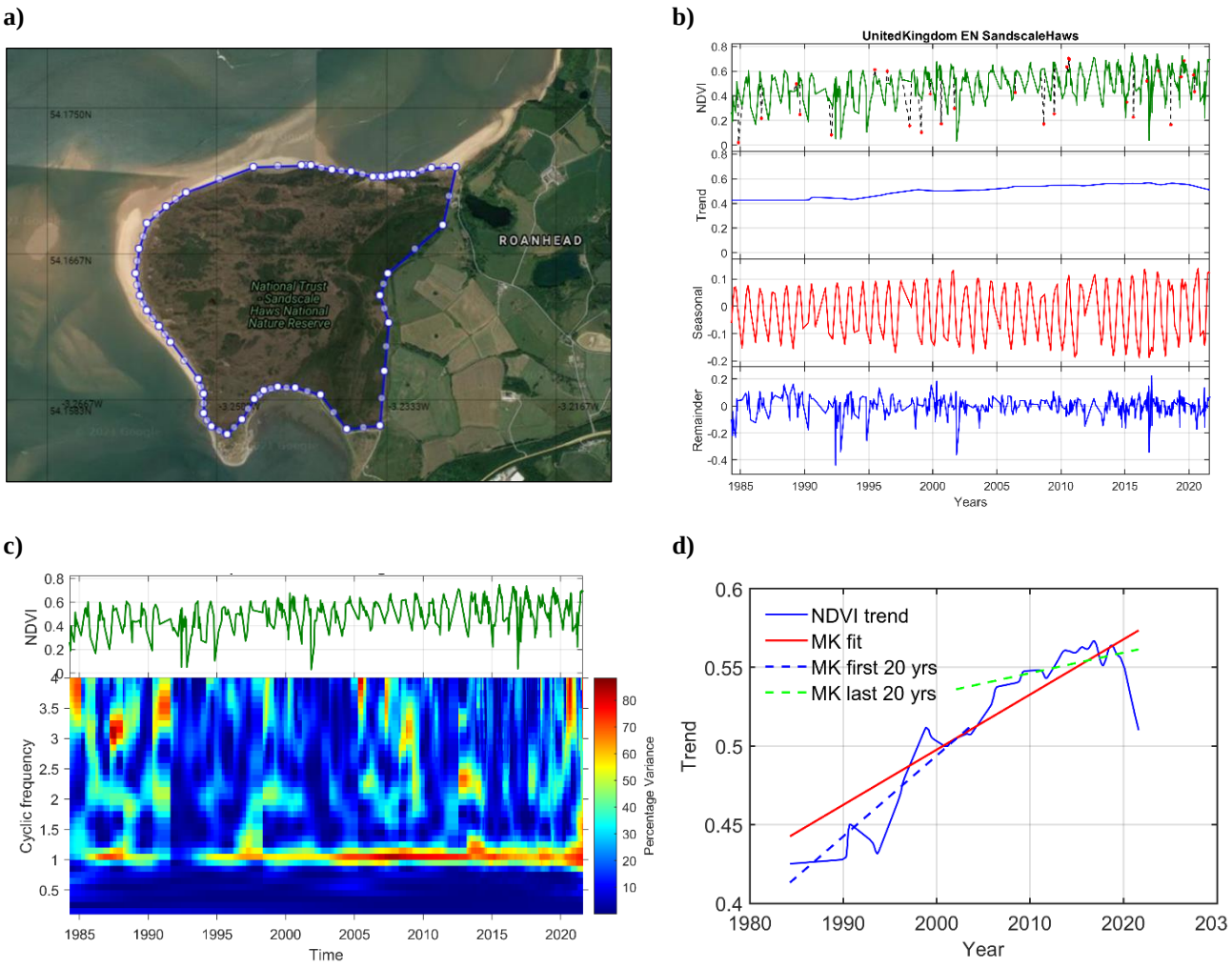

Figure C.4. (a) Sandscale Haws, UK (*Source*: Google Earth Pro 7.3.4.8248); (b) JUST decomposition (Ghaderpour and Vujanovic, 2020); (c) Spectrogram (LSWA; Ghaderpour and Pagiatakis, 2017); (d) Mann-Kendall test performed on the *NDVI* trend component with the two 20-year line fits also illustrated.

Sandscale Haws is a coastal foreland dune system with an area of 1.8 km^2. It is located on the southern coast of the Duddon Estuary in NW England and is attributed a status of National Nature Reserve since the end of the 20th century (Pye et al., 2020). The climate of the region is cool temperate moist and shows long-term trends of increasing temperature and precipitation. The wind speed, on the other hand, has been declining for more than a century. Such combination of warmer, wetter and less windy conditions illustrate the typical changes in the meteorological parameters in NW Europe which result in dune stabilisation (Pye and Blott, 2020). Other environmental conditions, such as increased nitrogen deposition, increased levels of CO_2, as well as changes in the land use practices (among them grazing) may have also played a role, although not a major one.

The highest temperatures are recorded in August and the lowest in February. The average annual precipitation reaches 1013 mm, with April, May and June being the driest months. The potential

evapotranspiration is the strongest in June and July and exceeds the monthly rainfall. Regarding the wind speed, the nearby airfield reports 5.5 m/s at 10 m height which is approximately 1 m/s higher in winter than in spring and summer. Wind gusts exceeding 7 m/s are recorded in all months, but may further increase to approximately 9 m/s between November and January.

The *NDVI* data analysis shows that the Sandscale Haws site has one of the largest mean vegetation indices, $\overline{NDVI}$ = 0.517, and a relatively high amplitude of seasonal fluctuations, $\Delta NDVI$ = 0.233. This fact is reflected in the LSWA spectrogram in Figure C.4(c), where the main peak is at the scale of 1 year, but relatively high-energy peaks appear also at half a year and less, e.g., at 4 months.

The identified greening is seen to decelerate slightly over the last 20 years which may be due to hysteresis effect in the response of vegetation to wind stilling (Figure C.4d). The analysis of the local meteorological time series confirms the presence of a combination of trends which is particularly favourable for vegetation growth ($T\uparrow$, $P\uparrow$, $W\downarrow$). Therefore, it can be concluded that the ongoing greening at Sandscale Haws is in agreement with the expected climate-related trend.

C.5. Guerrero Negro, Mexico (Greening trend, $\overline{NDVI}$ << 0.3 / Subtropical dry, hyperarid climate / T↑, P↓, W↑)

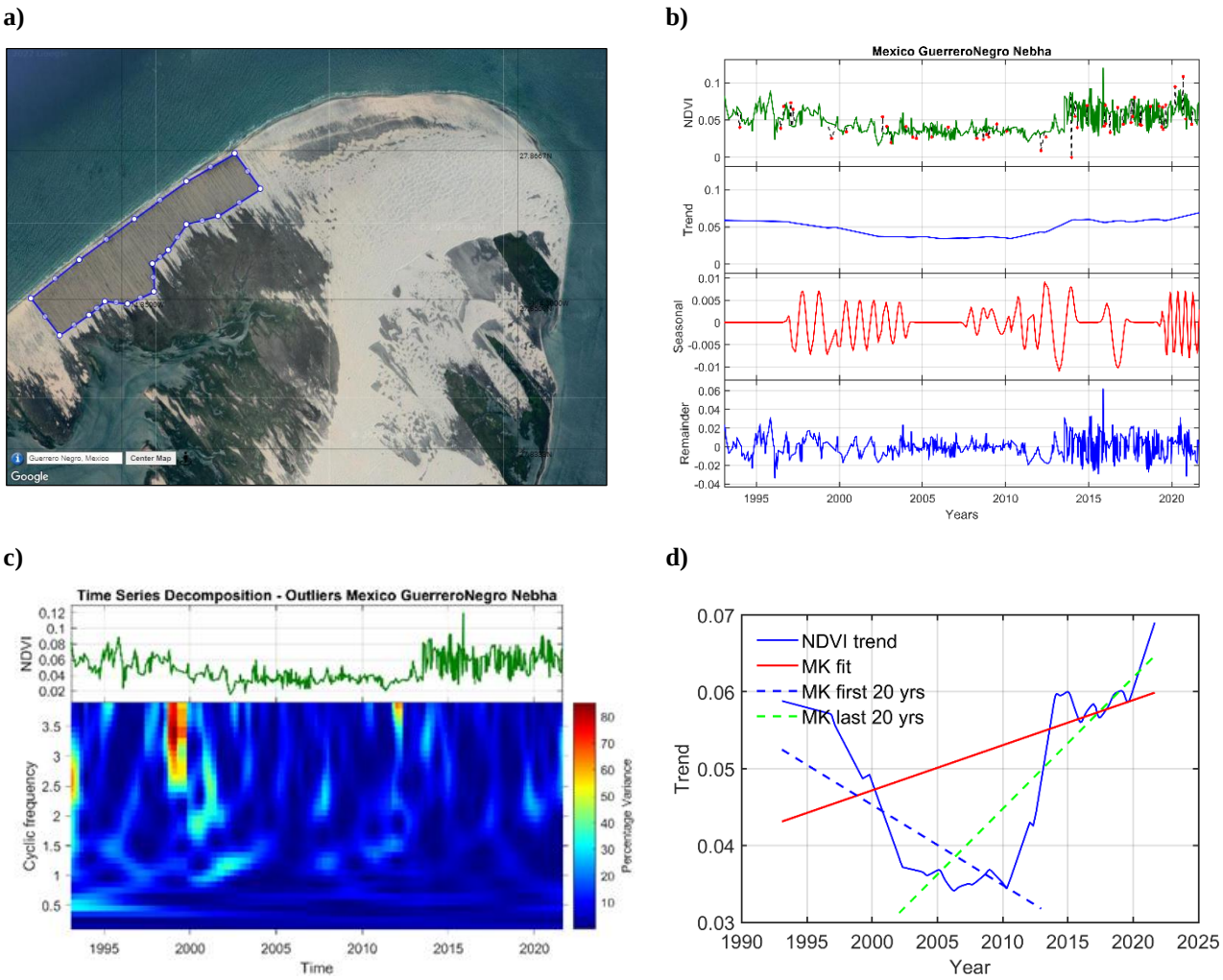

Figure C.5. (a) A segment from Guerrero Negro dunefield located south of Laguna Ojo de Liebre, Baja California, Mexico. The segment illustrates the typical for arid climates sand sheets and nebkha dunes developed under low sediment supply (*Source*: Google Earth Pro 7.3.4.8248); (b) JUST decomposition (Ghaderpour and Vujanovic, 2020); (c) Spectrogram (LSWA; Ghaderpour and Pagiatakis, 2017); (d) Mann-Kendall test performed on the *NDVI* trend component with the two 20-year line fits also illustrated.

The Guerrero Negro dunefield (Figure C.5a) is located on the tidally-flooded barrier islands to the west of the town of Guerrero Negro, Baja California, Mexico (Ewing and Kocurek, 2010). The large transgressive dunefield has formed in the hyper-arid settings of the subtropical dry climate of the region, characterised with strong onshore NW winds and extensive supply of sediments from the beach. The mean monthly maximum and minimum temperatures are between 20 – 29°C in summer and 8 – 20°C in winter. The winter rainfall is scarce, ~35 mm/year, on the average (Fryberger et al., 1990).

Figure C.5(a) shows fragment of the dunefield which has been studied here. It is located to the south of the largest lagoon in the area, Laguna Ojo de Liebre, and is dominated by aeolian sand sheets and lines of nebkha dunes next to a larger area of active dunes. Nebkha are typical dune forms in arid and

semi-arid climates and are usually associated with reduced sediment supply (Hesp, 2013; Hesp et al., 2021). On the other hand, strong winds and abundant supply of sand promote active aeolian transport in the neighbouring dunefields.

As described by Fryberger et al. (1990), there are two seasonal wind patterns acting at the site. In summer (March – October), the wind is unidirectional, onshore, and may reach up to 12 m/s. In winter, the pattern is bidirectional, with the strongest sea breeze of about 9 m/s, and a more gentle breeze offshore of less than 5 m/s. Therefore, the dunes display the fastest advance in summer as a result of high wind power, significant evaporation rates and local hydrodynamic conditions (the occurrence of the highest tides).

The present analysis of the dune dynamics at Guerrero Negro returned the lowest average vegetation content among all dune sites ($\overline{NDVI}$ = 0.049 *NDVI*). Moreover, the *NDVI* values hardly reach 0.1 *NDVI*, especially before 2013, which points to an area of predominantly bare sand. The *NDVI* trendline is visibly nonlinear, revealing a decrease below the average for the period between 2000 – 2012 (Figure C.5b, d).

The estimated non-parametric trends for the first and last 20 years of the studied period, on the other hand, show a tendency of negligible acceleration from sand mobilisation towards dune stabilisation. In the present case, the two periods overlap, as can be seen in Figure C.5(d). This is because the analysed time series are shorter due to missing data in the first years of measurements (the period with available data is 1993 – 2021). It should be noted that the dune area to the right of the studied site exhibits a continuous negative trend since the dunes there are very mobile under the current climatic conditions which makes vegetation colonisation impossible.

Finally, the temporal series of the climatic variables at Guerrero Negro show that between 1993 and 2021 the mean daily temperature and wind speed increased ($Q_T > 0$, $Q_W > 0$), while the mean daily precipitation decreased ($Q_P < 0$). These conditions ($T\uparrow$, $P\downarrow$, $W\uparrow$) agree with the reported local climate at the dunefield and together indicate a tendency for increasing mobility, although the considered dune polygon exhibits different dynamics due to presence of sparse vegetation resulting in the formation of nebkha dunes.

C.6. Younghusband Peninsula (North), Australia (Greening trend, $\overline{NDVI} < 0.3$ / Warm temperate dry / T↑, P↓, W↓)

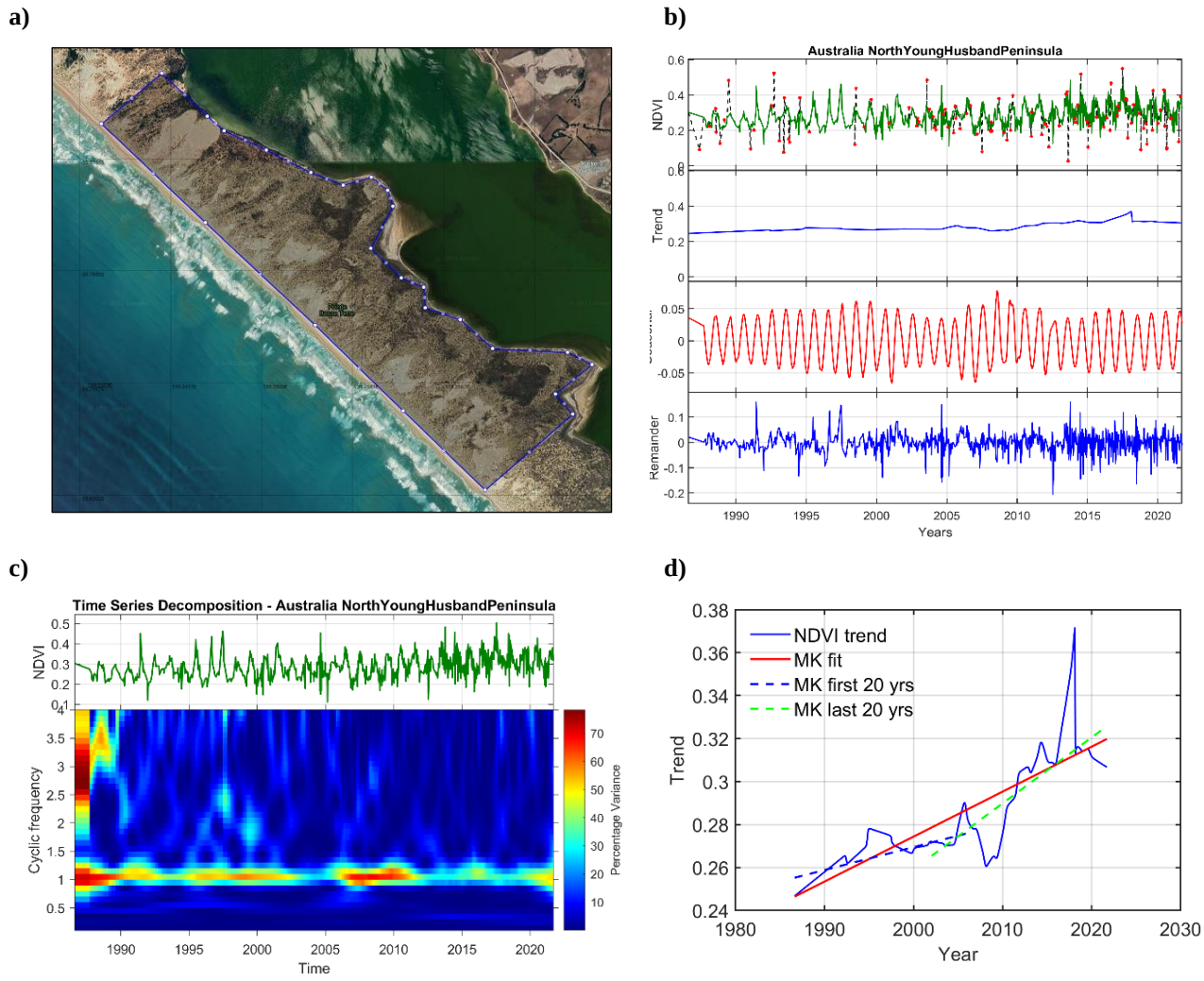

Figure C.6. (a) Younghusband Peninsula, Australia (*Source*: Google Earth Pro 7.3.4.8248); (b) JUST decomposition (Ghaderpour and Vujanovic, 2020); (c) Spectrogram (LSWA; Ghaderpour and Pagiatakis, 2017); (d) Mann-Kendall test performed on the *NDVI* trend component with the two 20-year line fits also illustrated.

The Younghusband Peninsula is located at the southeast coast of south Australia (Figure C.6a). It represents one of the longest continuous transgressive dune systems in Australia, with approximately 190 km length. The width of the Peninsula is between 1 and 2 km and the dunes can grow as high as 40 m (Harvey, 2006; Moulton et al., 2019).

The climate of the region can be classified as warm temperate dry (Figure 2.3; Sayre et al., 2020) and is characterised by hot, relatively dry summers and wet, mild winters. The rainfall is unevenly distributed along the Peninsula, decreasing from northwest to southeast, from 468 to 586 mm/year. The Younghusband Peninsula experiences very strong SW winds, which can reach up to 18 m/s (Moulton et al., 2019). These winds drive the dune migration landward.

In a recent study, Moulton et al. (2019) suggest three potential drivers of observed significant increase (between 7 and 40%) in vegetation cover on the northwest side of the Peninsula over the last ~70 years. Those include local climate, in terms of rainfall and wind regime, and land-use change, in terms of grazing by rabbits. Correlation analysis and comparison of trends in the studied variables led to the conclusion that cases of sudden decline of the rabbit population had the largest effect on the dune dynamics. Another important factor is the largely varying levels of precipitation, from above the average to prolonged droughts (Moulton et al., 2019).

The non-parametric MK test confirmed the greening trend at the Younghusband dunefield. The change is relatively slow though, such as the average vegetation cover maintains on the limit between bare sand and vegetated surface ($\overline{NDVI}$ = 0.29 *NDVI*). In addition, the amplitude of the seasonal fluctuations is also very low ($\Delta NDVI$ = 0.09 *NDVI*). The observed increase in *NDVI* in Figure C.6(b) between 2008 and 2013 can be possibly associated with rapid decline in the rabbit population. Moreover, during that period, significant peaks of around 70% percentage variance can be observed in the spectrogram at annual frequency (Figure C.6c). Furthermore, the vegetation change has accelerated slightly over the second 20-year period, remaining positive (Figure C.6d).

The total daily averaged precipitation have declined with time ($Q_P < 0$), which somewhat contradicts the identified increase in vegetation. However, contrary to Moulton et al. (2019), who reported an increase in the sand drift potential, the climatic time series for the wind speed showed reduced wind potential ($Q_W < 0$), which may support dune stabilisation by allowing spatial expansion of vegetation.

For this site, the combination of climatic trends ($T\uparrow$, $P\downarrow$, $W\downarrow$) does not promote directly greening. Greening has been attributed to the reduction in the rabbit population (land cover use) affecting the average vegetation cover.

C.7. Fenambosy Chevrons, southern Madagascar (Mobilising trend, $\overline{NDVI}$< 0.3 / Subtropical dry, semi-arid climate / T↑, P↓, W↑)

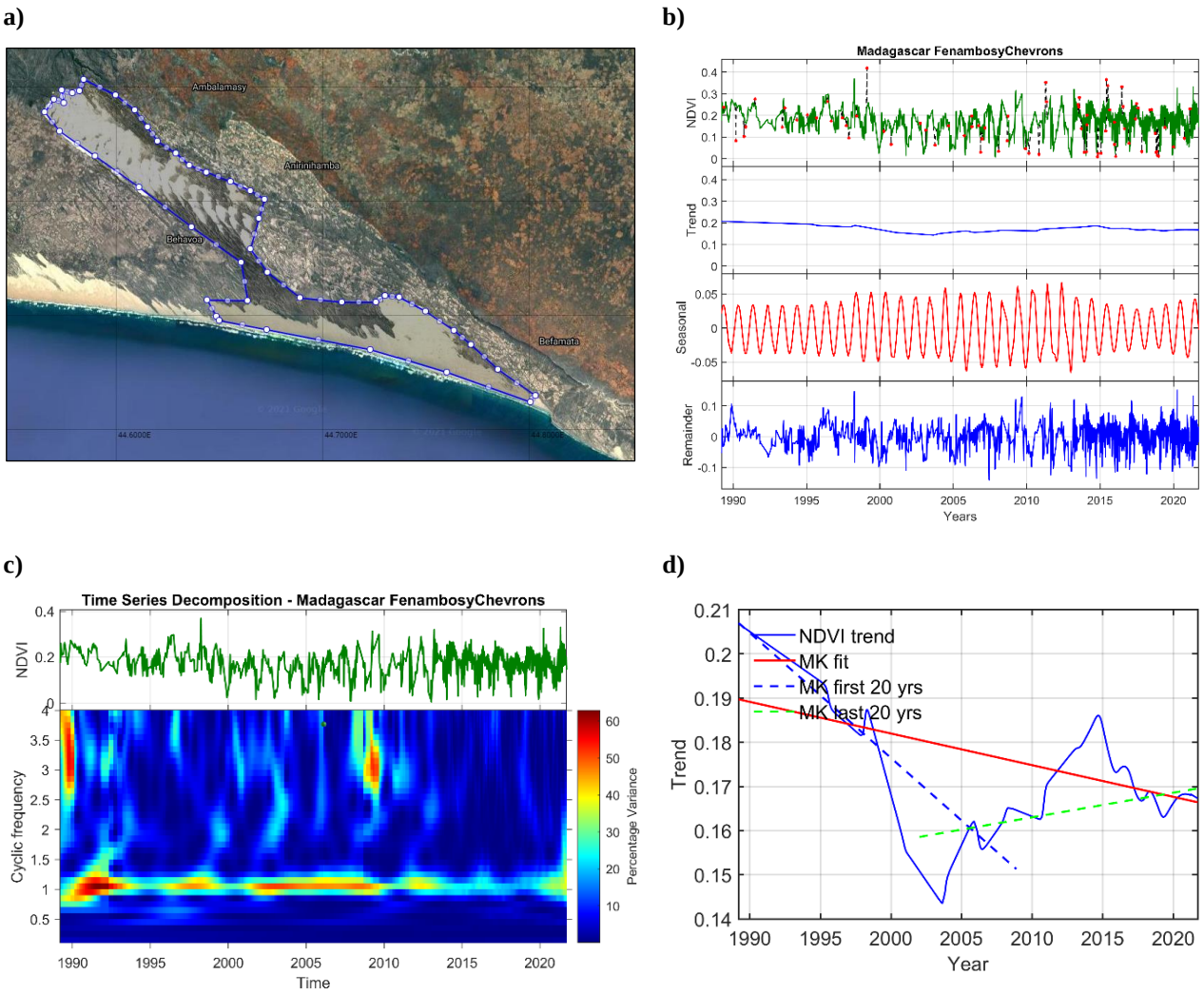

Figure C.7. (a) Fenambosy Chevrons, Madagascar (*Source*: Google Earth Pro 7.3.4.8248); (b) JUST decomposition (Ghaderpour and Vujanovic, 2020); (c) Spectrogram (LSWA; Ghaderpour and Pagiatakis, 2017); (d) Mann-Kendall test performed on the *NDVI* trend component with the two 20-year line fits also illustrated.

Four chevron dune sites from S Madagascar have been sampled from the available Landsat imagery and analysed here, among which is the Fenambosy dunefield presented in Figure C.7(a) (Abbott et al., 2016; Vimpere et al., 2019). They exemplify dune mobilisation over time. The climate of the studied region is subtropical dry (Figure 2.3; Sayre et al., 2020), or tropical savannah, following the Köppen-Geiger classification (Vimpere et al., 2019). The dunes experience the effect of a pronounced dry season (< 60 mm of precipitations for the driest month) alternated with a wet season.

The Fenambosy chevron extends obliquely to the shoreline over approximately 28 km distance inland and has a width of about 6 km (Figure C.7a). Two distinct types of dunes coexist in the dunefield: fixed parabolic dunes and active transverse dunes with ongoing wind erosion (bistability; Yizhaq et al., 2009). Land used for agricultural purposes was excluded from the studied dune area.

The *NDVI* signal is dominated by the trend component, since the seasonal fluctuations are very low ($\overline{NDVI}$ = 0.172, as compared to $\Delta NDVI$ = 0.078). Furthermore, the initially negative trend changed to positive, although with a milder slope (Figure C.7d, Appendix C). It can also be seen in Figure C.7(d) that the last 5 years of the study period obey again a diminishing trend. These nonlinear changes over time are also visible in the spectrogram (Figure C.7c). Namely, significant spectral peaks at 60% variance are recorded for the annual seasonal fluctuations, but also occasionally appear at a 4-month frequency.

In terms of the local climate, Fenambosy shows increasing daily temperatures ($Q_T > 0$), while the daily precipitation is decreasing ($Q_P < 0$) and the wind speed is increasing ($Q_W > 0$). Such changes ($T\uparrow$, $P\downarrow$, $W\uparrow$) are in agreement with the current dynamic state of the dunes and also characterise the other three sampled chevron dunes on Madagascar.

Vimpere et al. (2019) describe the chevrons on Madagascar and others worldwide as sand deposits reflecting past wind regimes, due to the strong correlation found between dune geomorphology and recurrent local breezes with speed of 5.5 to 7.9 m/s.

C.8. Rubjerg Knude, Denmark (Mobilisation trend, $\overline{NDVI}$ = 0.327 / Cool temperate moist climate / T↑, P↑, W↑)

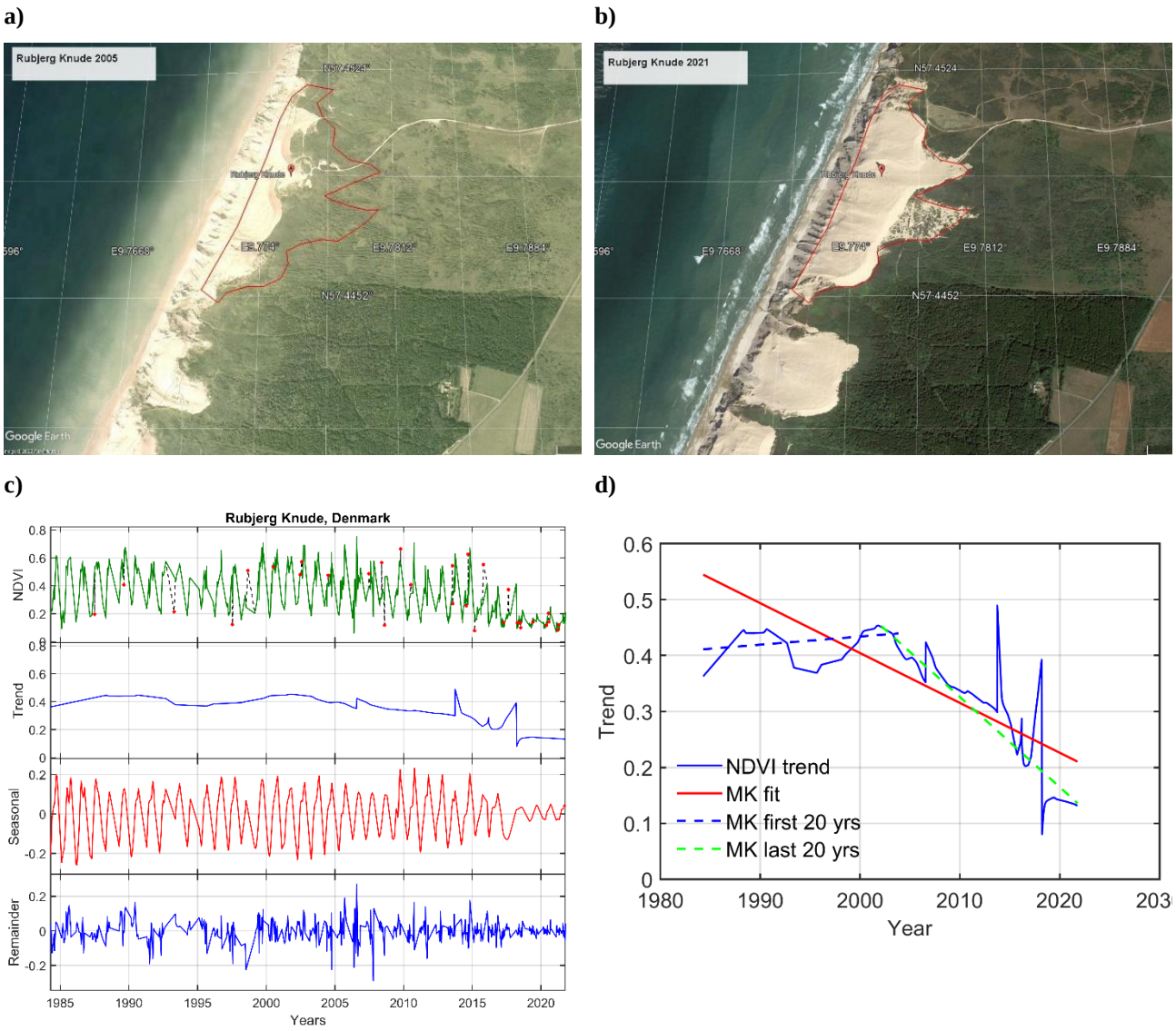

Figure C.8. (a, b) Rubjerg Knude, Denmark in 2005 and 2021, respectively (*Source*: Google Earth Pro 7.3.4.8248); (c) JUST decomposition (Ghaderpour and Vujanovic, 2020); (d) Mann-Kendall test performed on the *NDVI* trend component with the two 20-year line fits also illustrated.

Rubjerg Knude is a large cliff-top dune with a height of up to 40 m, located on the western coast of Jutland Peninsula, Denmark. The crest of the dune is at about 90 m above the mean sea level. It is a highly mobile dune evolving in a cool temperate climate.

The formation of the modern dune began after 1885 (the end of the Little Ice Age in Europe). The start of the period is associated with accelerated erosion of the cliff underneath followed by a coastal retreat. Saye et al. (2006) report a recent vertical dune growth rate of approximately 1 m/year between 1975 and 1980 which has declined since then.

Dominant winds influencing the dune mobility are the westerly and southwesterly onshore winds. Moreover, the seaward side of the dune continues to experience erosion and the sand is blown to the dune crest first and then further inland, up to 2 km from the crest of the dune. The rate of sand deposition inland decreases exponentially with the distance. Direct sediment transport from the beach is rare, due to the almost vertical lower cliff.

Management practices attempting to stop the inland migration of the dune include brushwood planting and have had limited effect. Figure C.8(a, b) allow to compare the dunefield in 2005 and 2021. The delineated polygon in red illustrates the location and dimensions of the dune at present. The retreat of the shoreline can be clearly seen, as well as the landward shift of the dune crest by approximately 5 m.

Furthermore, the present study has shown that Rubjerg Knude is the only dune from the group of identified mobile dunes here with $\overline{NDVI} > 0.3$. This possibly reflects the vegetated surfaces that have been buried by the sand of the advancing dune. The seasonal amplitude is also relatively high, $\Delta NDVI = 0.294$ (Figure C.8c).

With respect to the partial trends over the two 20-year periods, it could be concluded that the rate of long-term change in the dune cover has decelerated from slightly positive to a significant negative (Figure C.8d). The trend direction changed around 2005 (Figure C.8a).

Finally, the climatic conditions at the site reveal tendency of increasingly warmer, wetter and windier conditions ($T\uparrow$, $P\uparrow$, $W\uparrow$). They support aeolian transport, although the daily precipitation is also increasing. High aeolian transport is possible, since the strong onshore winds may outweigh the effect of rain which impedes the availability of sand for transportation due to increased moisture content.

C.9. Dune du Pilat, France (Mobilisation trend, $\overline{NDVI}$ << 0.3 / Warm, temperate moist climate / T↑, P↑, W↓)

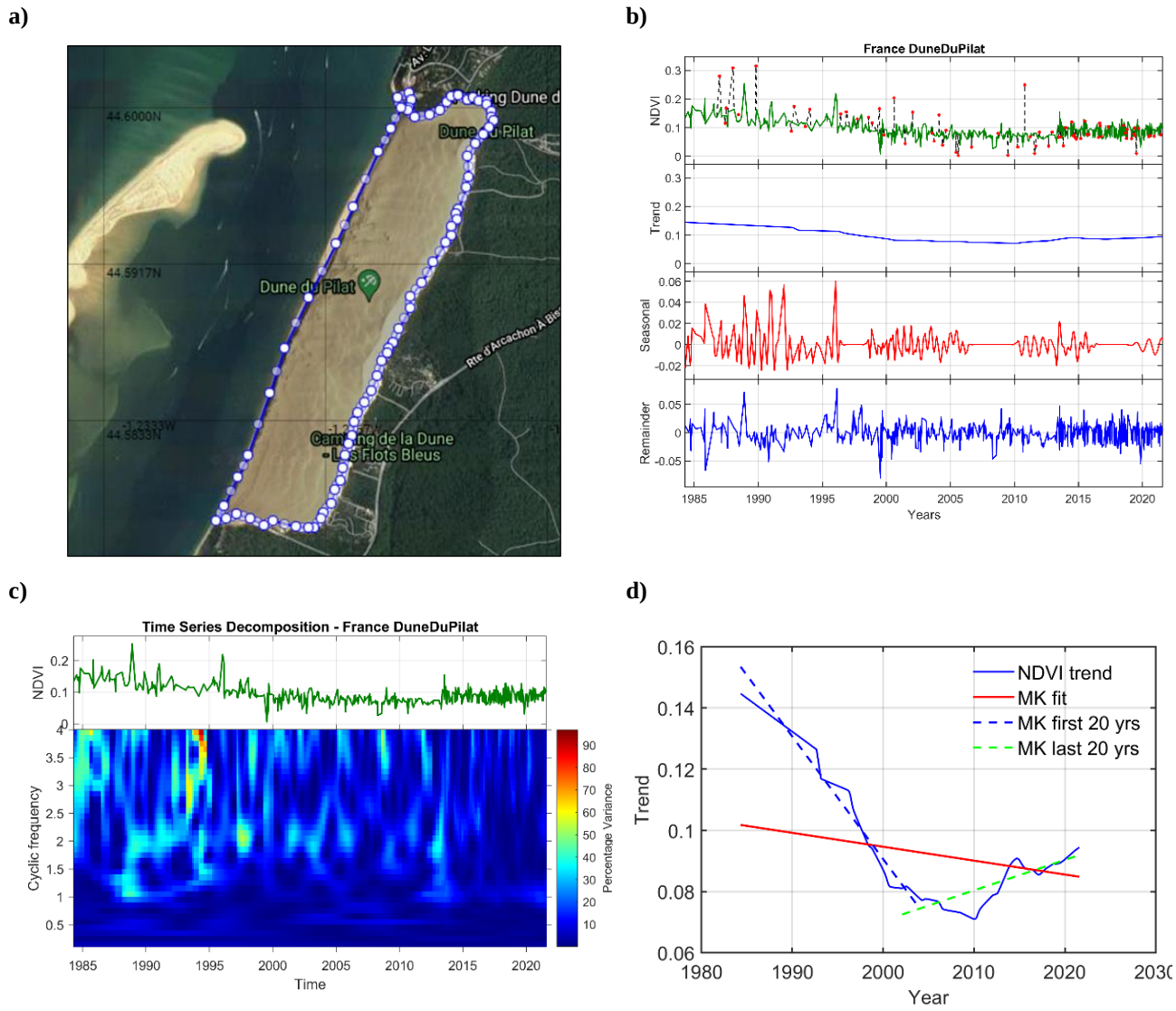

Figure C.9. (a) Dune du Pilat, France (*Source*: Google Earth Pro 7.3.4.8248); (b) JUST decomposition (Ghaderpour and Vujanovic, 2020); (c) Spectrogram (LSWA; Ghaderpour and Pagiatakis, 2017); (d) Mann-Kendall test performed on the *NDVI* trend component with the two 20-year line fits also illustrated.

Dune du Pilat is located on the Aquitaine coast, SW France. It is the largest coastal dune in Europe which has a vast open sand area and is actively migrating, thus threatening the nearby infrastructure and touristic installations (Clarke et al., 2002). According to Gabarrou et al. (2018), the current dune dimensions are: 2500 m length, 107 m height and 500 m width.

Based on in-situ measurements, an average displacement of 4.9 m/year was reported by Gabarrou et al. (2018), which compares well with a modelled advance speed of 3 m/s. The parabolic dunes on top of which has been evolving Dune du Pilat were stabilised with pine trees in the late 19th century and nowadays this forest plays an important role to slow down the migration rates of the dune.

In terms of local climate, the dune is exposed to dominant winds blowing perpendicular to the shore, with velocities of above 8 m/s, thus exceeding the threshold for effective sand transport. The main source of sediments is the beach where sand, reworked by waves and currents, is constantly supplied.

The dunefield has $\overline{NDVI}$ = 0.092, the lowest in the group of mobile dunes and one of the smallest among the whole sample of selected dune sites here. It is slightly higher than the corresponding value for the Brazilian Lençois Maranhenses dunefield ($\overline{NDVI}$ = 0.08; Figure C.9(a) and the Russian Efa Dune ($\overline{NDVI}$ = 0.07), although the latter is classified as greening. As compared to Rubjerg Knude, the average vegetation cover of Dune du Pilat is significantly smaller. The seasonal amplitude is very low, $\Delta NDVI$ = 0.009, which indicates dominance of the trend component (Figure C.9b).

The spectrogram in Figure C.9(c) reveals sporadic presence of low vegetation before 2000, which is confirmed by the Mann-Kendall test results (Figure C.9d). Furthermore, Figure C.9(d) shows a slight change of slopes from positive to negative and acceleration at around 2010.

Overall, the climatic variables at the site display increasing temperature and precipitation trends combined with decreasing drift potential ($T\uparrow, P\uparrow, W\downarrow$), which is a climatic combination favouring dune stabilisation. However, in the case of Dune du Pilat, the major factors supporting dune mobility are the frequent intensive winds and the coastal erosion that brings large amount of sand to the dune.